ρ_{ij} $(i \neq j)$ are negligible, or else we may regard formula (3) as an indication of the order of magnitude of formula (2). Finally, an unbiased estimate of formula (3) may be shown to be

$$\sum_i A_i^2 p_i (1 - p_i)/(n_i - 1), \qquad (4)$$

and the square root of this was used to estimate the standard deviation mentioned above.

PART V. TARGET COMPONENTS: SPECIAL STUDIES

A. REACTIONS OF SIMPLE SYSTEMS UNDER BLAST LOADING*

by D. Montgomery and A. H. Taub

Abstract

The differential equation $M\ddot{x} + F(x) = p(t)$ was considered for some simple cases of blast loading. The main problem was to find the relation between p_o (peak pressure acting on target) and t_o (duration of pressure wave) in order that the maximum solution (maximum value of displacement x) of the equation would be a specified quantity. If this were known it would mean, for example, that for a target such as a brick wall the relation between p_o and t_o that would just cause the target to fail -- that is, reach a critical displacement with zero velocity -- could be determined. In the solution, the right-hand side of the equation was assumed linear, and $F(x)$ was taken (i) as constant and (ii) as linear from the origin to x_1 and then remaining constant for larger values of x up to x_3 (the maximum value of x). A formula is developed that makes it easy to calculate from the limiting case ($x_1 = 0$) what the situation is for a given value of x_1/x_3 provided this value is not too large.

1. Introduction

In discussing the behavior of various targets under blast loading it is often possible to reduce the mathematical problem to that of a one-dimensional system governed by the equation

$$M \frac{d^2x}{dt^2} + F(x) = p(t), \qquad (1)$$

where x is the displacement of the system, $F(x)$ is the restoring force, M is the equivalent mass of the system, and $p(t)$ is the force [= pressure × area] acting on the system where $p(t)$ is dependent on time.

Equations of this form arise in many problems; for example, if the target is elastic and has various modes of vibration, its response is determined by solving a set of equations of the type of Eq. (1) where $F(x)$ is of the form $k_n x$. Again, this equation is found in the treatment given by Christopherson[1/] in R.C. 349 of the action of brick walls. There it is shown that $F(x)$ may be replaced by a constant.

In the application we have in mind (blast wave) the function $p(t)$ is zero for negative time, has a finite initial value p_o at $t = 0$, decreases to

---

*First published as AES-12a (OSRD-5393a).

1/ A modification of the impulse criterion for blast damage, by D. G. Christopherson, R.C. 349, Sept. 1942.

zero again at time t_o, and becomes negative thereafter, rising to zero at some later time. The problem with which we are mainly concerned may be stated as follows:

> What relation must exist between p_o and t_o in order that the maximum of the solution of Eq. (1) be a specified quantity, say x_3?

If the solution of this problem is known, then for a target such as a brick wall we can determine the relation between p_o and t_o that will just cause the target to fail -- that is, reach a critical displacement with zero velocity. The quantity p_o is called the peak pressure acting on the target, and t_o is called the duration of the pressure wave. The area under the pressure-time curve between $t = 0$ and $t = t_o$, called the positive impulse, may be related to p_o and t_o. The result may then be expressed in terms of the peak pressure and positive impulse just necessary to cause failure. If the relation between peak pressure and impulse acting on the target and the same quantities in the blast wave are known, then for any charge weight a distance can be determined that is the limiting distance at which the target is destroyed. In order to perform the last calculation the dependence of peak pressure and impulse in the blast wave on weight of charge and distance must be known. These quantities must be corrected for reflection, diffraction, and motion of the target in order to obtain the peak pressure and impulse acting on the target.

This paper will be concerned with the determination of the relation between peak pressure and impulse <u>acting on the target</u> for a given maximum displacement for special cases of Eq. (1). The specializations made are as follows:

$$p(t) = p_o\left(1 - \frac{t}{t_o}\right).$$

Case I: $F(x) = \text{constant} = P,$

or

Case II: $$F(x) = \begin{cases} \dfrac{P}{x_1}\, x, & 0 \le x \le x_1; \qquad \text{(a)} \\ P, & x \ge x_1. \qquad \text{(b)} \end{cases}$$

Case I is a limiting case of case II. If the desired deflection is x_3 and if x_1/x_3 approaches zero, then general existence theorems guarantee that the solutions in case II approach those in case I. However, there is no guarantee that a given value of x_1/x_3, say 0.01 for example, will bring the solutions near each other to an accuracy of about the same size. Actually we find that the solutions can differ to a greater degree than 0.01 in this case, although the difference is not excessive. We exhibit numerical calculations bearing on this point, and we also develop a formula that makes it easy to calculate from the limiting case what the situation is for a given value of x_1/x_3 provided this value is not too large. We consider only cases where $x_3 > x_1$ since in such cases a target will be destroyed when it reaches a deflection x_3 with zero velocity. At the end we also take up a related question whose description we postpone.

2. Solution for case II

We shall treat case I as a special case of case II and proceed first to obtain the solutions in the latter case.

In the interval from 0 to x_1 the solution is as follows:

$$x = \frac{p_o}{M\omega^2}\left[\frac{\sin\omega t}{\omega t_o} - \frac{t}{t_o} + 1 - \cos\omega t\right], \tag{2}$$

where $\omega^2 = P/Mx_1$, and hence in this interval

$$\dot{x} = \frac{p_o}{M\omega^2 t_o}\left[\cos\omega t + \omega t_o \sin\omega t - 1\right]. \tag{3}$$

Let t_1 be the time at which the displacement reaches x_1. Making use of the fact that $\omega^2 = P/Mx_1$, we see that

$$x_1 = \frac{p_o x_1}{P}\left[\frac{\sin\omega t_1}{\omega t_o} - \frac{t_1}{t_o} + 1 - \cos\omega t_1\right].$$

Dividing by x_1 and rearranging, we find as the equation determining t_1

$$\omega t_o \cos\omega t_1 + \omega t_1 - \sin\omega t_1 = \omega t_o\left(1 - \frac{P}{p_o}\right). \tag{4}$$

We let $\dot{x}_1$ be the value of $\dot{x}$ at t_1 and we denote by I the quantity $\frac{1}{2}p_o t_o$ which is the area under the curve $p(t)$ from 0 to t_o. Then from Eq. (3)

$$\frac{M\dot{x}_1}{I} = \frac{2}{\omega^2 t_o^2}(\omega t_o \sin \omega t_1 + \cos \omega t_1 - 1). \tag{5}$$

When t is greater than t_1 and x is greater than x_1 Eq. (1) becomes

$$M\ddot{x} = p(t) - P = (p_o - P) - \frac{p_o}{t_o} t.$$

Making use of the fact that $x = x_1$ and $\dot{x} = \dot{x}_1$ when $t = t_1$, we find that

$$M\dot{x} = M\dot{x}_1 + \left[p_o\left(1 - \frac{t_1}{t_o}\right) - P\right](t - t_1) - \frac{p_o}{2t_o}(t - t_1)^2 \tag{6}$$

and

$$Mx = Mx_1 + M\dot{x}_1(t - t_1) + \frac{1}{2}\left[p_o\left(1 - \frac{t_1}{t_o}\right) - P\right](t - t_1)^2 - \frac{p_o}{6t_o}(t - t_1)^3. \tag{7}$$

Let t_3 be the value of t at which the solution given by Eq. (7) has its maximum value, and let x_3 be this maximum. When $t = t_3$ the left-hand side of Eq. (6) is zero and we obtain

$$M\dot{x}_1 = \frac{p_o}{2t_o}(t_3 - t_1)^2 - \left[p_o\left(1 - \frac{t_1}{t_o}\right) - P\right](t_3 - t_1).$$

Let $\tau_3 = (t_3 - t_1)/t_o$. Rearrangement gives

$$\frac{M\dot{x}_1}{I} = \tau_3^2 - 2\left[\left(1 - \frac{t_1}{t_o}\right) - \frac{P}{p_o}\right]\tau_3.$$

Solving for τ_3,

$$\tau_3 = \left(1 - \frac{t_1}{t_o} - \frac{P}{p_o}\right) \pm \left[\frac{M\dot{x}_1}{I} + \left(1 - \frac{t_1}{t_o} - \frac{P}{p_o}\right)^2\right]^{1/2}, \tag{8}$$

where we must choose the sign before the square root so as to make τ_3 positive. In developing the approximation formula we consider the case where $1 - t_1/t_o - P/p_o$ is positive.

To find x_3 we substitute this value in Eq. (7):

$$Mx_3 = Mx_1 + t_o\tau_3\left\{M\dot{x}_1 + \frac{1}{2}\left[p_o\left(1 - \frac{t_1}{t_o}\right) - P\right]t_o\tau_3 - \frac{p_o t_o}{6}\tau_3^2\right\}.$$

Replace $M\dot{x}_1$ by its value from the equation preceding Eq. (8):

$$Mx_3 = Mx_1 + \frac{p_o t_o^2 \tau_3^2}{6}\left[2\tau_3 - 3\left(1 - \frac{t_1}{t_o} - \frac{P}{p_o}\right)\right]. \qquad (8a)$$

Now $p_o = \frac{p_o}{P} P = \frac{p_o}{P} M\omega^2 x_1$, and hence

$$x_3 = x_1 + \frac{1}{6}\frac{p_o}{P}\cdot\omega^2 t_o^2 x_1 \tau_3^2\left[2\tau_3 - 3\left(1 - \frac{t_1}{t_o} - \frac{P}{p_o}\right)\right]. \qquad (9)$$

Instead of plotting p_o against t_o it is more convenient to plot $I/\sqrt{2PMx_3}$ against p_o/P, and we shall next derive a formula expressing the first of these quantities in terms of the second in the limiting case. In this case $t_1 = x_1 = 0$. Here Eq. (9) becomes meaningless because in Eq. (9) we have used the expression P/x_1 for a slope. However, from Eq. (8a), in this case

$$Mx_3 = \frac{t_o^2 \tau_3^2 p_o}{6}\left[2\tau_3 - 3\left(1 - \frac{P}{p_o}\right)\right],$$

and also in this same case by Eq. (8)

$$\tau_3 = 2\left(1 - \frac{P}{p_o}\right).$$

Hence

$$2PMx_3 = \frac{16PI^2}{3p_o}\left(1 - \frac{P}{p_o}\right)^3 \qquad (10)$$

and

$$\frac{I^2}{2PMx_3} = \frac{3}{16}\frac{p_o}{P}\frac{1}{\left(1 - \frac{P}{p_o}\right)^3}. \qquad (11)$$

From Eq. (11) a table of values may be computed relating p_o/P and $I/\sqrt{2PMx_3}$. Table I and the graph of $x_1/x_3 = 0$ in Fig. 1 present these values.

Table I. Values of $I/\sqrt{2PMx_3}$ in the limiting case.

$\frac{p_o}{P}$	$\frac{I}{\sqrt{2PMx_3}}$	$\frac{p_o}{P}$	$\frac{I}{\sqrt{2PMx_3}}$
1.25	5.413	6	1.394
1.5	2.756	7	1.444
2	1.732	8	1.496
3	1.378	9	1.550
4	1.333	10	1.604
5	1.353		

Notice that for some computations in case II it is convenient to use the following relation

$$\frac{I}{\sqrt{2PMx_3}} = \frac{\frac{1}{2}\frac{p_o}{P}\omega^2 x_1 M t_o}{\sqrt{2M^2\omega^2 x_1 x_3}} = \frac{1}{2\sqrt{2}}\frac{p_o}{P}\sqrt{\frac{x_1}{x_3}}\,\omega t_o. \qquad (12)$$

CONFIDENTIAL

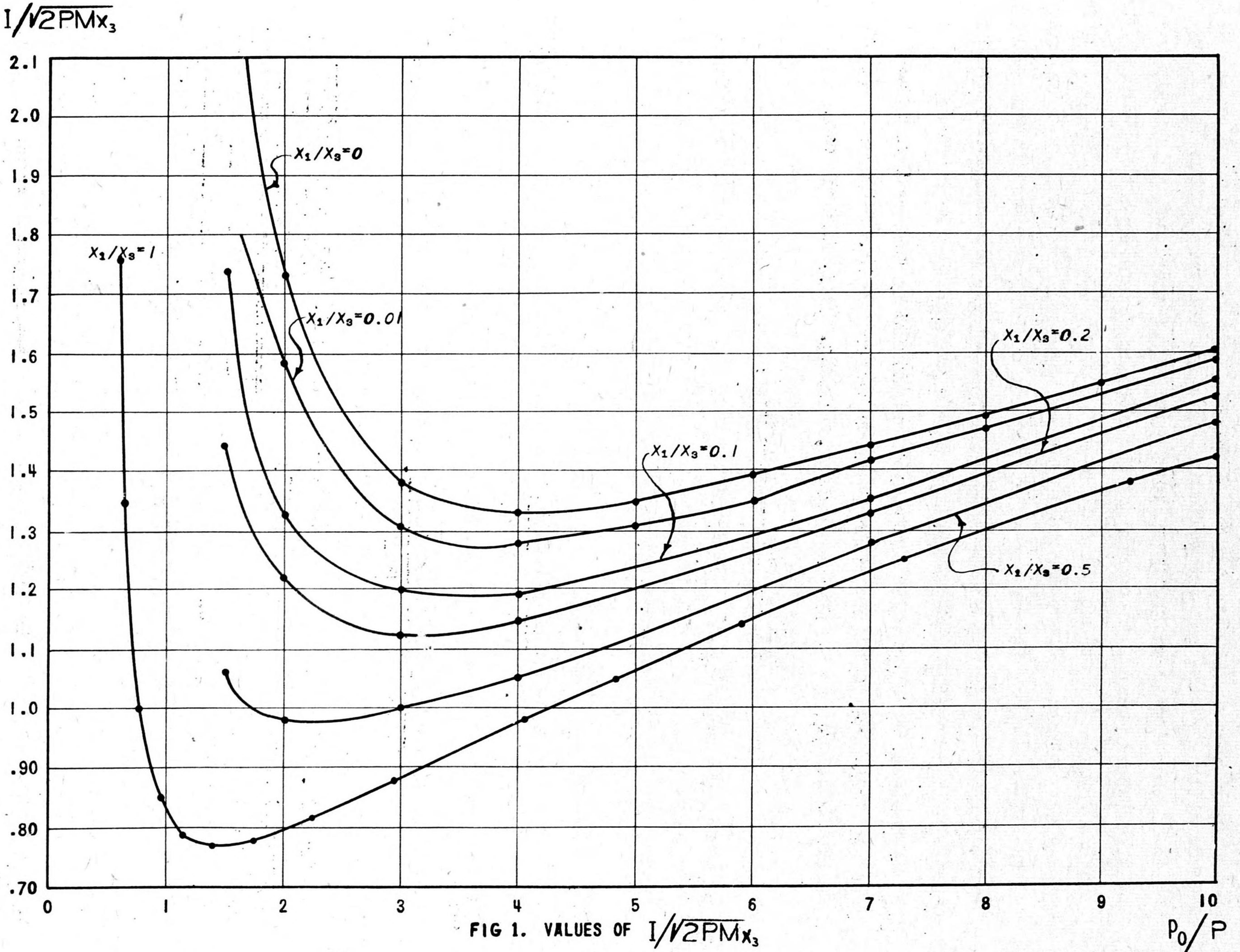

FIG 1. VALUES OF $I/\sqrt{2PMx_3}$

Princeton University Station

Division 2, NDRC

The quantity $I^2/2PMx_3$ has the following physical interpretation; it is the ratio of the kinetic energy given to the target if the loading is truly impulsive (the impulse I is communicated before any displacement or velocity is acquired by the target) to the static work done on the target when it is displaced to failure. This ratio would be one for impulsive loading. Actually in the limiting case this ratio is a function of P/p_o and its minimum value is 4/3. Thus the fact that the loading is spread out over a finite time has an appreciable effect on the behavior of the system.

The fact that the value of $I/\sqrt{2PMx_3}$ rises slowly for values of p_o/P greater than four, implies that in this range of p_o/P the "impulse criterion" is approximately true. That is, if the impulse in the pressure wave acting on the structure is greater than and approximately the minimum value the target will break, provided of course p_o/P is greater than four. In the range where p_o/P is less than two, but greater than one, the value of $I/\sqrt{2PMx_3}$ changes very rapidly for small changes in p_o/P. This means that the breaking of the target is following a pressure criterion.

3. Approximation formulas

We shall now find a method to obtain approximately the value of $I/\sqrt{2PMx_3}$ for a given value of x_1/x_3 from the value of $I/\sqrt{2PMx_3}$ in the limiting case. The equations we need for this purpose are Eqs. (4), (5), (8), and (9).

For convenience we collect these formulas in one place

$$\omega t_o \cos \omega t_1 + \omega t_1 - \sin \omega t_1 = \omega t_o \left(1 - \frac{P}{p_o}\right), \tag{4}$$

$$\frac{\dot{M}x_1}{I} = \frac{2}{\omega^2 t_o^2} (\omega t_o \sin \omega t_1 + \cos \omega t_1 - 1), \tag{5}$$

$$\tau_3 = \left(1 - \frac{t_1}{t_o} - \frac{P}{p_o}\right) + \left[\frac{\dot{M}x_1}{I} + \left(1 - \frac{t_1}{t_o} - \frac{P}{p_o}\right)^2\right]^{1/2}, \tag{8}$$

$$x_3 = x_1 + \frac{x_1}{6} \frac{p_o}{P} \omega^2 t_o^2 \tau_3^2 \left[2\tau_3 - 3\left(1 - \frac{t_1}{t_o} - \frac{P}{p_o}\right)\right]. \tag{9}$$

Suppose that P/p_o is fixed. If we also fix ωt_o, then ωt_1 is determined by Eq. (4). Then $\dot{M}x_1/I$ is given by Eq. (5) and, since $t_1/t_o = \omega t_1/\omega t_o$, τ_3 is given by Eq. (8) and x_1/x_3 is determined by Eq. (9). Hence for each value of P/p_o there will be a value of ωt_o which gives x_1/x_3 a fixed value.

Assuming that x_1/x_3 and P/p_o are fixed we now estimate what the value of ωt_o will be when x_1/x_3 is small.

For a first rough estimate assume that $t_1 = 0$ and that $\tau_3 = 2(1 - P/p_o)$ as in the limiting case. Then from Eq. (9)

$$\frac{x_3}{x_1} = 1 + \frac{2}{3}\frac{p_o}{P}\omega^2 t_o^2\left(1 - \frac{P}{p_o}\right)^3.$$

We may drop the one as unimportant when x_3/x_1 is large and get as a first estimate $(\omega t_o)_1$ of ωt_o,

$$(\omega t_o)_1^2 = \frac{3\,\frac{x_3}{x_1}\,\frac{P}{p_o}}{2\left(1 - \frac{P}{p_o}\right)^3}. \tag{13}$$

We now assume that a second approximation $(\omega t_o)_2$ is given by

$$(\omega t_o)_2 = \beta(\omega t_o)_1, \tag{14}$$

where β is a quantity to be determined.

From Eq. (4) it is seen that a good approximation to ωt_1 is

$$\omega t_1 = \text{arc cos}\left(1 - \frac{P}{p_o}\right), \tag{15}$$

and from Eq. (5) an approximation for $\dot{M}x_1/I$ is

$$\frac{\dot{M}x_1}{I} = \frac{2 \sin \omega t_1}{\omega t_o}. \tag{16}$$

We also make the following estimates for τ_3 and τ_3^2:

$$\tau_3 = 2\left(1 - \frac{t_1}{t_o} - \frac{P}{p_o}\right) + \frac{\dot{M}x_1}{I}\,\frac{1}{2\left(1 - \frac{t_1}{t_o} - \frac{P}{p_o}\right)} \tag{17}$$

and

$$\tau_3^2\left[2\tau_3 - 3\left(1 - \frac{t_1}{t_o} - \frac{P}{p_o}\right)\right] = 4\left(1 - \frac{P}{p_o}\right)^3 - 12\left(1 - \frac{P}{p_o}\right)^2\frac{t_1}{t_o} + 6\,\frac{\dot{M}x_1}{I}\left(1 - \frac{P}{p_o}\right). \tag{18}$$

The value $(\omega t_o)_1$ has been chosen so that the desired value of x_3/x_1 is given by

$$\frac{x_3}{x_1} = \frac{2}{3}\frac{p_o}{P}(\omega t_o)_1^2\left(1 - \frac{P}{p_o}\right)^3, \tag{19}$$

but substitution of Eq. (18) in Eq. (9) and use of the second approximation $(\omega t_o)_2 = \beta(\omega t_o)_1$ gives

$$\frac{x_3}{x_1} = 1 + \frac{1}{6}\frac{p_o}{P}\beta^2(\omega t_o)_1^2\left[4\left(1 - \frac{P}{p_o}\right)^3 - 12\left(1 - \frac{P}{p_o}\right)^2\frac{t_1}{t_o} + 6\frac{\dot{M}x_1}{I}\left(1 - \frac{P}{p_o}\right)\right].$$

Equating these two values, again dropping the one as unimportant when x_3/x_1 is large, and dividing, we find

$$4\left(1 - \frac{P}{p_o}\right)^3 = \beta^2\left[4\left(1 - \frac{P}{p_o}\right)^3 - 12\left(1 - \frac{P}{p_o}\right)^2\frac{t_1}{t_o} + 6\frac{\dot{M}x_1}{I}\left(1 - \frac{P}{p_o}\right)\right].$$

Hence

$$\beta^2 = \frac{1}{1 + \alpha},$$

where

$$\alpha = \frac{1}{1 - \frac{P}{p_o}}\left[\frac{3/2}{1 - \frac{P}{p_o}}\frac{\dot{M}x_1}{I} - 3\frac{t_1}{t_o}\right].$$

Substituting the relation given by Eq. (16) and remembering that $t_1/t_o = \omega t_1/\omega t_o$,

$$\alpha = \frac{3}{\left(1 - \frac{P}{p_o}\right)^2}\left[\sin \omega t_1 - \left(1 - \frac{P}{p_o}\right)\omega t_1\right]\frac{1}{(\omega t_o)_2},$$

and then using the relations given in Eqs. (13), (14), and (15),

$$\alpha = \frac{1}{\beta}\frac{3}{\left(1 - \frac{P}{p_o}\right)^2}\left[\sin\left\{\arccos\left(1 - \frac{P}{p_o}\right)\right\} - \left(1 - \frac{P}{p_o}\right)\arccos\left(1 - \frac{P}{p_o}\right)\right]\left[\frac{2\left(1 - \frac{P}{p_o}\right)^3\frac{x_1}{x_3}}{3\frac{P}{p_o}}\right]^{1/2}$$

or

$$\alpha = \frac{\gamma\sqrt{\frac{x_1}{x_3}}}{\beta},$$

where

$$\gamma = 3\left[\frac{2\,\frac{p_o}{P}}{3\left(1-\frac{P}{p_o}\right)}\right]^{1/2}\left[\sin\left\{\arccos\left(1-\frac{P}{p_o}\right)\right\} - \left(1-\frac{P}{p_o}\right)\arccos\left(1-\frac{P}{p_o}\right)\right].$$

Hence

$$\beta^2 = \frac{1}{1+\alpha} = \frac{1}{1+\frac{\gamma\sqrt{\frac{x_1}{x_3}}}{\beta}},$$

$$\beta = -\frac{\gamma\sqrt{\frac{x_1}{x_3}}}{2} + \sqrt{1+\frac{\gamma^2 x_1/x_3}{4}},$$

$$\beta \cong 1 - \frac{\gamma}{2}\sqrt{\frac{x_1}{x_3}} + \frac{\gamma^2}{8}\frac{x_1}{x_3}. \qquad (20)$$

Table II. Values of γ and β.

$\frac{p_o}{P}$	γ	$\frac{\gamma}{2}$	$\frac{\gamma^2}{8}$	β for $\frac{x_1}{x_3}=0.01$
1.25	4.323	2.162	2.337	0.760
1.5	2.767	1.384	0.958	.852
2	1.677	0.838	.351	.920
3	0.959	.480	.115	.953
4	.688	.344	.0592	.966
5	.522	.261	.0341	.974
6	.425	.212	.0225	.979
7	.359	.180	.0162	.982
8	.311	.156	.0122	.984
9	.274	.137	.0094	.986
10	.245	.122	.0074	.988

Thus we have achieved our purpose — to find the approximate value of β. A table of values of $\gamma/2$ and $\gamma^2/8$ as well as the values of β when $x_1/x_3 = 0.01$ is given in Table II.

If we replace ωt_o in Eq. (12) by $(\omega t_o)_1$ we see that we obtain the value of $I/\sqrt{2PMx_3}$ for the limiting case. Hence the factor β is also the factor which when multiplied by $I/\sqrt{2PMx_3}$ in the limiting case yields the value (approximately) for any value of x_1/x_3.

Table III shows $I/\sqrt{2PMx_3}$ as computed in certain cases and as given by the approximation formula derived above. It can be seen that the approximation formula is quite accurate in these cases.

Hence, to get a good estimate of $I/\sqrt{2PMx_3}$ for a given small value of x_1/x_3, compute β from Eq. (20), using in many cases the values of $\gamma/2$ and $\gamma^2/8$ from Table II. Then multiply β and the limiting value of $I/\sqrt{2PMx_3}$ from Table I. This approximation formula is quite accurate when x_1/x_3 is small, and is fairly accurate for values of x_1/x_3 as large as 0.3 or 0.4. Figure 1 gives the values of $I/\sqrt{2PMx_3}$ for various values of x_1/x_3 between 0 and 1. The case $x_1/x_3 = 1$ may be handled as follows. In this case $F(x)$ is a straight line and[2/]

Table III. Comparison of exact and approximate values of $I/\sqrt{2PMx_3}$

$\frac{p_o}{P}$	$\frac{x_1}{x_3}$	Exact Value of $\frac{I}{\sqrt{2PMx_3}}$	Value Given by Approximation Formula
1.5	0.0205	2.280	2.265
2.0	.0424	1.457	1.458
2.0	.0124	1.577	1.578
3.0	.0150	1.300	1.299
3.0	.0069	1.324	1.324
4.0	.0223	1.269	1.266
4.0	.0129	1.283	1.281
7.0	.0091	1.420	1.420
10.0	.0220	1.575	1.575
10.0	.0125	1.583	1.582

$$x_3 = \frac{2p_o}{M\omega^2}\left[1 - \frac{\text{arc tan } \omega t_o}{\omega t_o}\right];$$

using the fact that $\omega^2 = \frac{P}{Mx_3}$, we obtain

$$\frac{P}{p_o} = 2\left[1 - \frac{\text{arc tan } \omega t_o}{\omega t_o}\right].$$

We find also in this case, by Eq. (12),

$$\frac{I}{\sqrt{2PMx_3}} = \frac{1}{2\sqrt{2}}\frac{p_o}{P}\omega t_o.$$

The graphs for this case and for the cases where $x_1/x_3 = 0.0$, 0.01, 0.1, 0.2, and 0.5 are shown in Fig. 1.

The curves of Fig. 1 all have vertical asymptotes on the left. To find them proceed as follows. Looking at the Eqs. (4), (5), (8), (9), and (12),

---

2/ The following equation is derived by solving the differential equation for $x(t)$. Determine the time at which the maximum is obtained from the equation $\dot{x}(t_1) = 0$. Substitute this value of t_1 in the equation $x(t_1) = x_3$. See R.C. 6, "The design of buildings against air attack (Part 2)," March 1939.

let ωt_o approach infinity. Then τ_3 approaches zero. Let $\frac{p_o}{P}$, $\frac{1}{2} \leqq \frac{p_o}{P} \leqq 1$, be fixed, and attempt to find the corresponding value of x_1/x_3. Since $1 - t_1/t_o - P/p_o$ is negative, the approximation for τ_3 given by Eq. (17) is to be replaced by the expression obtained by the choice of signs in Eq. (8) which makes τ_3 positive. This gives

$$\tau_3 = \frac{-\dot{M}x}{I} \frac{1}{2(1 - t_1/t_o - P/p_o)}.$$

Since $t_1/t_o = \omega t_1/\omega t_o$ is negligible compared to $1 - P/p_o$, we obtain

$$\tau_3 = \frac{\sin \omega t_1}{\omega t_o (P/p_o - 1)}.$$

Substituting in Eq. (19) and replacing $\sin^2 \omega t_1$ by $2P/p_o - (P/p_o)^2$ we obtain

$$\frac{x_3}{x_1} = 1 + \frac{1}{6} \frac{p_o}{P} \frac{2P/p_o - (P/p_o)^2}{(P/p_o - 1)^2} [\tau_3 - 3(1 - P/p_o)].$$

Making use of the fact that τ_3 is small compared to $3(1 - P/p_o)$ we write

$$\frac{x_3}{x_1} = 1 + \frac{1}{6} \frac{2 - P/p_o}{(P/p_o - 1)^2} 3(P/p_o - 1)$$

$$= 1 + \frac{2 - P/p_o}{P/p_o - 1}$$

and

$$\frac{x_1}{x_3} = \frac{2P/p_o - 2}{P/p_o}.$$

This may be written

$$\frac{p_o}{P} = 1 - \frac{1}{2} \frac{x_1}{x_3}.$$

Hence this is the location of the vertical asymptotes for the curve associated with x_1/x_3. When $x_1/x_3 = 0$ the asymptote is at 1, and as x_1/x_3 increases to 1 the position of the asymptote shifts linearly to $\frac{1}{2}$.

As we have seen, the curves all have a vertical asymptote given as above. After this they drop rather soon to a minimum and then rise gradually. The position of the minimum varies from about 1.5 for $x_1/x_3 = 1$ to 4 for $x_1/x_3 = 0$.

4. Comparison of case II to an elastic system

Returning to the differential equation Eq. (1), we discuss next a problem which arises in connection with F(x) as given in case II and as given in still another case called case III.

The function $F(x) = kx$ where $k = P/x_1$ is the value given in (a) of case II. Thus the curve of case III is merely a continuation of the straight line with which the curve in case II begins. Suppose that the desired maximum deflection in case II is x_3 and that the desired maximum deflection in case III is x_3'. The area A_2 under the curve II from 0 to x_3 is

$$A_2 = kx_1x_3 - \frac{kx_1^2}{2}.$$

The area under the curve III from 0 to x_3' is

$$A_3 = \frac{kx_3'^2}{2}.$$

Under some conditions it is reasonable to suppose that if $A_2 = A_3$, then the p_o and t_o which produce a maximum deflection x_3 in case II will produce a maximum deflection x_3' in case III. This conjecture will be examined below, and it will be shown that it is not always true.

For $A_2 = A_3$, the following must hold

$$x_3'^2 = 2x_1x_3 - x_1^2,$$

or when x_1 is small,

$$x_3'^2 = 2x_1x_3. \tag{21}$$

Let x_{III} be the maximum deflection in case III. Then

$$x_{III} = \frac{2p_o}{M\omega^2}\left[1 - \frac{\text{arc tan } \omega t_o}{\omega t_o}\right]$$

$$= 2\frac{p_o}{P}x_1\left[1 - \frac{\text{arc tan } \omega t_o}{\omega t_o}\right].$$

For small values of x_1 this is approximated fairly well by

$$x_{III} = 2\frac{p_o}{P}x_1.$$

In case II assume that x_1/x_3 is so small that the maximum deflection x_{II} is approximately equal to what it would be in the limiting case,

$$x_{II} = \frac{1}{M}\frac{2}{3}\left(1 - \frac{P}{p_o}\right)^3 p_o t_o^2.$$

According to Eq. (21) we wish to compare the quantities

$$4\left(\frac{p_o}{P}\right)^2 x_1^2 \quad \text{and} \quad \frac{4}{3M}\left(1 - \frac{P}{p_o}\right)^3 p_o t_o^2 x_1.$$

It is clear that in general these two quantities do not approximate each other, and as a further check it is easy to choose special values of the constants which show a substantial discrepancy between the two quantities.

As a numerical example suppose that $M = 1$, $t_o = 1$, $\frac{P}{p_o} = \frac{1}{2}$ and $\frac{x_{II}}{x_1} = 100$.

Then

$$x_{II} = \frac{p_o}{12},$$

$$x_{III} = 4x_1,$$

and

$$\frac{x_{II}}{x_1} = 100 = \frac{p_o}{12x_1},$$

$$p_o = 1200x_1.$$

We wish to compare the quantities

$$16x_1^2 \quad \text{and} \quad \frac{p_o x_1}{6},$$

or

$$16x_1 \quad \text{and} \quad \frac{p_o}{6},$$

or

$$16x_1 \quad \text{and} \quad 200x_1.$$

These quantities differ by a factor of more than 12. For this numerical case practically all of the action takes place while the right-hand side of the differential equation is positive.

B. REMARKS ON REACTIONS UNDER BLAST LOADING*

by H. F. Bohnenblust, D. Montgomery, and A. H. Taub

Abstract

This paper makes a few observations concerning the differential equation $Md^2x/dt^2 + F(x) = p(t)$, which is the equation for the reaction of a system under a blast. The equation is put in a certain canonical form involving certain dimensionless quantities. Some results are presented for the case where $F(x) = Cx$ and the conclusion may be drawn that at least in a large range of cases the negative phase of the blast is not of major importance.

1. Introduction

When a system is acted upon by a blast its motion is specified by the equation

$$M \frac{d^2x}{dt^2} + F(x) = p(t), \tag{1}$$

where M is the mass, $F(x)$ is the restoring force, and $p(t)$ is the force acting on the system as a result of the blast. Notice that $p(t)$ is equal to the pressure multiplied by the area under consideration.

We shall express Eq. (1) in terms of certain dimensionless quantities with which it is convenient to work. We assume throughout that $p(t)$ has the following form:

$$p(t) = p_o \pi(t/t_o),$$

and we let x_m be a certain fixed value of x which is to be the maximum displacement of the system; the word maximum here is used to refer to the first maximum occurring in time. The problem to be considered is that of finding relations between the parameters which will ensure that the system has x_m as its maximum displacement.

2. Canonical forms

In addition to p_o the following quantities will be found to be of use.

$$I = \int_o^{t_o} p(t)\, dt = p_o t_o \int_o^1 \pi(t)\, dt = p_o t_o k,$$

*First published as AES-14a (OSRD-6007a).

where

$$k = \int_o^1 \pi(t)\, dt \ ,$$

$$I_{oo} = \left[2M \int_o^{x_m} F(x)\, dx\right]^{\frac{1}{2}} ,$$

$$p_{oo} = \frac{1}{x_m} \int_o^{x_m} F(x)\, dx \ .$$

In place of $\underline{t}$ and $\underline{x}$ we use the variables $\underline{\tau}$ and $\underline{\xi}$, where

$$\tau = t/t_o \ ,$$

and

$$\xi = x/x_m \ .$$

We also let

$$\phi(\xi) = \frac{F(x_m\xi)x_m}{\int_o^{x_m} F(x)\, dx} = \frac{F(x_m\xi)}{p_{oo}} \ .$$

With these new symbols Eq. (1) becomes

$$\frac{d^2\xi}{d\tau^2} + \frac{p_{oo}t_o^2}{Mx_m}\phi(\xi) = \frac{p_o t_o^2}{Mx_m}\pi(\tau)$$

or

$$\frac{d^2\xi}{d\tau^2} + \frac{p_{oo}I^2}{Mx_m p_o^2 k^2}\phi(\xi) = \frac{p_o I^2}{Mx_m p_o^2 k^2}\pi(\tau) \ .$$

However, by making use of the quantities involved this may be written as

$$\frac{d^2\xi}{d\tau^2} + \frac{2}{k^2}\left(\frac{p_{oo}}{p_o}\right)^2\left(\frac{I}{I_{oo}}\right)^2\phi(y) = \frac{2}{k^2}\frac{p_{oo}}{p_o}\left(\frac{I}{I_{oo}}\right)^2\pi(\tau) \ .$$

Let $x = p_o/p_{oo}$, $y = I/I_{oo}$ (notice that $\underline{x}$ here is a different quantity from the $\underline{x}$ in the original statement) so that the equation is

$$\frac{d^2\xi}{d\tau^2} + \frac{2}{k^2}\frac{y^2}{x^2}\phi(\xi) = \frac{2y^2}{k^2 x}\pi(\tau) \ . \qquad (2)$$

In an important special case $F(x) = Cx$ and in this case $\phi(\xi) = 2\xi$. Therefore in this, the case of the linear restoring force, Eq. (2) becomes

$$\frac{d^2\xi}{d\tau^2} + \frac{4}{k^2}\frac{y^2}{x^2}\xi = \frac{2}{k^2}\frac{y^2}{x}\pi(\tau) \ . \qquad (3)$$

Let

$$\omega = \frac{2y}{kx} \ .$$

Then Eq. (3) becomes

$$\frac{d^2\xi}{d\tau^2} + \omega^2\xi = \frac{\omega y}{k}\pi(\tau) \ . \qquad (4)$$

In Eqs. (2) and (4) the quantity $\underline{k}$ is a constant once $\pi(\tau)$ has been given, and the problem therefore is to determine for a fixed $\pi(\tau)$ the relation between $\underline{x}$ and $\underline{y}$ or $\underline{\omega}$ and $\underline{y}$ which will guarantee that the maximum (that is, the first maximum) displacement is exactly one.

We denote the desired relation by $y = h(x)$. It would be highly desirable to be able to show in the general case that this relation depends, except for negligible variations, on a few simple properties of the functions $\phi(\xi)$ and $\pi(\tau)$. This goal has not been reached although certain progress toward it has been attained at least under simplified hypotheses.

3. Linear restoring forces

In this section we consider Eq. (4), that is, the case of the linear restoring force. For convenience we write the equation again,

$$\frac{d^2\xi}{d\tau^2} + \omega^2\xi = \frac{\omega y}{k}\pi(\tau) \ . \qquad (4)$$

The solution of Eq. (4) is

$$\xi = \frac{y}{k}\int_0^\tau \pi(\tau')\,\sin\,\omega(\tau - \tau')\,d\tau' \ , \qquad (5)$$

and we have

$$\dot{\xi} = \frac{y\omega}{k}\int_0^\tau \pi(\tau')\,\cos\,\omega(\tau - \tau')\,d\tau' \ . \qquad (6)$$

Let $P(\tau) = \int_0^\tau \pi(\tau')\,d\tau'$. Then ξ and $\dot{\xi}$ may also be written as follows:

$$\xi = \frac{y\omega}{k} \int_0^\tau P(\tau') \cos \omega(\tau - \tau')\, d\tau' , \tag{7}$$

$$\dot{\xi} = \frac{y\omega}{k}\left[P(\tau) - \omega\int_0^\tau P(\tau') \sin \omega(\tau - \tau')\, d\tau'\right] . \tag{8}$$

About the various quantities involved here the following assumptions are made:

(a) $P(\tau) \geqq 0$ for all τ,

(b) $\pi(0) = 1$, $\pi(1) = 0$, $\pi(\tau)$ is positive if $\tau < 1$, and negative if $\tau > 1$,

(c) $\pi(\tau)$ has at most one critical point which is a minimum and occurs when $\tau > 1$.

It is convenient to make some assumption about the maxima or their location in order to prove Theorem 2 which follows. For this purpose we choose the following, which seems reasonable for the phenomena studied:

(d) The first maximum of ξ is the largest maximum, or at any rate the largest in the interval $0 < \tau < \pi/\omega$. (One must occur in this interval, as will be shown.)

Notice that $P(0) = 0$. From Eq. (6) it can be seen that $\dot{\xi}$ is positive when τ is sufficiently small. In view of this and Theorem 1, which follows, we see that $\xi(\tau)$ must have a maximum between 0 and π/ω.

Theorem 1: $\dot{\xi}(\pi/\omega)$ is negative.

Proof: From Eq. (6)

$$\dot{\xi}(\pi/\omega) = \frac{y\omega}{k} \int_0^{\pi/\omega} \pi(\tau') \cos(\pi + \omega\tau')\, d\tau'$$

$$= -\frac{y\omega}{k} \int_0^{\pi/\omega} \pi(\tau') \cos \omega\tau'\, d\tau' .$$

Hence it will be sufficient to prove

$$\int_0^{\pi/\omega} \pi(\tau) \cos \omega\tau\, d\tau > 0. \tag{9}$$

In order to prove inequality (9) we consider various cases.

Case I. Assume $\pi/\omega < 1$. Then inequality (9) is obvious.

Case II. Assume $\pi/2\omega < 1 < \pi/\omega$. Then,

$$\int_0^{\pi/\omega} \pi(\tau) \cos \omega\tau \, d\tau = \int_0^{\pi/2\omega} \pi(\tau) \cos \omega\tau \, d\tau + \int_{\pi/2\omega}^{1} \pi(\tau) \cos \omega\tau \, d\tau + \int_1^{\pi/\omega} \pi(\tau) \cos \omega\tau \, d\tau. \tag{10}$$

Of the three integrals on the right-hand side of Eq. (10) the first and third are positive and the second is negative. From the nature of the functions involved we see that the negative contribution of the second term is not as great as the positive contribution of the first term. This proves inequality (9) in case II.

Case III. Assume $1 \leqq \pi/2\omega$. Then,

$$\int_0^{\pi/\omega} \pi(\tau) \cos \omega\tau \, d\tau = \int_0^{\pi/2\omega} \pi(\tau) \cos \omega\tau \, d\tau + \int_{\pi/2\omega}^{\pi/\omega} \pi(\tau) \cos \omega\tau \, d\tau. \tag{11}$$

The second integral on the right-hand side is positive. Integrating the first integral by parts,

$$\int_0^{\pi/2\omega} \pi(\tau) \cos \omega\tau \, d\tau = [P(\tau) \cos \omega\tau]_0^{\pi/2\omega} + \omega \int_0^{\pi/2\omega} P(\tau) \sin \omega\tau \, d\tau$$

$$= \omega \int_0^{\pi/2\omega} P(\tau) \sin \omega\tau \, d\tau.$$

This proves that the first integral on the right-hand side of Eq. (11) is also positive and hence inequality (9) is demonstrated in case III, and the proof of Theorem 1 is now complete.

In the following we use subscripts in an obvious way to denote the constants associated with $\pi_1(\tau)$, $\pi_2(\tau)$, and so forth.

Theorem 2: If $k_1 = k_2 = k$, if ω is fixed, and if $\pi_1(\tau) \geqq \pi_2(\tau)$ then $y_1 \leqq y_2$.

Proof: From Eq. (5)

$$1 = \frac{y_2}{k} \int_0^{\tau_2} \Pi_2(\tau') \sin \omega(\tau_2 - \tau')\, d\tau' \qquad (12)$$

and

$$1 = \frac{y_i}{k} \int_0^{\tau_1} \Pi_1(\tau') \sin \omega(\tau_i - \tau')\, d\tau'. \qquad (13)$$

Notice that in view of Theorem 1, the part of the integrand involving the sine in Eq. (12) as well as in Eq. (13) is positive. Also by assumption (d), $\xi(\tau_1)$ gives the largest value of $\underline{\xi}$ in the interval $0<\tau<\pi/\omega$ when $\Pi_1(\tau)$ is used. Hence if we assume $y_i > y_2$

$$\frac{y_1}{k}\int_0^{\tau_1} \Pi_1(\tau')\sin\omega(\tau_1 - \tau')d\tau' > \frac{y_1}{k}\int_0^{\tau_2} \Pi_1(\tau')\sin\omega(\tau_2 - \tau')d\tau'$$

$$> \frac{y_2}{k}\int_0^{\tau_2} \Pi_2(\tau')\sin\omega(\tau_2 - \tau')d\tau' .$$

But the first and third terms of this inequality are equal by Eqs. (12) and (13). Therefore the assumption that $y_1 > y_2$ has led to a contradiction. This proves Theorem 2.

Theorem 3: If $k_1 = k_2 = k$ and if $\Pi_1(\tau) \geqq \Pi(\tau) \geqq \Pi_2(\tau)$, then if we consider the graph of $\underline{y}$ against $\underline{x}$ for $\Pi(\tau)$ this graph will be between the corresponding graphs for $\Pi_1(\tau)$ and $\Pi_2(\tau)$.

Proof: Theorem 2 proves a similar result for the graphs of $\underline{y}$ against $\underline{\omega}$. In changing from the $\underline{\omega},\underline{y}$-graphs to the $\underline{x},\underline{y}$-graphs we map the positive quadrant of the $\underline{\omega},\underline{y}$-plane onto the positive quadrant of the $\underline{x},\underline{y}$-plane by the equations

$$\omega = \frac{2y}{kx} ,$$

$$x = x .$$

This is a homeomorphism of the one quadrant on the other, and hence if a

curve is between two others it will continue to be so after the transformation.

Theorem 4: If $\int_0^\tau P(\tau)d\tau$ is bounded, then in the relation between $\underline{y}$ and $\underline{x}$ which makes $\xi_{max} = 1$ we may conclude that $\underline{y}$ is unbounded when $\underline{x}$ becomes infinite.

Proof: We see from Eq. (7) that for $\xi_{max} = 1$ when $\tau = \tau_m$ we have

$$y = \frac{k}{\omega \int_0^{\tau_m} P(\tau') \cos \omega(\tau_m - \tau')\, d\tau'} . \qquad (14)$$

We know that

$$\omega = \frac{2y}{kx} .$$

when

$$k = \int_0^1 \pi(\tau)\, d\tau$$

is a fixed constant once $\pi(\tau)$ is known in $0<\tau<1$. Assume now that $\underline{y}$ is bounded when $\underline{x}$ is large. Then $\underline{\omega}$ approaches zero as $\underline{x}$ tends toward infinity. But

$$\left| \int_0^{\tau_m} P(\tau') \cos \omega(\tau_m - \tau')\, d\tau' \right| \leq \int_0^{\tau_m} |P(\tau')|\, d\tau' = \int_0^{\tau_m} P(\tau')\, d\tau' .$$

The last integral on the right-hand side is bounded by hypothesis. Hence the assumption that $\underline{y}$ is bounded leads to a contradiction in view of Eq. (14).

4. Special cases

We consider now two special cases of the linear case which can be solved completely.

Case (a) $\pi(\tau) = 1 - \tau$ for all τ.

In this case the solution is

$$\xi = \frac{2y}{\omega}\left[1 - \tau + \frac{\sqrt{\omega^2 + 1}}{\omega} \sin(\omega\tau - \varepsilon)\right],$$

when $\varepsilon = \arctan \omega$.

We find that

$$\xi_{max} = \frac{4y}{\omega}\left(1 - \frac{\arctan \omega}{\omega}\right)$$

so that for $\xi_{max} = 1$ we have

$$y = \frac{\omega^2}{4(\omega - \arctan \omega)} \cdot \tag{15}$$

Case (b) $\begin{cases} \pi(\tau) = 1 - \tau , & 0 \leqq \tau \leqq 1; \\ \pi(\tau) = 0 , & 1 \leqq \tau \leqq \infty . \end{cases}$

For $\tau_m < 1$ the solution is as before. This corresponds to a value of $\omega \geqq 2.3$, approximately. For smaller values of ω we find

$$\xi_{max} = \frac{2y}{\omega^2}\sqrt{\omega^2 + 2 - 2\sqrt{\omega^2 + 1}\cos(\omega - \varepsilon)} .$$

Hence for $\xi_{max} = 1$ we have

$$y = \frac{\omega^2}{2\sqrt{\omega^2 + 2 - 2\sqrt{\omega^2 + 1}\cos(\omega - \varepsilon)}} . \tag{16}$$

Equations (15) and (16) determine graphs of y against ω and hence of y against x. The latter two graphs are plotted in Fig. 1. If we assume that $\pi(\tau) = 1 - \tau$ between 0 and 1 and that elsewhere it is between case (a) and case (b), then the associated graph for y against x would be between those given here. If we draw a curve about half way between these two we obtain a graph which must fit any such case to within a fairly reasonable degree of error. If we took considerably larger values of x this would not remain true, but for the range considered the conclusion may be drawn that the negative phase of the blast is not of major importance.

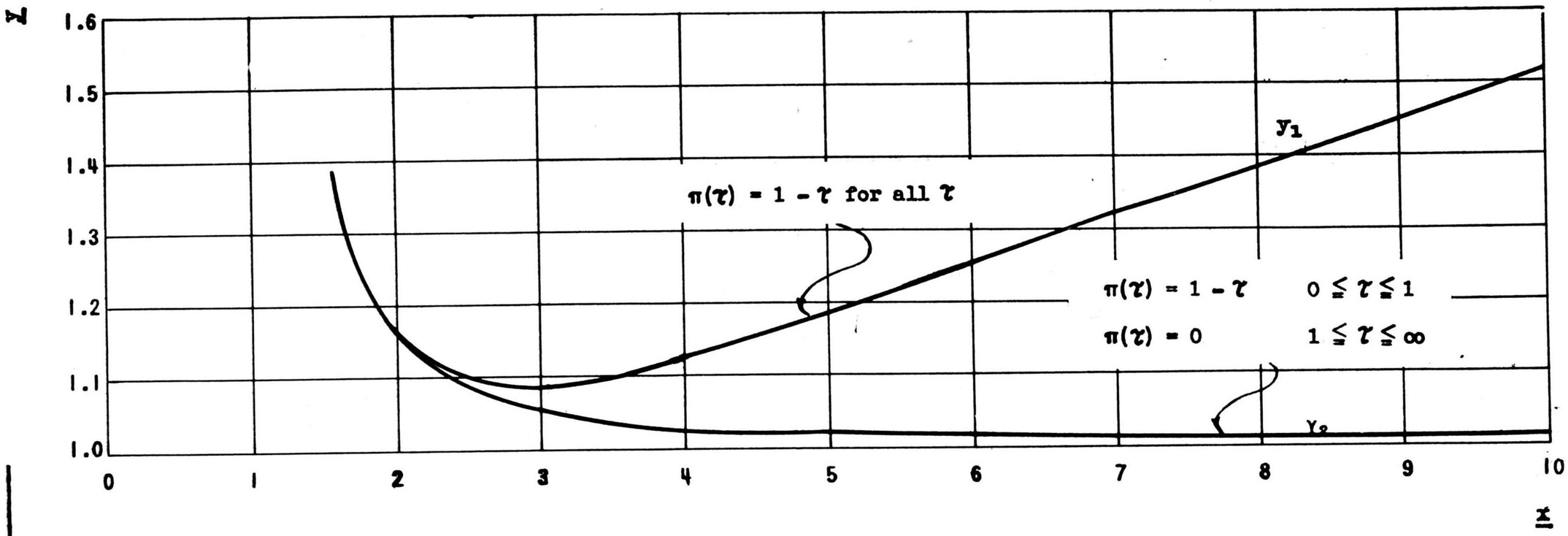

Fig. 1. Relation between $\underline{x}$ and $\underline{y}$ to make $\xi_{max} = 1$.

Princeton University Station

Division 2, NDRC

C. DAMAGE TO REINFORCED-CONCRETE WALL PANELS BY DETONATION OF CONTACT AND REMOTE CHARGES*

by Ira M. Freeman

Abstract

This paper sketches a calculation of the general damage to be expected due to blast from a bomb detonating in contact with or some distance from a reinforced concrete wall. The mechanism of failure is assumed to be communication of impulse to the material of the wall, followed by dissipation of the resulting energy either in plastic stretching of the reinforcing bars or in disruption of the concrete or both. The form of the existing empirical equation for damage to wall panels is confirmed, and the resulting values of the constants give good agreement with test data. The theory also provides a correlation of data taken under various conditions. A Weapon Data Sheet (6A6) based on the available data as reduced by the above method has been prepared.

1. Introduction

Reinforced-concrete panels of moderate thickness constitute component parts of a number of different structures, both of strategic and of tactical importance. It is therefore of some interest to know the type and extent of damage to be expected when a bomb or charge detonates in contact with or near a wall having air on both sides. A moderate amount of experimental information, based on some fifty incidents, is available for studying the question. Most of these data are from British model tests and a few derive from American full-scale experiments. The walls tested were in nearly all cases rectangular panels with face dimensions between three and twenty-five times the thickness. They were supported for the most part along all four edges, and results showed no appreciable difference between freely supported and clamped edges. Charge weights in these experiments ranged from less than 2 oz to nearly 1700 lb. The explosives used were P.A.G., TNT, Pentolite, Composition C-2, and P.E. Concrete compressive strengths varied from 2200 to 4000 lb/in^2 (cylinder test).

*First published as EWT-3h (OSRD-5176h).

On the basis of an examination of descriptions, photographs, and sketches, it was found possible to assign to each incident a characterization of degree of damage such as "slight," "moderate," "heavy," or "breaching." The way in which a wall shows damage in the "air-air" case under consideration here differs from that for underground walls ("earth-air"). For the former, the first three damage categories invariably involve cracking of the panel, with some rear-face scabbing for the more severe classes. On the other hand, contact charges of sufficient size usually produce a more local effect in which the wall is perforated by removal of concrete over a roughly circular region, with or without accompanying bending, removal, or rupture of all or part of the reinforcing bars in this region. For all but this last damage class, the ratio of permanent central deflection to span correlates roughly with the degree of damage, as was previously found to be true of the "earth-air" case.[1/]

In addition to the kinds of damage described in the foregoing, an actual bomb produces fragment scars on the front face and may cause a few fragment perforations of the wall. This type of damage is not under consideration here.

2. Notation

The English gravitational system of units will be used. Let the following notation be adopted:

Symbol	Definition
t	Thickness of wall
w	Weight of charge
r	Distance of charge from wall
$H[=ht]$	Breadth of wall, that is, the smaller face dimension
$L[=\ell t]$	Span of wall, that is, the larger face dimension
Q	Final central deflection of wall
ρ	Radius of bending of panel
W	Total weight of wall panel
D	Density of wall material
$s[=nt]$	Center-to-center spacing of reinforcing bars in each mat

1/ Weapon Data Sheet 6A5, OSRD Report 6053.

Symbol	Definition
$a[=ct^2]$	Cross-sectional area of one bar
bt	Distance between front and rear mats
F	Fraction of volume occupied by reinforcing
E	Strain energy per unit volume in steel bars
e	Final elongation of each bar
q	Effective length of each bar subject to strain
R	Mean radius of annulus of rupture of concrete
$S[=ut]$	Semi-width of annulus
z	Ratio of radius of annulus to radius of charge
α	Shear angle
K	Maximum tangential force on lateral face of annulus
τ	Maximum shearing stress in concrete
G	Shear modulus of elasticity for concrete
I	Air-blast impulse per unit area, side on
J	Total impulse delivered to impulse pendulum by contact charge
σ	Charge shape factor in impulse pendulum formula
$\varkappa$	Density of explosive

3. Analysis for remote shots

When the damage is in the form of a single central crack, the elongation e of each longitudinal bar is given by [Fig. 1(a)]:

$$\frac{\frac{1}{2}e}{bt} = \frac{Q}{\frac{1}{2}L},$$

or

$$e = 4\frac{Q}{L}bt. \qquad (1)$$

If, representing the other extreme, failure is assumed to be by bending along, say, a circular arc, with many finer cracks in place of a single larger one [Fig. 1(b)], the elongation is found from $(L+e)/(\rho+bt) = L/\rho$. Using the sagitta formula $\rho \approx L^2/8Q$ gives $e = 8b(Q/L)t$, or twice the value given by Eq. (1). The calculation will be continued using the value given by Eq. (1), remembering that the actual one may be somewhat greater, particularly if there are several cracks in place of only one.

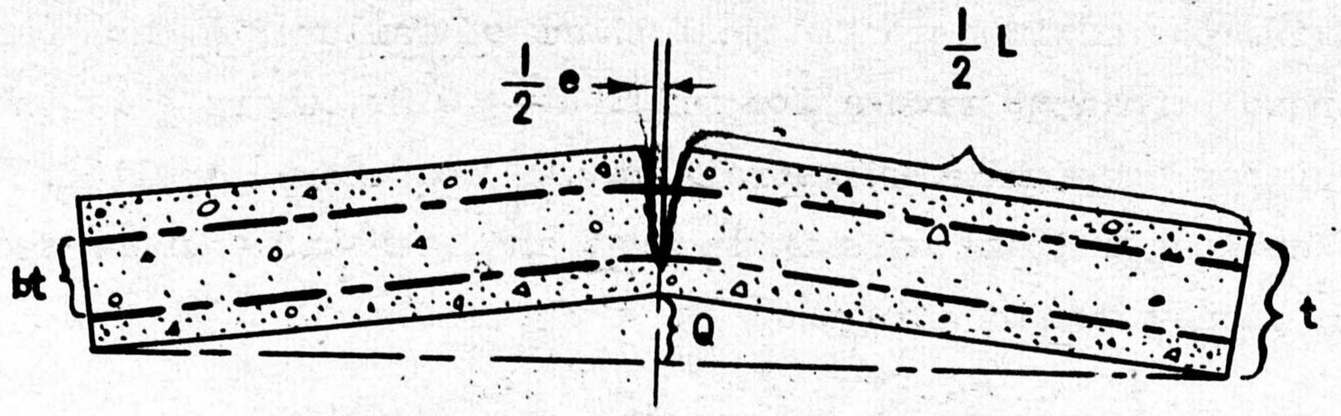

Fig. 1(a).

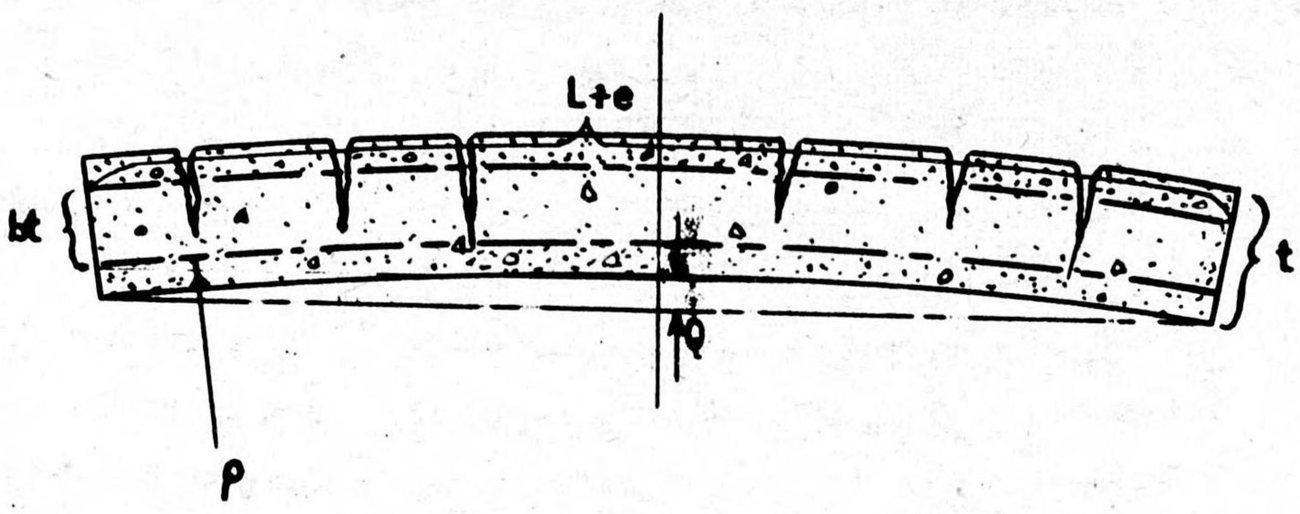

Fig. 1(b).

Fig. 1. Elongation of longitudinal bar when damage is (a) in the form of a single central crack, (b) by bending along a circular arc with many finer cracks in place of a single larger one.

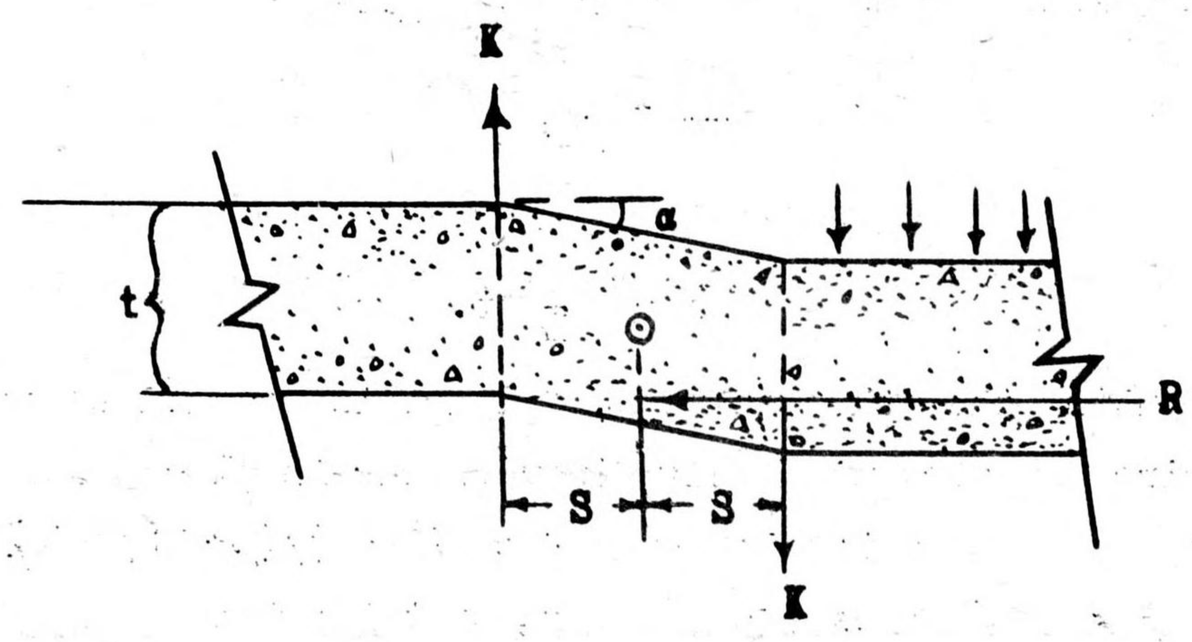

Fig. 2. Representation of damage by a contact charge.

Taking the maximum strain just short of failure in each bar to be 0.2, the extreme permanent elongation will be $e = 0.2q$, where q is the effective length of bar over which the strain may be considered applied. There are $H/s = ht/nt$ longitudinal bars in the mat and each has a cross-sectional area ct^2. The energy expended is then

$$Eq\,\frac{h}{n}\,ct^2 = E\,\frac{e}{0.2}\,\frac{h}{n}\,ct^2 = \frac{20Ebhc}{n}\cdot\frac{Q}{L}\,t^3. \qquad (2)$$

The impulse imparted to the wall by a noncontact shot is taken to be simply ILH; the equivalent kinetic energy is then

$$\frac{(ILH)^2 g}{2W} = \frac{k^2 gh\ell w^{4/3} t}{2Dr^2}, \qquad (3)$$

since $I = kw^{2/3}/r$ for air blast and $W = DHLt$.

Actually, the total impulse given to the wall may differ from that specified by the above formula, particularly for very near shots. Reflection of the wave will increase the delivered impulse by a factor of at least two for weak blast and considerably more for strong blast. Recoil of the member during application of the pressure, as well as possible diffraction around the edges, would operate toward decreasing the amount of impulse actually delivered. In the absence of quantitative information on these questions, the simple assumption mentioned was adopted.

Equating the expressions in Eqs. (2) and (3) we get

$$\frac{r}{w^{1/3}} = \frac{k}{2}\sqrt{\frac{gn\ell}{10DEbc(Q/L)}}\cdot\frac{w^{1/3}}{t}. \qquad (4)$$

It is convenient to introduce the fractional volume of the reinforcing, F.[2/] If there are two mats, $F = (4/nt)\cdot(ct^2)/t = 4c/n$. Equation (4) may then be written

$$\frac{r}{w^{1/3}} = k\sqrt{\frac{g\ell}{10DEFb(Q/L)}}\cdot\frac{w^{1/3}}{t} = A\,\frac{w^{1/3}}{t}. \qquad (5)$$

2/ In using F as the measure of the effect of reinforcing, it is of course assumed that the size and arrangement of the bars is in accordance with reasonable design practice.

4. Analysis for contact shots

As a simple representation of damage by a contact charge, assume first that the detonation impulse is imparted to a circular portion of the slab, treated as being initially rigid, and that this portion communicates shearing stresses to a surrounding annulus up to the point of failure of the concrete in shear (Fig. 2).

The average maximum shearing force, K, on each lateral face of the annulus will be approximately equal to $2\pi Rt\alpha G$ (see Sec. 2 for notation). The total work done in the shearing process will then amount to $\frac{1}{2}K \cdot 2S\alpha = 2\pi\alpha^2 GRSt$, or since $\gamma = \alpha G$, this energy will be

$$\text{Total work} = \frac{2\pi\gamma^2 RSt}{G}. \qquad (6)$$

Experiments with the impulse pendulum[3/] have yielded the empirical relation $J = jw(\ell_1\ell_2/\ell_3^2)^{1/6} = jw\sigma$ for the impulse delivered by contact explosion. Here ℓ_1 and ℓ_2 are the dimensions of the face of a rectangular charge in contact with the slab and ℓ_3 is the third dimension. The kinetic energy imparted to the circular piece of the panel punched out is then

$$J^2 g/2W = j^2\sigma^2 w^2 g/2D\pi R^2 t. \qquad (7)$$

The size of the breach produced in a panel must depend in some way on both the size of the charge and on the thickness of the wall, other factors being held constant. The greater part of the test results is for bomb-like charges (cylinders) in the "side-on" position, that is, with the axis parallel to the slab. The length-to-diameter ratio of a cylinder representing the charge in an average GP bomb is about 5:2. Inspection of the data suggests that the mean radius of the annulus of rupture is simply a multiple z of the cylinder radius, while the semi-width of the annulus may be taken to be a certain fraction u of the slab thickness. Values adopted for these constants were estimated from sketches and photographs accompanying the test reports and are given in the following.

3/ Tests thus far reported are described in Ref. 6 (see List of References at end of paper).

Equating Eqs. (6) and (7) and introducing z, u, and $\mathscr{l}$, we obtain finally for a cylindrical charge of length-diameter ratio 5:2

$$\frac{W^{1/3}}{t} = z\left(\frac{4\pi r^2 Du}{5j^2\sigma^2 gG\mathscr{l}}\right)^{1/3} = B'. \qquad (8)$$

The result just obtained probably marks a lower bound for the critical $W^{1/3}/t$ for breaching by a contact shot, since some energy must in reality go toward breaking up the circular plug and its surrounding annulus, toward imparting kinetic energy to the fragments, and toward disrupting the bond of or severing some of the reinforcing bars.

An estimate of an upper bound for B might be gotten, on the other hand, by supposing that all of the work is done in producing plastic strain in the bars crossing an area of the panel comparable in size with the circular plug considered in the foregoing. The volume of steel subject to strain will then be $\pi R^2 Ft$ and the strain energy absorbed will be $\pi ER^2 Ft$. Equating, as before, to the available energy given by Eq. (7) we now get for the cylinder

$$\frac{W^{1/3}}{t} = \frac{\pi z^2}{j\sigma(5\pi\mathscr{l})^{2/3}}\sqrt{\frac{2DEF}{g}} = B''. \qquad (9)$$

5. Numerical values: Comparison with experimental data

Let the following numerical values be adopted:

$h = 7.5$; $\mathscr{l} = 12$; $n = 5/4$; $b = 0.8$;

$D = 150$ lb/ft^3; $\mathscr{x} = 100$ lb/ft^3;

$c = 7.5 \times 10^{-4}$, that is, 3/8-in. bars in a 1-ft wall;

$k = 7.8$ lb$^{1/3}$-sec/ft (0.054 lb$^{1/3}$-sec-ft/in^2) for TNT;

$Q/L = 0.05$; $j = 92$ sec; $\tau = 350$ lb/in^2; $G = 700\,000$ lb/in^2;

$E = 1.2 \times 10^6$ ft-lb/ft^3 (8300 lb/in^3); $F = \frac{1}{2}$ percent;

$u = \frac{1}{4}$; $z = (500\pi)^{1/3} R/W^{1/3}$ for 5:2 cylinder.

Substitution in Eq. (5) gives $A = 0.26$; hence we may write

$$\frac{r}{W^{1/3}} = 0.26\,\frac{W^{1/3}}{t}. \qquad (5a)$$

Further, Eq. (8) yields

$$\frac{W^{1/3}}{t} = B' = 0.28 \qquad (8a)$$

and, by Eq. (9),

$$\frac{W^{1/3}}{t} = B'' = 2.1. \qquad (9a)$$

It should be noted that B' turns out numerically smaller than B'', in agreement with the discussion following Eq. (8).

Equation (5a) gives the result for remote shots; either Eq. (8a) or Eq. (9a) describes the case of contact shots. If a single relation can be written to embrace both cases, it will, on dimensional grounds, have the form $r/W^{1/3} = f(t/W^{1/3})$. Further, for remote shots we must have $r \propto W^{2/3}$ since an impulse criterion was assumed and $I = kW^{2/3}/r$. For contact shots ($r = 0$) the equation must yield a critical value of $t/W^{1/3}$ corresponding to each given degree of damage. This circumstance requires $t/W^{1/3} = \text{const.}$ when $r = 0$. Fulfillment of these conditions then requires the equation to be of the form

$$\frac{r}{W^{1/3}} = A\,\frac{W^{1/3}}{t} - AB. \qquad (10)$$

This relation has the same form as the empirical Ministry of Home Security formula used by British workers in correlating data on shelter-wall damage.4/

Equation (10) has the form

$$y = \frac{A}{x + AB}, \qquad (10a)$$

where $x = r/W^{1/3}$ and $y = t/W^{1/3}$. The curve is thus a rectangular hyperbola with displaced vertical axis. Using $A = 0.26$ with $B = 0.28$ and $B = 2.1$ in turn in Eq. (10a), two curves will be obtained, and it is logical to assume that these curves will mark extremes within which the true relation must lie. Accordingly, these curves are plotted in Fig. 3, together with the experimental points which were adjusted to care for differences in reinforcing, type of explosive, and so forth, as will be explained below. Considering the many factors involved, the agreement between the points and the position and trend of the curves is satisfactory and indicates that the large variations in some of the factors in the analysis must act to balance each other to a great extent.

4/ See, for example, Ref. 5 (List of References).

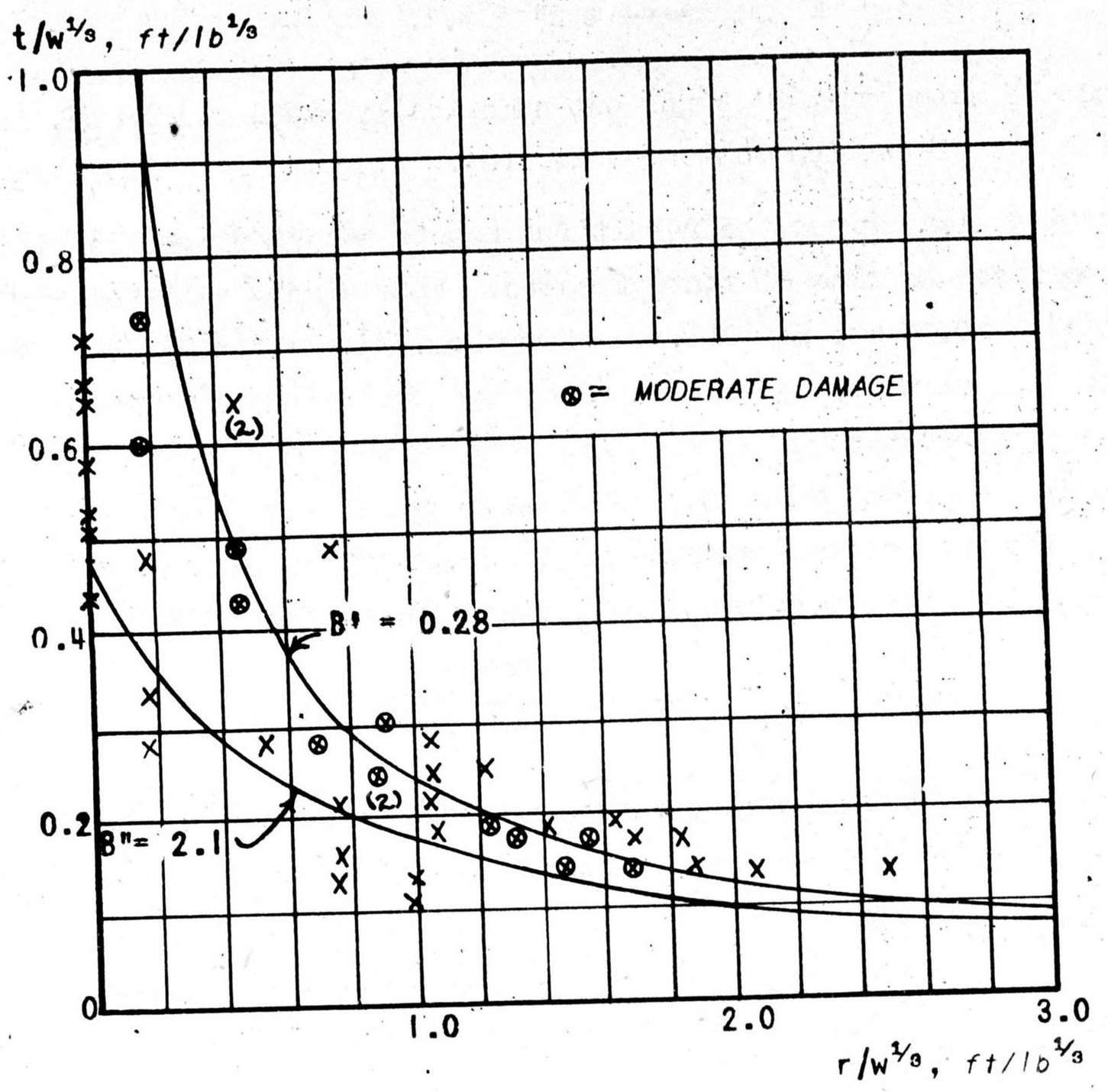

Fig. 3. Plot of $y = \frac{A}{x + AB}$ for A = 0.26 and for two indicated values of B. Experimental points were adjusted to allow for differences in reinforcing, type of explosive, and so forth.

6. Comparison of bombs end-on and side-on in contact

While the greater part of the data refer to bombs or cylindrical charges side-on, it is a matter of practical interest to inquire the relation of expected effects for bombs in this position and in the end-on position. Let us examine the way in which the charge shape and orientation enter into the analysis. Referring to Eqs. (8) and (9), it is seen that the critical wall thickness for a contact shot will be proportional to either $\underline{\sigma}$ or to $\sigma^{2/3}$, depending on which expression for $\underline{B}$ is used. For the 5:2 cylinder end-on, $c_{n,\sigma} = (\pi/25)^{1/6} = 0.71$ and $\sigma^{2/3} = 0.80$. For a cylinder side-on, there is some question as to what to take for the three applicable dimensions, since a flat surface is not in contact with the slab. However, assuming a roughly equivalent rectangular parallelepiped, the value of $\underline{\sigma}$ for the side-on case turns out to be about 1.1 and to two significant figures $\sigma^{2/3}$ is also 1.1. Hence the ratios of the critical thicknesses, end-on to side-on, are

$$\frac{T_{end}}{T_{side}} = \frac{0.71}{1.1}\ 0.65 \quad \text{or else} \quad \frac{0.80}{1.1} = 0.73. \tag{11}$$

No data directly applicable to testing this result could be found, but some results for scabbing of panels by $\frac{1}{2}$-lb Engineer blocks of TNT are available in Ref. 7. A study of the relevant incidents described there indicates that the thicknesses for roughly 50-percent chance of scabbing on the back surface with these blocks are, end-on to side-on, in the ratio 0.8 to 1. This is not far different from the ratios given in Eq. (11). It may be assumed, as a rough rule, that the breachable thickness end-on is about three-quarters of that side-on for bombs in contact. For remote positions, the ratio is probably close to unity.

7. Adjustment of data by use of the theory

As mentioned in Sec. 5, the course of the damage curves represented by Eq. (10) will depend on the values of the parameters $\underline{A}$ and $\underline{B}$. According to the analysis, these in turn depend on various physical factors -- geometrical and material constants of the slabs, degree of reinforcing, type of explosive as it affects impulse, and so forth.

It is evident from Eq. (10a) that for the damage categories other than breaching, the ordinates to the curve will be controlled largely by the

value of A, particularly for x not too small. The effect on the plot when x assumes small values may be computed as follows: If A is to be altered by a factor ϕ (temporarily assuming B constant), it is seen from Eq. (10a) that y will now have a new value $Y = \phi A/(x + \phi AB)$. If the new ordinate were to be computed simply by multiplying the original y by ϕ, the result would be $Y' = \phi y = \phi A/(x + AB)$. The fractional error thus introduced will then be $(Y' - Y)/Y$, which is seen to be equal simply to $B(\phi - 1)y$. If $B = 0.2$ -- the value finally determined by actually fitting the slight-damage curve -- and $\phi = 1.7$ as determined below, then the fractional error for even the item having the largest y on this curve, namely, 0.43, amounts to 0.06. Consequently, it appears that simple correction of the original ordinates by a factor ϕ will give a result whose accuracy is well within that of the raw data.

The method of correcting the data will now be outlined. For convenience, the expressions for the parameters, as given in Eqs. (5), (8), and (9), are repeated here:

$$A = k\sqrt{\frac{g\ell}{10DEFb(Q/L)}},$$

$$B' = z\left(\frac{4\pi\tau^2 Du}{5j^2\sigma^2 gG\mathscr{L}}\right)^{1/3},$$

$$B'' = \frac{\pi z^2}{j\sigma(5\pi\mathscr{L})^{2/3}}\sqrt{\frac{2DEF}{g}}.$$

Of the quantities involved in A, ℓ and b will assume various values (but over a limited range) from one test to another. The factors most likely to affect the value of A are k and F. The remaining factors will be sensibly constant for slabs experiencing a given degree of damage (given Q/L).

Considering only k and F, it was decided to reduce all data to the case of light reinforcing ($F = \frac{1}{4}$ percent by volume) and TNT as the explosive charge ($k = 7.8$ lb$^{1/3}$-sec/ft; see Sec. 5). The experimental walls had either about $\frac{1}{4}$ percent or 3/5 percent steel by volume. Since the expression above shows that A is proportional to $F^{-1/2}$, the points for the walls with medium reinforcing should be corrected by a factor $\sqrt{3/5 \div \frac{1}{4}} = 1.55$. Concerning the explosive effect, it is known from experiment that, referred to TNT, blast

impulse values from P.A.G. are about 0.9, while those from Pentolite, P.E., and Composition C-2 are about 1.2. This factor is to be applied directly, since A$\propto$ k. The points for the slight-damage curve involved various combinations of the two degrees of reinforcing mentioned, and the explosives TNT, Pentolite, P.E., Composition C-2, and P.A.G. Consequently, to correct the points to light reinforcing and TNT, the proper combination of the above factors had to be applied in each case. For example, to adjust a point where medium reinforcing and P.A.G. were used, its ordinate was multiplied by (1.55)/0.9 = 1.7; one with light reinforcing and P.E. was multiplied by 1/1.2 = 0.83, and so forth.

It is interesting to note that, in almost every case, application of the corrections required by the theory brought the points for a given damage class into better position for drawing a smooth curve of the proper kind through them.

Thus, for slight damage, Fig. 4 shows the original data points, the corrected points, and the curve drawn to fit the latter. It will be seen that the departures of the adjusted points from their curve is less than those of the raw data from the best curve that could be drawn to represent them.

Adjustment of the curves for moderate and for heavy damage also was accomplished as described above. Because of the different mechanism involved, the breaching curve required a slightly different procedure. Here the determining factor is the constant B, and since there are two possible analytical expressions (B' and B") to use, the corrections dictated by the adjustment using each in turn were averaged. Of the factors entering B' and B", the only ones that lend themselves to adjustment are j and F. No experimental information is available on the values of j for various explosives, but it is probably justifiable to apply correction factors of the same order as those applied to k in the foregoing. The variation of F is known. Both corrections were applied. The net correction was very small in any case.

Finally, the curve for each damage category was plotted, with some slight adjustments indicated by judgment. The final curves, together with the values of the parameters, are shown in Fig. 5.

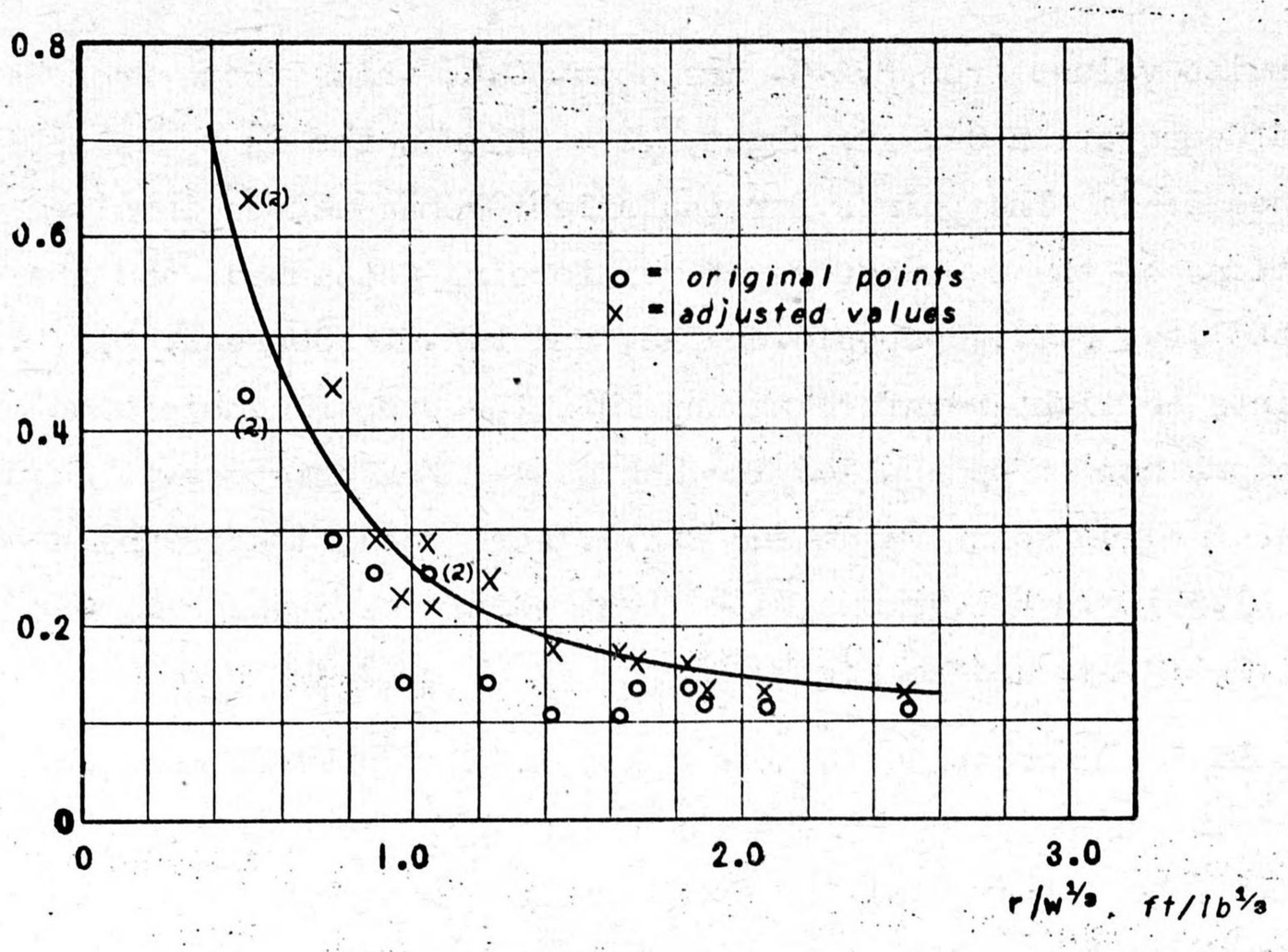

Fig. 4. Wall thickness for slight damage versus charge distance. Original data points, adjusted values, and a curve drawn to fit the latter.

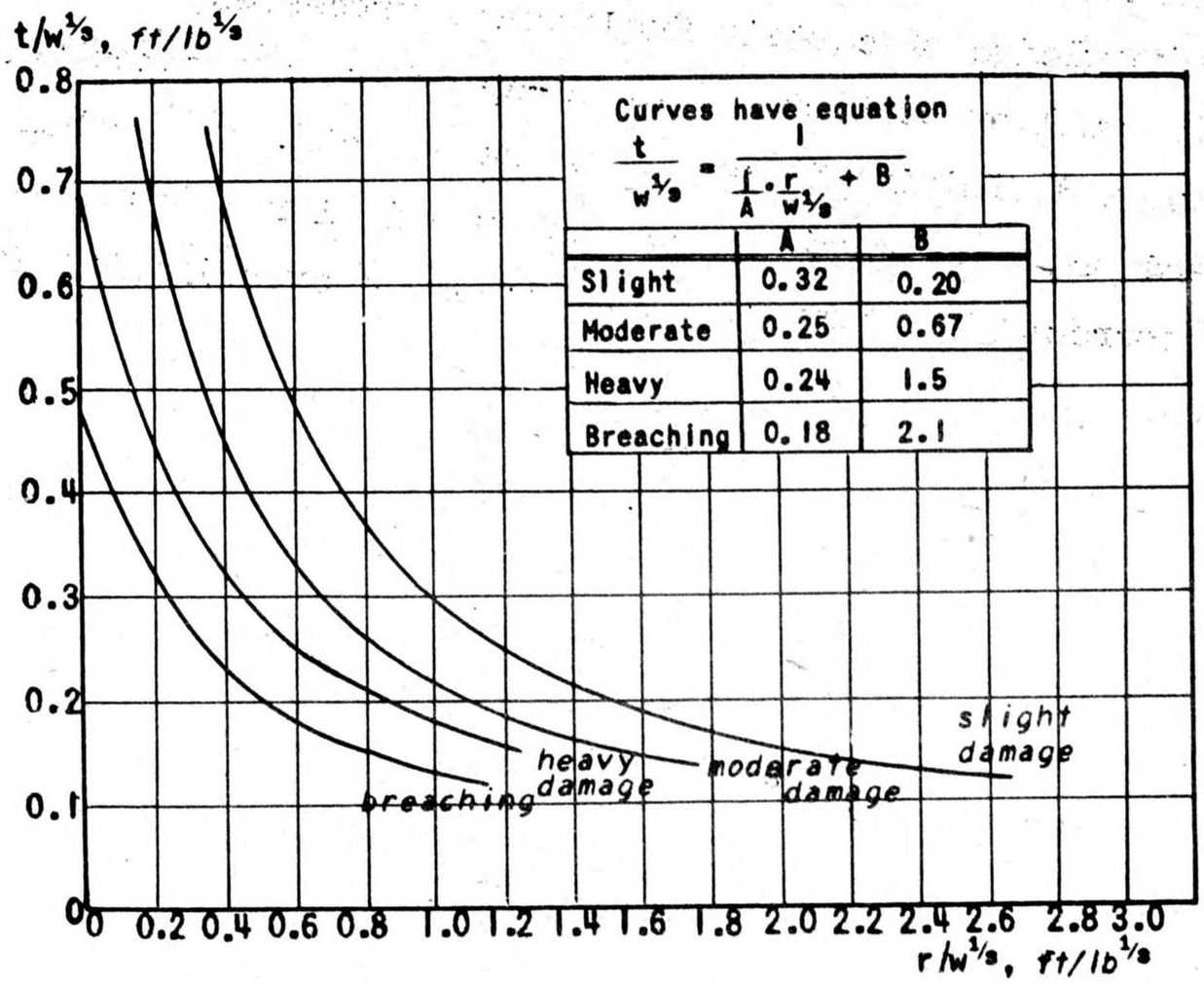

	A	B
Slight	0.32	0.20
Moderate	0.25	0.67
Heavy	0.24	1.5
Breaching	0.18	2.1

Fig. 5. Curves of wall thickness versus charge distance for four damage categories.

The dependence of the latter on the average value of Q/L is not precisely as indicated by the theoretical expression for A, but this is hardly to be expected in view of the wide range of Q/L in each category actually found experimentally.

The Weapon Data Sheet[5/] summarizing the results includes a table of wall thicknesses experiencing each given degree of damage due to the several American GP, SAP, and LC bombs detonating at various distances. These values, measured in feet and given to one decimal place, were taken from the final curves. It should be mentioned again that for bombs the results apply more nearly to the side-on position, particularly for contact shots.

8. Conclusion

The phenomenon of wall-panel damage by contact and noncontact explosions appears to find a semiquantitative explanation on the basis of impulse communicated to the wall by the detonation and subsequent dissipation of the corresponding energy by work done against the resistance of the wall materials. Because of the large number of variables which may be involved and our lack of quantitative knowledge of certain fundamental processes, such as impulse delivered to the wall by contact and close-up shots, the computation should not be regarded as a definitive theory of these effects. Nevertheless, the general trend and order of magnitude of the numerical results turn out to be essentially correct when compared with available experimental data.

5/ Weapon Data Sheet 6A6, OSRD Report 6053.

List of References

1. "Resistance of surface shelter walls to explosion," Road Research Lab., Ministry of Home Security, R.C. 222, May 1941.

2. "Resistance of reinforced concrete walls to severe blast," Road Research Lab., Ministry of Home Security, R.C. 304, Jan. 1942.

3. "Pillbox demolition by high explosive charges," Ballistic Research Laboratory Memorandum Report No. 299, Ordnance Dept., U.S.A., May 1944.

4. "Model and full-scale tests of resistance of reinforced concrete to attack by bombs nearby and in contact," Road Research Lab., Ministry of Home Security, R.C. 358, Sept. 1942.

5. "The design of bombproof structures," R. and E. Dept., Ministry of Home Security, R.E.N. 418, Oct. 1943.

6. "Impulse delivered to a plane slab by a contact explosion," Committee on Fortification Design, National Research Council, Memorandum Report M-11, June 1944.

7. "Contact explosions on concrete," Committee on Fortification Design, National Research Council, Interim Report No. 29, June 1944.

D. EFFECTS OF CONFINED BLAST ON BRICK CURTAIN WALLS*

by A. H. Taub and J. A. Wise

Abstract

Tests on explosions in a room 6 ft 5 in. square and 4 ft high with brick walls and concrete floor and roof indicate that the time of breaking of the walls is very long in comparison with the time necessary for multiple reflection of the pressure waves. A charge of 22 gm of Tetryl was sufficient to crack the walls in 17 msec after detonation. A charge of 44 gm of Tetryl completely disrupted the walls in about 35 msec after detonation. This implies that if comparisons of explosives in totally enclosed spaces are made in terms of impulse, this quantity should be measured at times long after the arrival of the initial pulse. Bare ½-lb and 1-lb charges of TNT detonated outside the room about 3 ft from the center of a wall previously damaged by 22 gm of Tetryl produced no further damage to the wall. When ½ lb of TNT was detonated inside and at the center of the structure, the walls were completely demolished and the frame was wrecked.

1. Introduction

It has been found in experiments conducted at Camp Gruber by the Underwater Explosives Research Laboratory on the relative effectiveness of explosives fired in nearly enclosed rooms[1/] that the ratio of the impulses from two different explosives is a function of the time at which the comparison is made; that is, for short times one explosive may be better than another, whereas if the time is long enough the situation may be reversed. The question of when a wall breaks then arises for a confined explosion, for obviously this time would determine the relative effectiveness of the explosive. To obtain data on this point, a model structure which was built for other purposes at Princeton University Station and which consisted of four columns, a roof slab, and a floor slab was completely enclosed with curtain walls consisting of one course of brick to form an enclosed room 6 ft 5 in. square by 4 ft high. Provision was made for detonating charges inside the structure and for measuring the displacement of a wall

---

*First published as AES-14d (OSRD-6007d).

1/ "Relative effectiveness of explosives fired in nearly enclosed rooms," by W. E. Gordon and H. M. Lang, AES-9d (OSRD-5011d), Apr. 25, 1945.

and the time of cracking of a wall. The program was interrupted before completion. It was originally proposed to determine the static resistance of the walls and to compare the behavior under both internal and external blast loading to that under static loading. It had also been proposed to examine the influence of venting by making walls with windows of various sizes. Only a comparison of internal and external blast loading was obtained.

2. Description of test

The test structure is illustrated in Fig. 1. It simulates a prototype to about 1/3 scale.

The walls were of single-thickness 4½-lb red face brick; individual bricks weighed between 4.1 and 4.35 lb. A Portland-cement mortar was used that had been set for about 10 days when the tests were made. The sides of the brick panels were attached with steel anchor strips, and the base of the brick wall rested on a roughened portion of the slab so that good bond was secured. The top mortar joint was formed with no special effort to secure good bond, and it was evident that there was less restraint there than on the sides or bottom.

The charges were suspended at the geometrical center of the room. In the first test, two pellets each of 22 gm of Tetryl were used; in the second test, only one such pellet was used. An Engineer special cap was used for the detonation.

High-speed motion pictures (approximately 6000 frames/sec) were taken so that one wall in each test was viewed in profile. At the center of the wall, a 3/4-in. steel prong about 6 in. long capped with a large ball bearing was used as a reference point for the pictures in the first test and was replaced by a 2-in. wide flat strip in the second test. Behind it, at the same level, a backboard was placed so as to form a background for making measurements of displacements on the film. A cap was placed in the field of view and exploded by the firing circuit. This gave the zero of time on the film. In the second test, aluminum-foil strips 0.00035 in. thick and about ½ in. wide were attached to the exterior face of the brick panel and connected to a single-sweep oscillograph so that a record of the time required for a crack to form in the brick wall could be obtained.

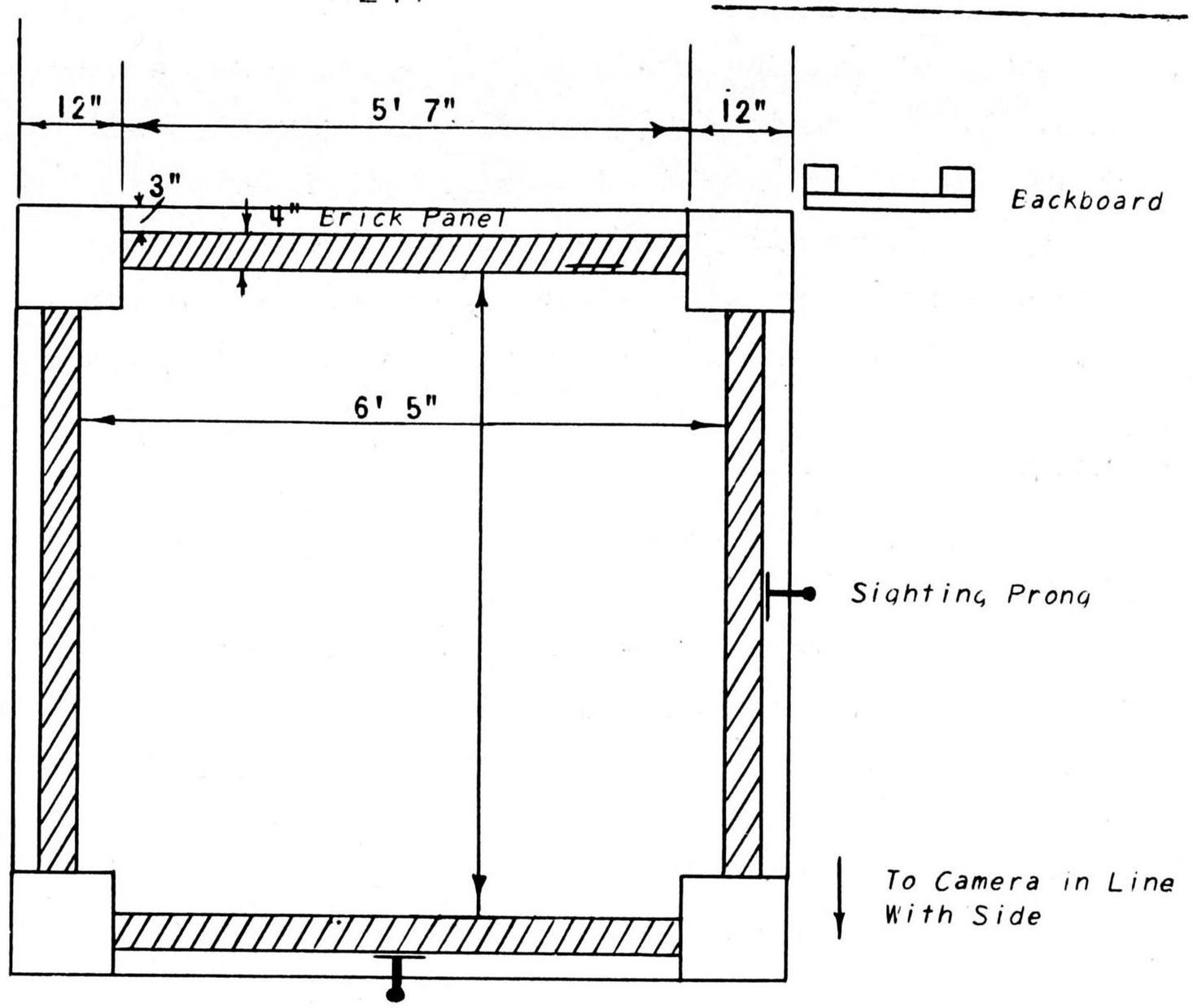

Plan (Section through second floor)

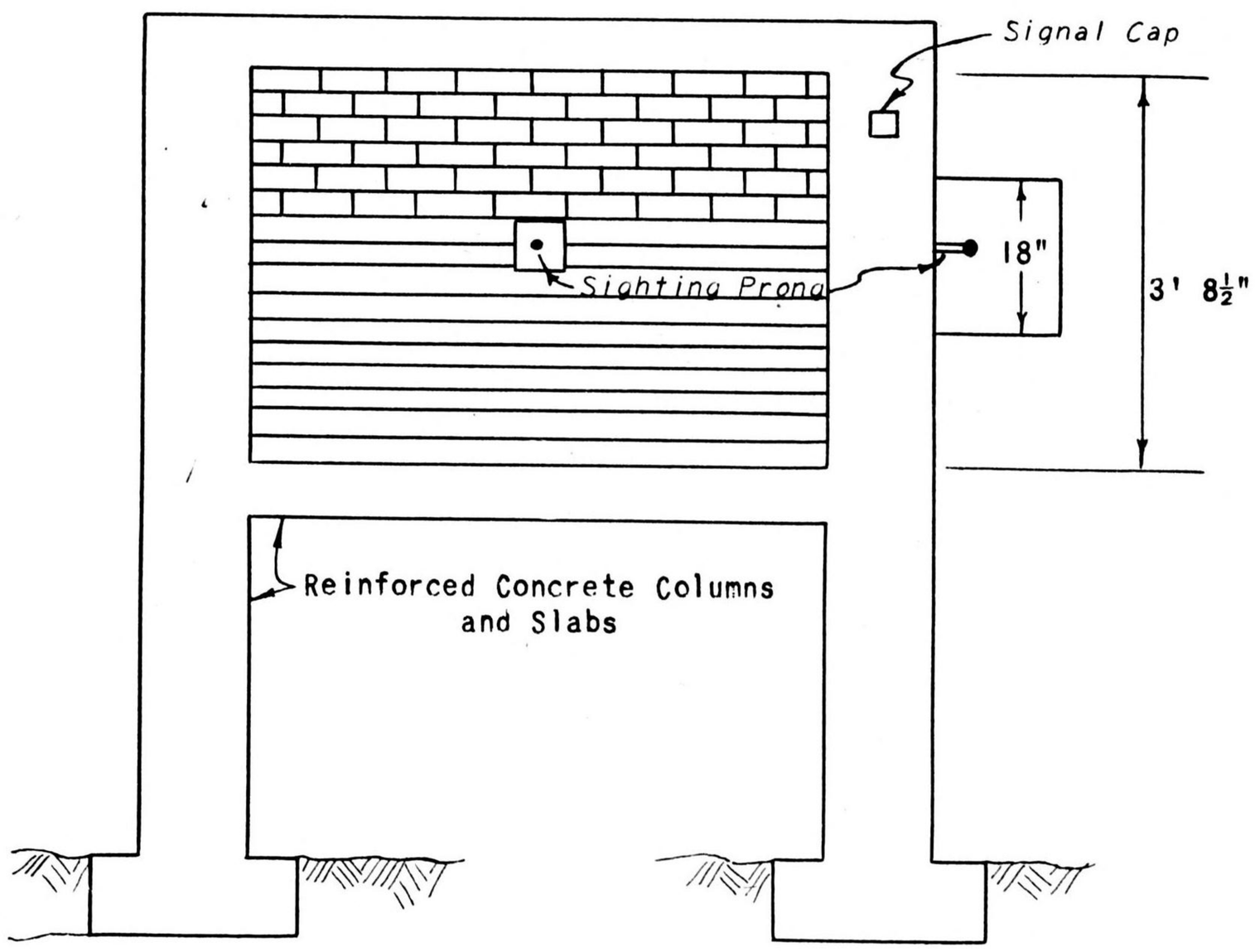

Elevation

Fig. 1. Test structure.

Princeton University Station
Division 2 NDRC

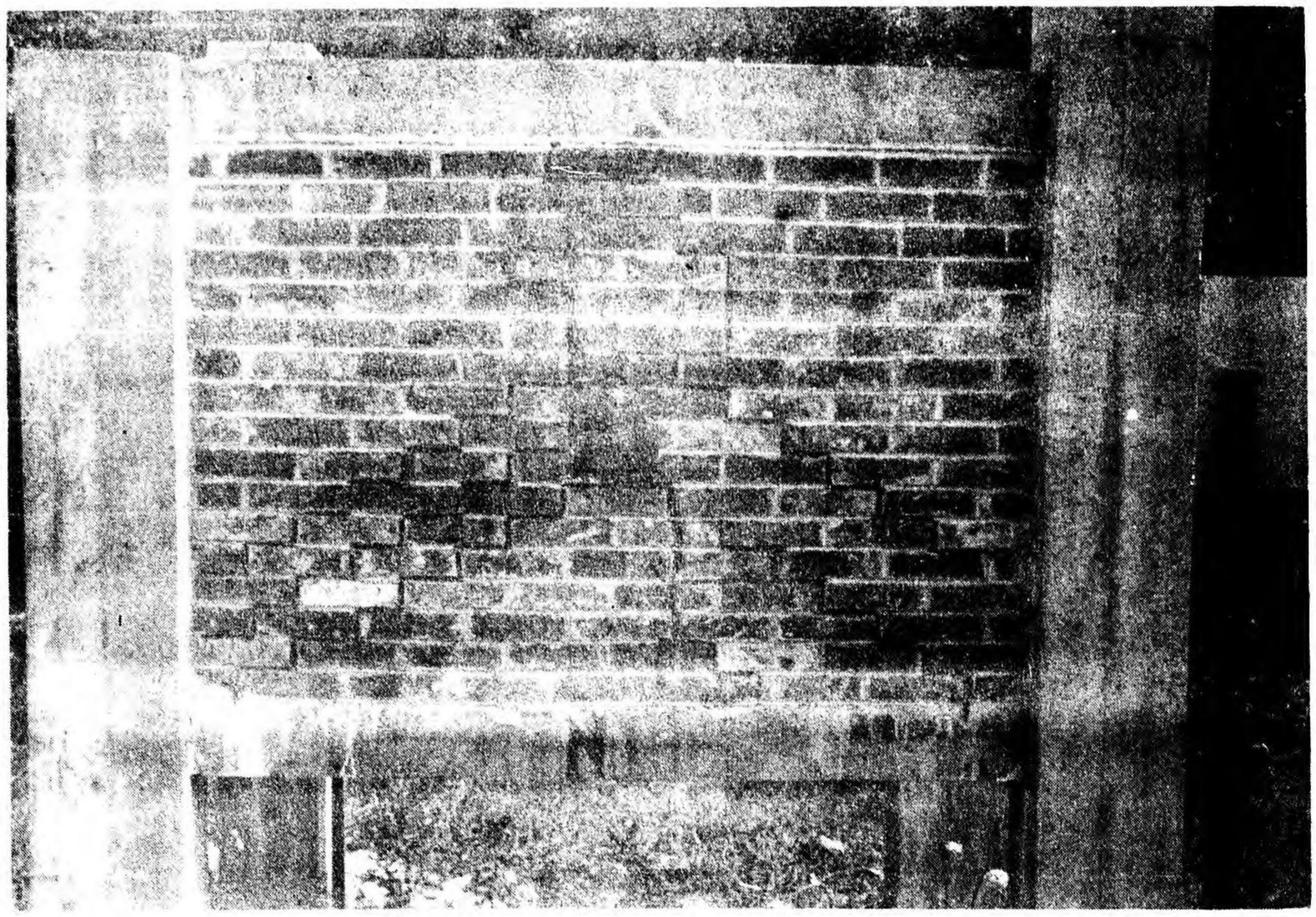

Fig. 2. North wall of test structure after detonation of one 22-gm pellet of Tetryl. Cracks have been indicated with crayon markings.

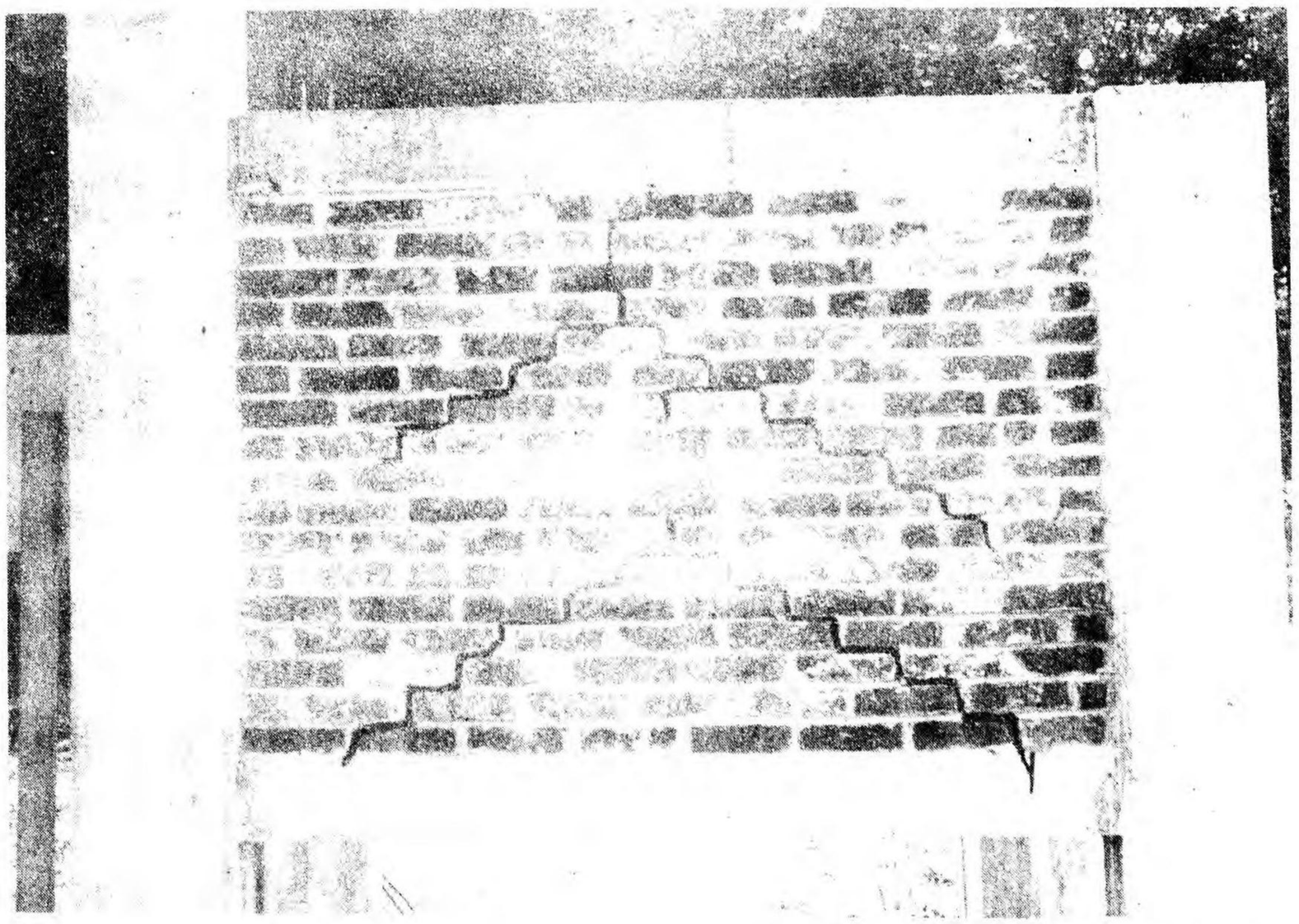

Fig. 3. East wall of test structure after detonation of one 22-gm pellet of Tetryl.

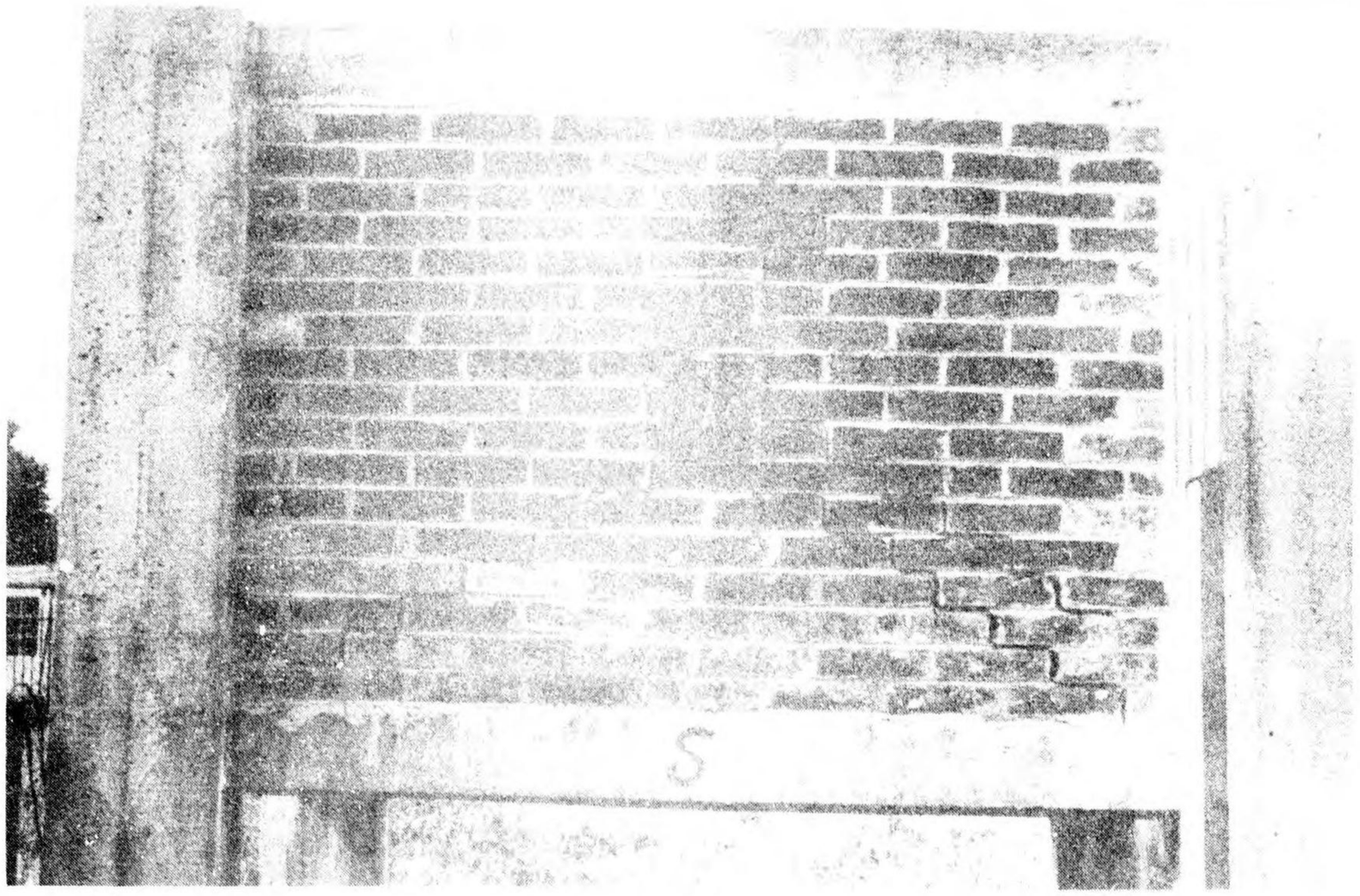

Fig. 4. South wall of test structure after detonation of one 22-gm pellet of Tetryl.

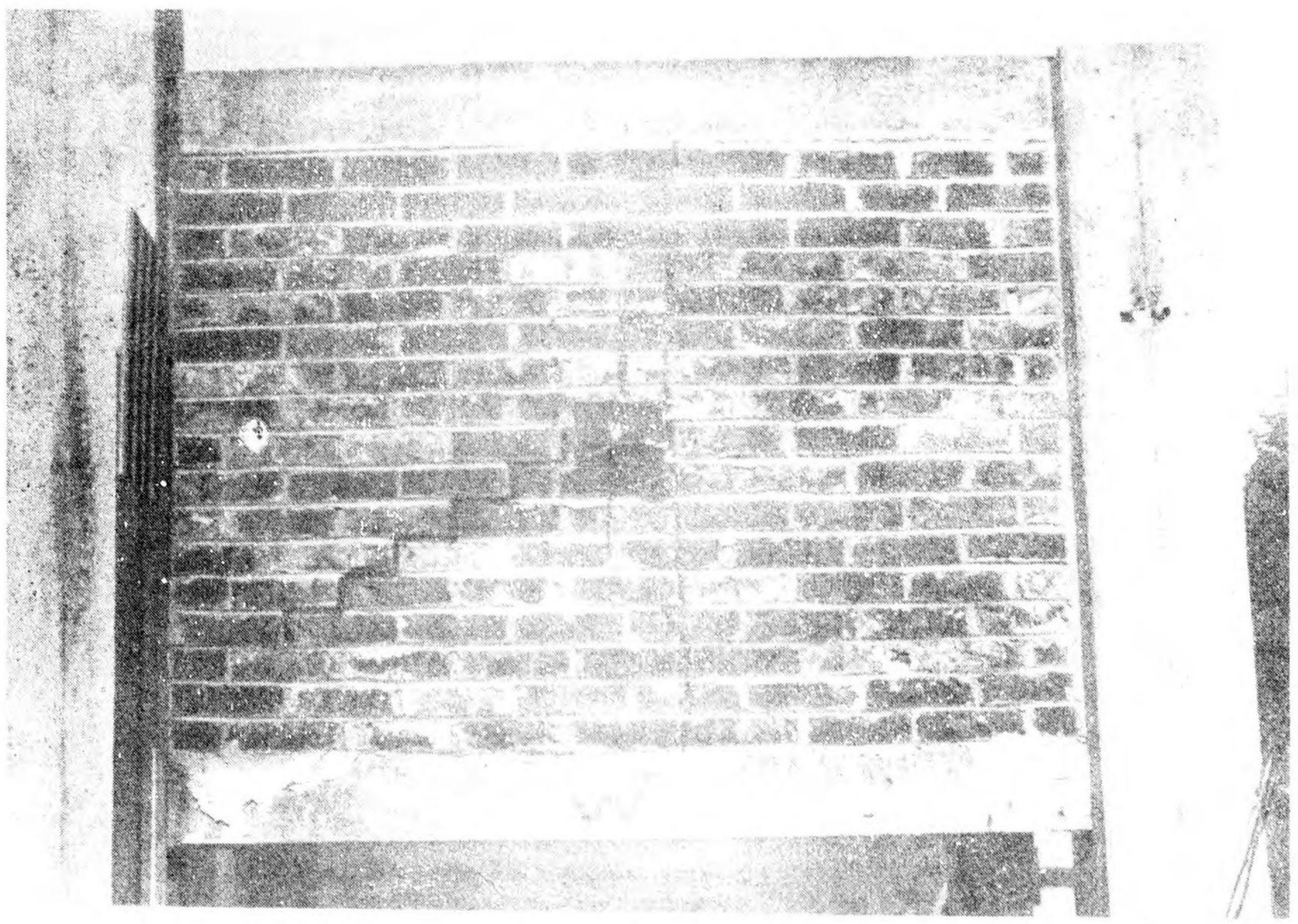

Fig. 5. West wall of test structure after detonation of one 22-gm pellet of Tetryl.

TABLE I
DATA

Time *msec*	Displacement *mm on film*	Time *msec*	Displacement *mm on film*
12	0.1	26	.4
13	.1	27	.8
14	.3	28	.7
15	.1	29	1.0
16	.1	30	1.1
17	.5	31	1.0
18	3	32	1.3
19	3	40	1.4
20	3	50	2.0
21	.3	60	2.6
22	.4	70	3.3
23	4	80	3.8
24	.7	90	4.3
25	.6	100	4.8

0.1mm. as measured on film equals 0.19 inches displacement of center of panel.

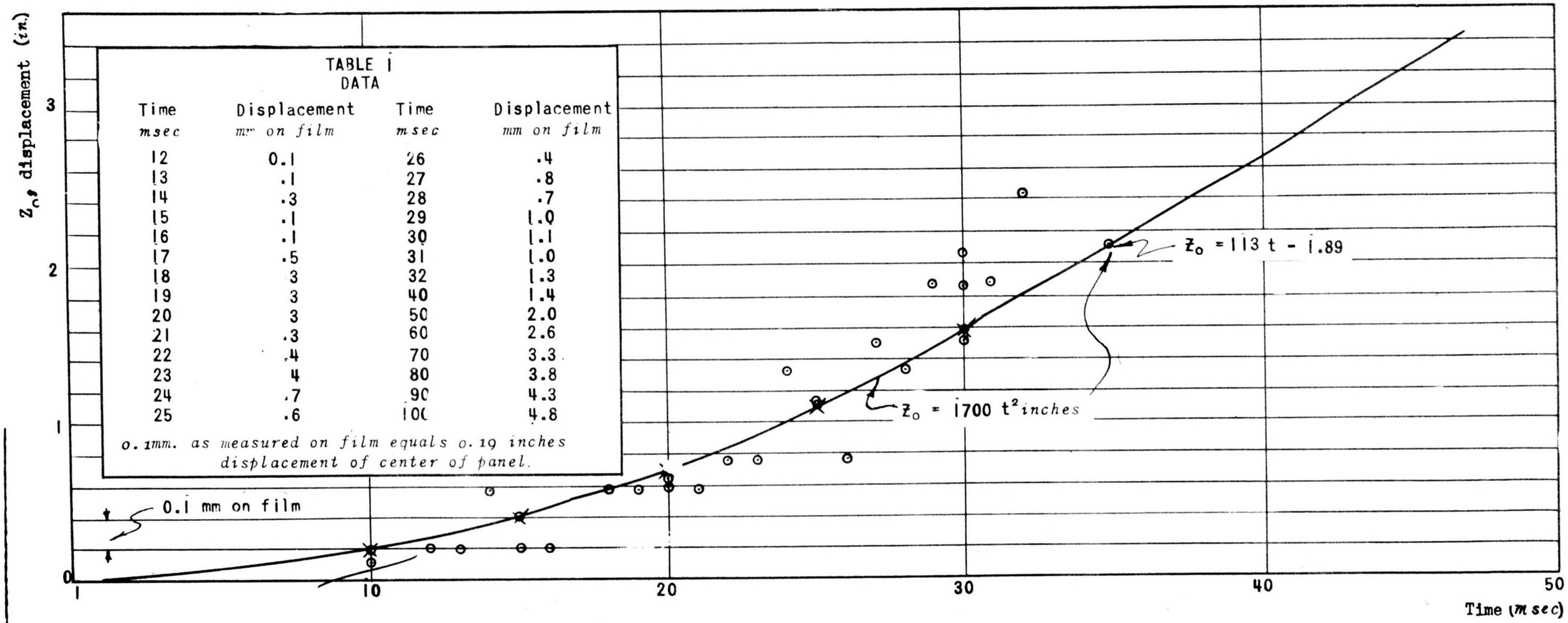

Fig. 6. Displacement versus time for center of wall subjected to interior explosion.

Princeton University Station
Division 2 NDRC

3. Results of tests

The explosion in the first test blew out the north wall completely and the major portion of each of the other walls as well. The bricks which remained indicated, from their position and the location of the cracks, that there had been some restraint against bending at the sides and bottom, but very little at the top. Most of the bricks were ejected without being cracked, but among both those ejected and those which remained some were cracked or split into pieces.

In the second test, cracks appeared in all four walls, but none of the walls were destroyed. Figures 2 to 5 are photographs showing the results of this test. An inspection of the results of the second test indicated that a smaller charge would have left the structure intact, whereas a larger one would have completely disrupted the walls. As the walls stood after the test they could support a small portion of the static load they were originally capable of withstanding.

The high-speed film record was examined under a comparameter and the scale of the pictures was obtained by measuring the width of column, height of panel, and height of backboard. The camera was at a considerable distance from the test frame so that the light rays forming the photographic image were practically parallel and no correction for depth or distance from camera was necessary. A synchronous timing circuit marked milliseconds on the film. The displacements of the reference prong were then read; they are listed and plotted in Fig. 6. The displacements were too small to be measured in the second test.

4. Interpretation of test data

The static behavior of the walls can be approximated by assuming that each panel does not deflect until its ultimate strength is reached and thereafter its deflection will be independent of the applied pressure.[2/] In reference 2 a square panel was assumed to crack along diagonals in such a manner that a constant bending moment along the cracks provided the internal resistance up to complete rupture. The difference between the applied pressure p and the static resisting pressure P will supply the force to accelerate the panel. The equivalent mass per unit area will be defined as that mass per unit area which would

---

2/ "A modification of the impulse criterion for blast damage," by D. G. Christopherson, R.C. 349.

respond with the observed motion of the center of the panel when subjected to an accelerating pressure p - P. In reference 2 it was shown that this equivalent mass per unit area, m', was m/2, where m is the actual mass per unit area. It can be shown that this is also valid for the rectangular panel. If we assume that the panel cracks along a vertical line at the center and swings like double doors opening, the equivalent mass per unit area, m', would be 2m/3. The photographs indicate that the actual behavior of the panel was intermediate between the two cases and hence the equivalent mass per unit area was between m/2 and 2m/3.

In the test panel m was 35 lb/ft^2 or 1.09 slug/ft^2 or 0.00755 slug/in.^{2} Therefore the equivalent mass per unit area was 0.00378 to 0.00503 slug/in.^{2} The time-displacement curves from the test, Fig. 6, show that the initial motion of the center of the panel was given by $Z_o = 1700\ t^2$, where Z_o (in.) is displacement and t (sec) is time. At about 35 msec the velocity became substantially uniform and the displacement could be represented by $Z_o = 113t - 1.89$. From this it was concluded that the cracks had opened sufficiently at that time to allow the gases to escape and thus to tend to relieve the internal pressure. The equation of motion in the initial stage would be

$$p - P = m'\ddot{Z}_o \ . \qquad (1)$$

Consequently p - P lies between

$$\left.\begin{aligned} p - P &= 0.00378 \times \frac{3400}{12} = 1.07 \text{ lb/in.}^2 \\ \text{and} \\ p - P &= 0.00503 \times \frac{3400}{12} = 1.42 \text{ lb/in.}^2 \end{aligned}\right\} \qquad (2)$$

The static resistance P of the panel is estimated to be about 1 lb/in.^{2}, based upon the data in reference 2 and also confirmed by an approximate analysis of the panel as an elastic plate. The peak pressure, of course, may be much greater, but its magnitude cannot be estimated from these data. The time of complete disruption is estimated to be about 35 msec and the corresponding central deflection, 2 in. From Eq. (2) then,

$$\begin{aligned} p - 1.0 &= 1.07 \text{ to } 1.42 \text{ lb/in.}^2 \ , \\ p &= 2.07 \text{ to } 2.42 \text{ lb/in.}^2 \end{aligned} \qquad (3)$$

This gives the estimated average or assumed uniform pressure within the panel.

In the second test, in which only one 22-gm pellet of Tetryl was used, the following calculation for pressure developed by the explosion was made. It is based on an analysis in PTM 19[3]. When a small amount of explosive is detonated in a closed room, the energy W_1 of the gas in the room before explosion is

$$W_1 = \frac{P_1 V}{\gamma - 1}, \tag{4}$$

where P_1 is the pressure, γ is the ratio of specific heats, and V is the volume of the room. The energy W_2 of the gas in the room after explosion is

$$W_2 = \frac{P_2 V}{\gamma - 1}. \tag{5}$$

The difference E of the energies must have come from the explosive and is equal to εw, where ε is energy per unit weight of charge and w is weight of charge. Therefore,

$$W_2 - W_1 = E = \varepsilon w = \frac{(P_2 - P_1)V}{\gamma - 1}. \tag{6}$$

Assuming γ equal to 1.4, we get

$$P_2 - P_1 = \frac{0.4\ \varepsilon w}{V}. \tag{7}$$

In the test, ε was taken as 988 cal/gm for Tetryl.[4] With w = 22 gm and $V = 165\ ft^3$,

$$P_2 - P_1 = 1.13\ lb/in^2.$$

This theoretical value agrees quite well with the estimated static strength of the wall. It is also about half the pressure obtained in Eq. (3) for the first test, in which exactly twice as much explosive was used.

3/ PTM 19, Princeton University Station, Division 2, NDRC, "Final pressure due to an explosion in a confined chamber."

4/ R. H. Kent, Jour. App. Physics 13, 348-354, June 1942.

A pressure-time record taken, say, at the center of the wall would probably consist of a zero pressure until the initial shock wave struck the wall; thereafter there would be an irregular rise due to successive reflections; this in turn would be followed by a fairly uniform pressure. The agreement between the various methods of estimating the uniform pressure acting on the walls suggests that the time necessary for the wall to move appreciably is very large compared to the time required for the uniform pressure to develop.

This means that for totally enclosed rooms the order of effectiveness of explosives in terms of impulse should be determined by measuring impulses over long intervals of time. This conclusion may not hold for such rooms where walls have an appreciable area of windows.

5. Effect of exterior explosion

At the conclusion of the tests with interior explosion, first a $\frac{1}{2}$-lb charge of TNT and then a 1-lb charge of TNT were detonated outside the test structure about 3 ft away from the center of one wall. The walls had been cracked by the 22-gm charge detonated within the structure; nevertheless they showed no appreciable effects as a result of the detonation of the exterior charges. The effect of confinement in enhancing the effect of the blast is clearly illustrated by this experiment.

When these results are compared with the Richmond Park experiments described in R.C. 425[5/] where 8 lb of RDX/TNT detonated on the ground 10 ft from a similar brick wall damaged it very heavily, one obtains a verification of the impulse criteria. For, in the Princeton tests the peak pressure was greater in the 1-lb shot, but the impulse was smaller than in the Richmond Park tests.

6. Damage to frame

At the conclusion of the second test, $\frac{1}{2}$ lb of TNT was detonated within the structure at the center and completely wrecked it. The four walls were completely blown out, some bricks being thrown about 80 ft. Figures 7 to 13 show the structure after this final test. It will be noticed that the junctions of columns and beams were particularly affected, because the anchorage of steel at those points was not adequate. The SE and NW columns cracked at points where vertical reinforcing bars were discontinued.

5/ "Blast tests on model houses," Civil Defense Research Committee, Ministry of Home Security, July 1944.

Fig. 7. Test structure viewed from the SE after detonation of ½ lb of bare TNT within structure at center.

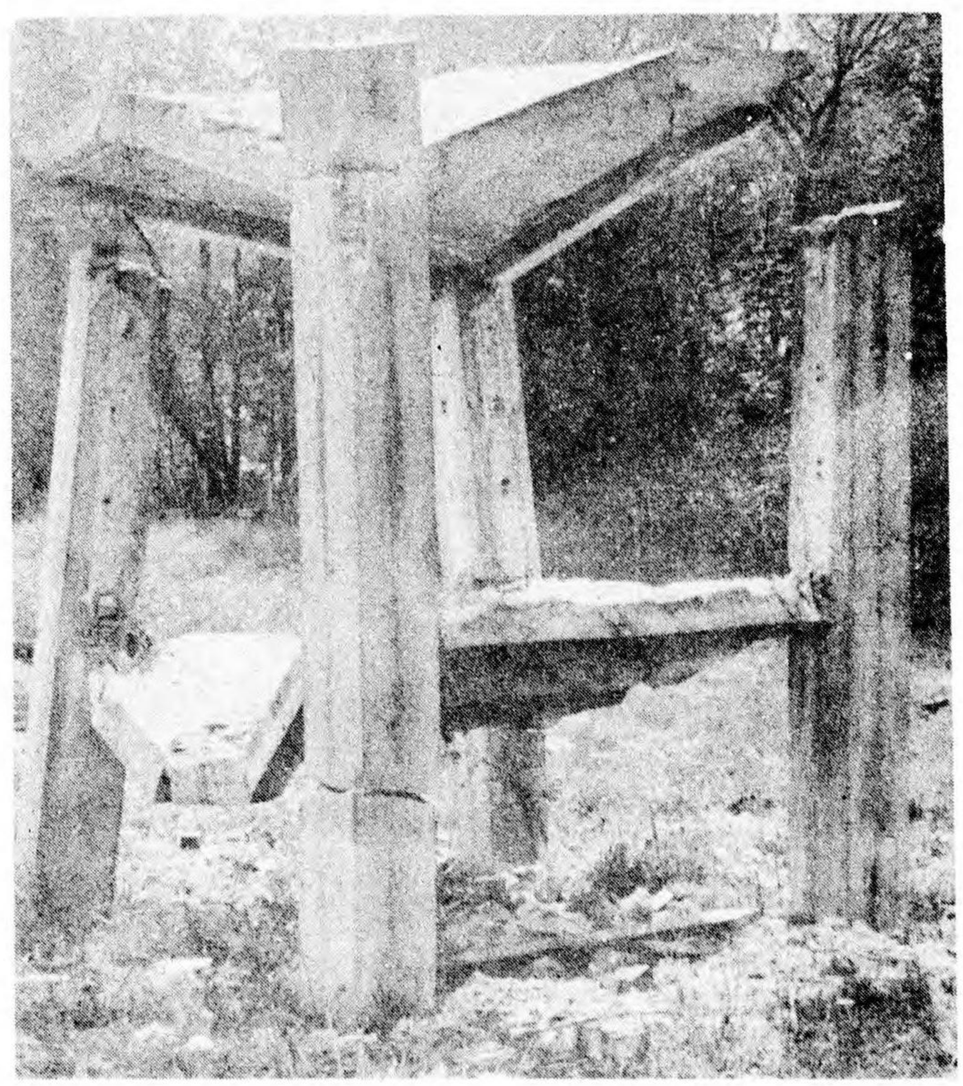

Fig. 8. Test structure viewed from the NW after detonation of ½ lb of TNT.

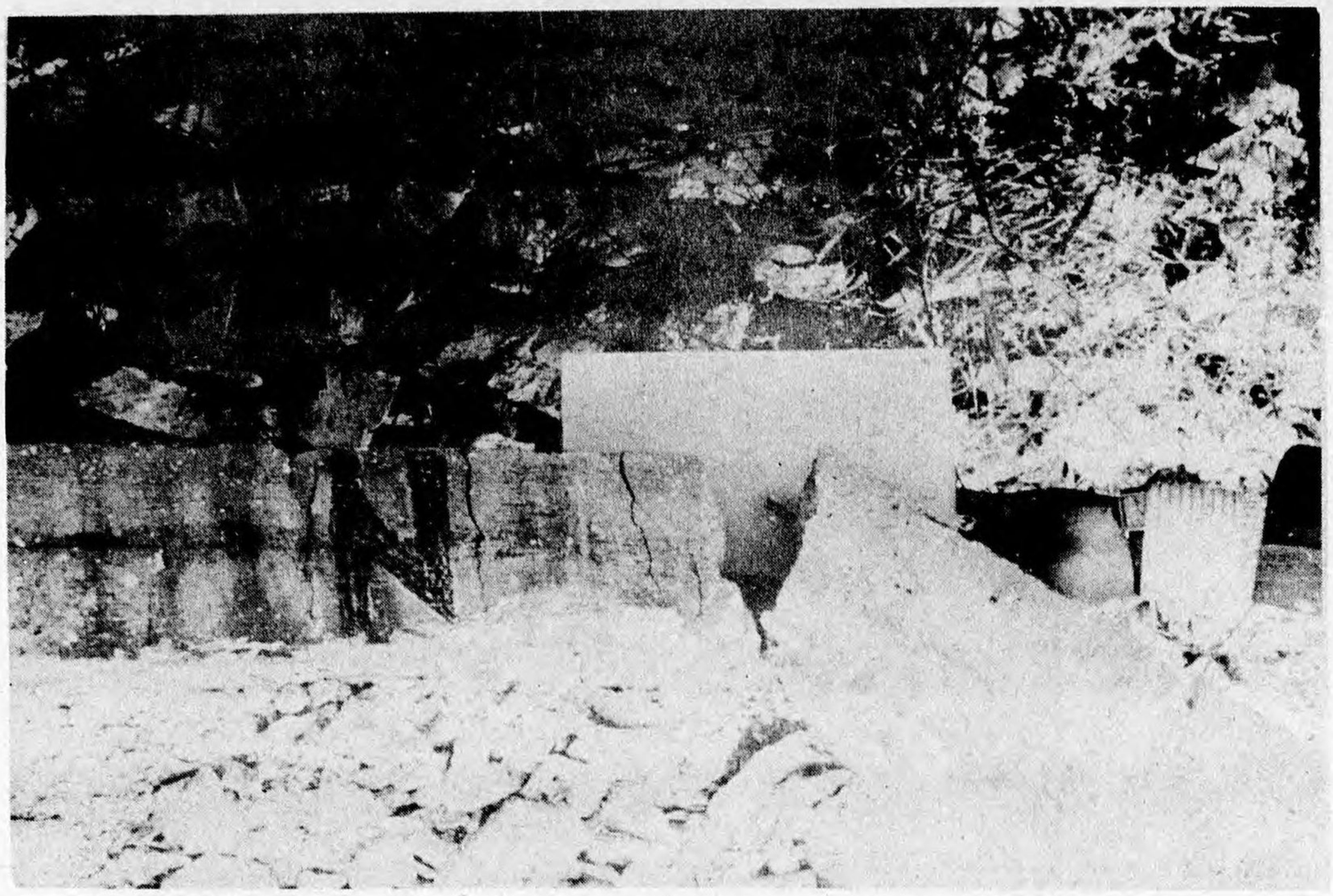

Fig. 9. First floor north spandrel beam after detonation of ½ lb of TNT. Note absence of tension reinforcing and consequent cracking.

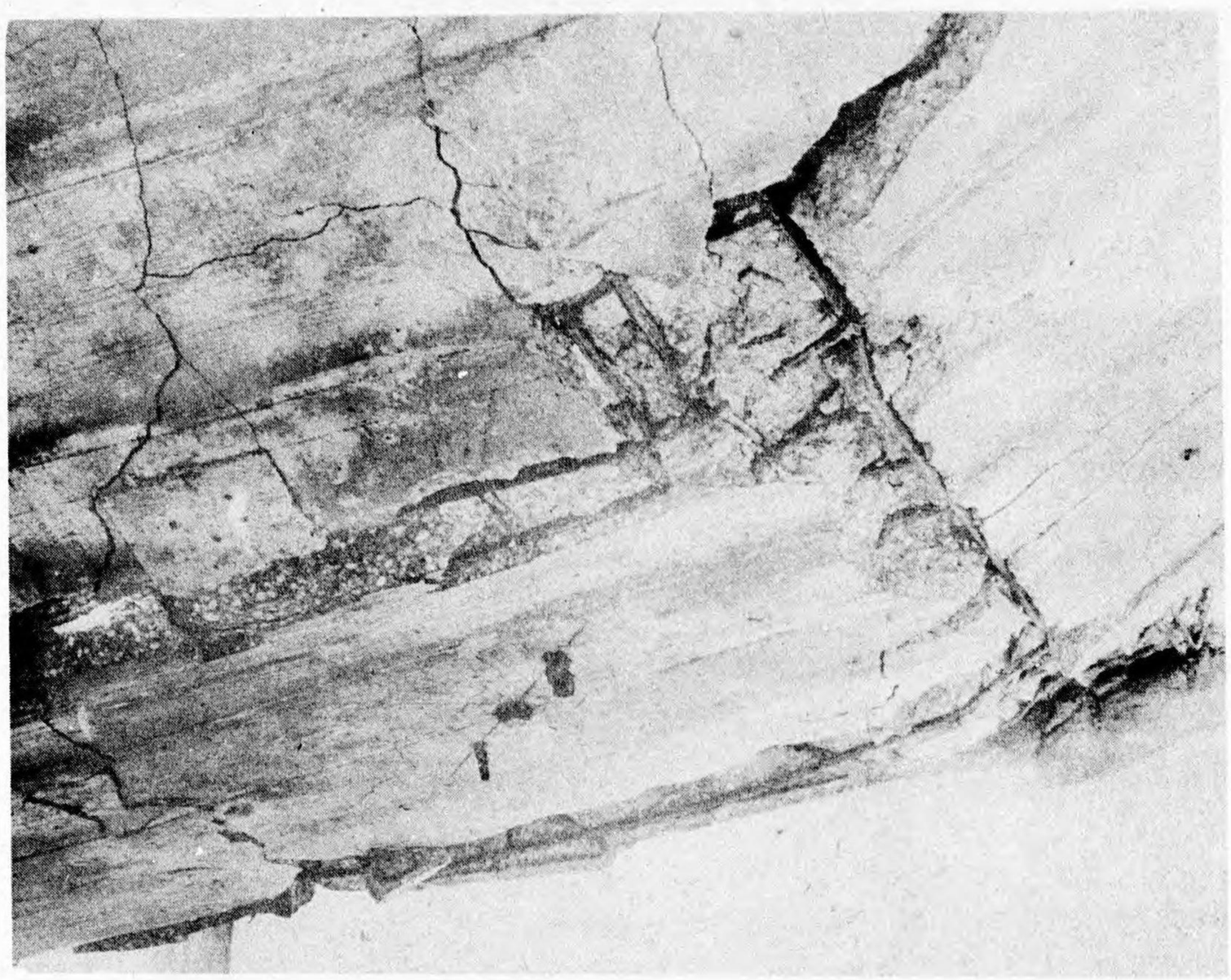

Fig. 10. Under side of first floor looking upward, after detonation of ½ lb of TNT. Only one bar failed in tension.

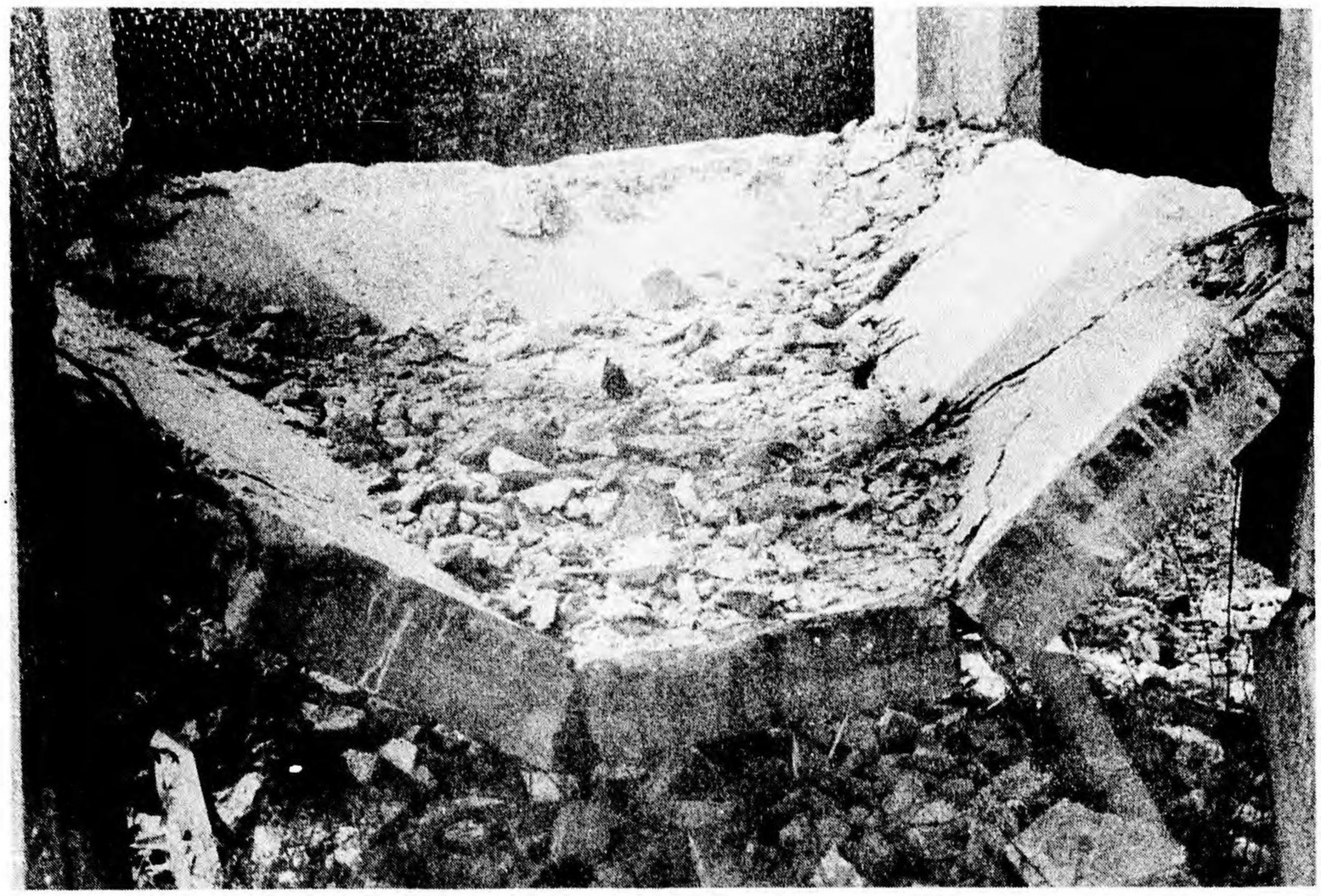

Fig. 11. Upper side of first floor looking down, after detonation of ½ lb of TNT.

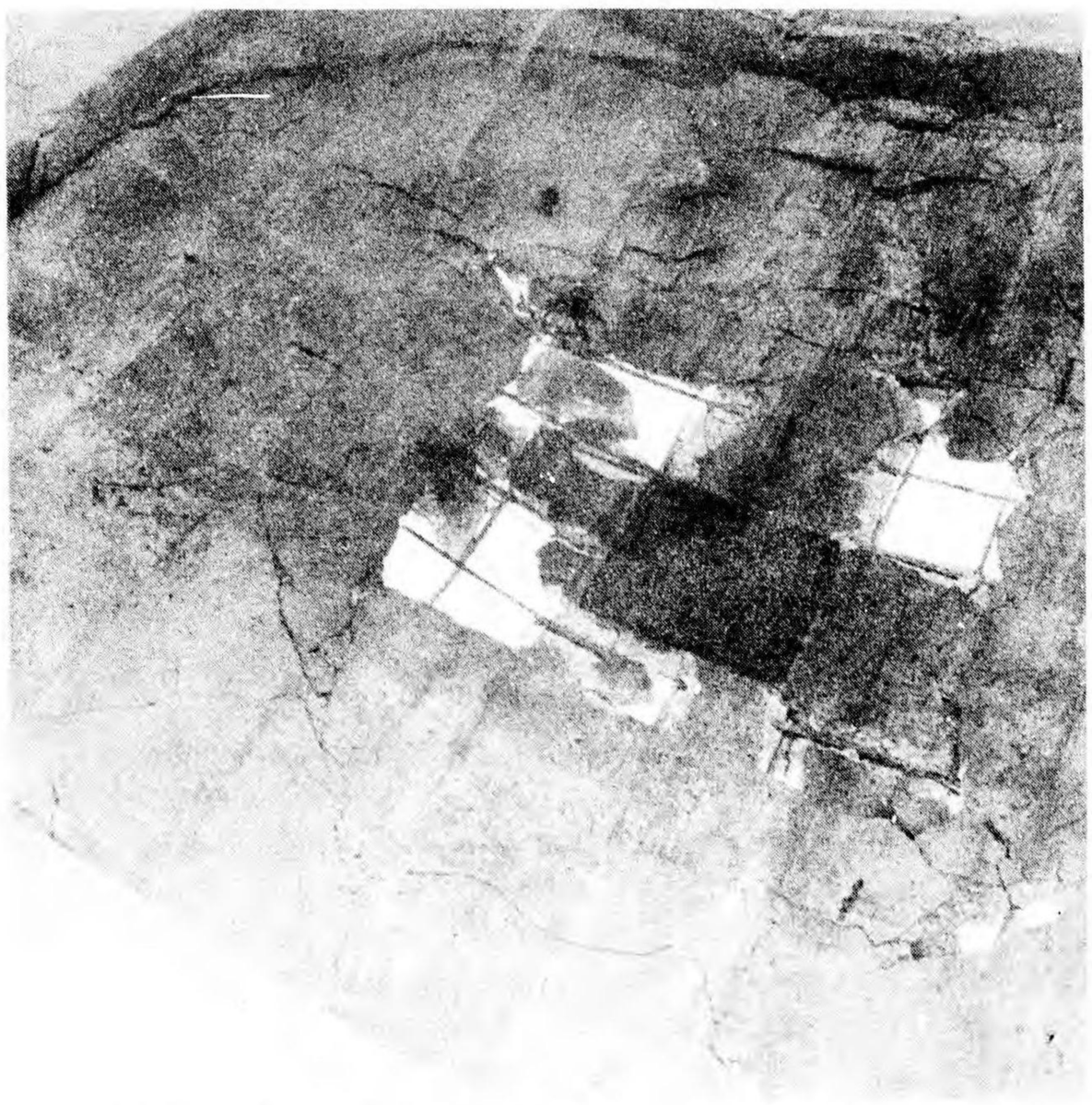

Fig. 12. Under side of roof looking up, after detonation of ½ lb of TNT.

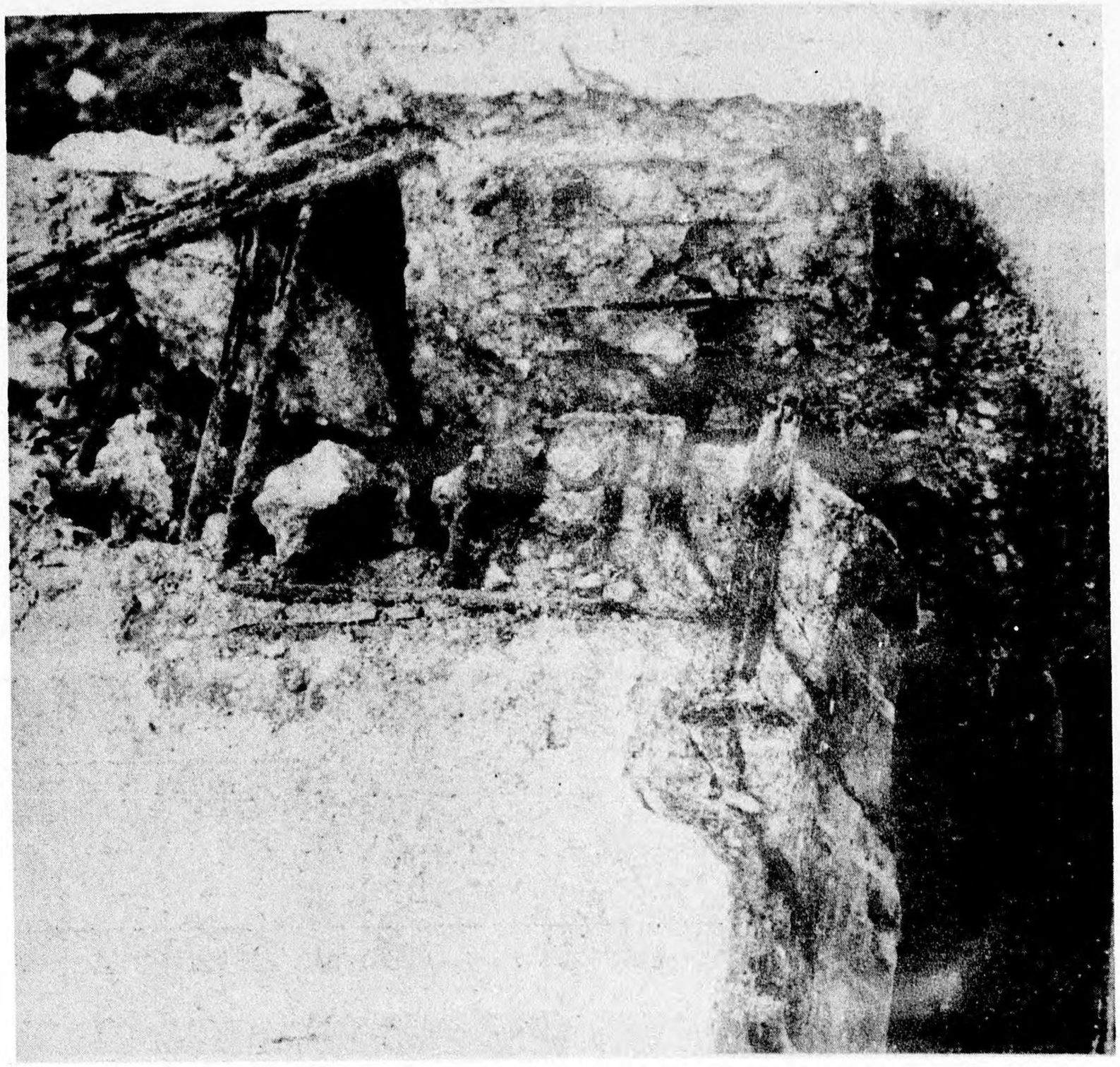

Fig. 13. Close-up of west end of north, first floor spandrel beam after detonation of ½ lb of TNT. Several bars failed in tension at this point and some pulled out because of insufficient bond.

E. DAMAGE TO UNDERGROUND REINFORCED-CONCRETE WALLS*

by I. M. Pei

Abstract

Data from model- and full-scale tests of damage to underground reinforced concrete walls, using charge weights ranging from 1/8 lb to 1000 lb, have been collected and analyzed. Results of this study are summarized in Tables I and II.

Table I. Radius of effectiveness (ft) of GP and SAP bombs against underground reinforced-concrete walls for the degree of damage indicated[a]

	Wall Thickness (ft) ⟶	1	2	3	4	5	6	7	8	9	10
100-lb GP AN-M30	Moderate	11.6	8.2	6.5	5.3	4.3	(2.5)	--	--	--	--
	Heavy	7.8	5.8	4.6	3.5	(1.8)	--	--	--	--	--
	Breach	5.6	4.2	2.9	--	--	--	--	--	--	--
250-lb GP AN-M57 500-lb SAP AN-M58	Moderate	--	12.4	10.1	8.5	7.2	6.3	(5.1)	(2.9)	--	--
	Heavy	--	8.7	7.1	6.0	4.9	(3.8)	--	--	--	--
	Breach	--	6.3	5.0	3.7	--	--	--	--	--	--
500-lb GP AN-M64 1000-lb SAP AN-M59	Moderate	--	18.0	14.7	12.7	11.1	9.8	8.6	7.6	(6.6)	(4.7)
	Heavy	--	12.4	10.5	9.0	7.8	6.8	5.7	(4.2)	--	--
	Breach	--	9.0	7.5	6.3	4.9	2.5	--	--	--	--
1000-lb GP AN-M65	Moderate	--	--	21.0	18.2	16.2	14.6	13.2	11.9	10.9	9.9
	Heavy	--	17.0	14.6	12.9	11.5	10.3	9.1	8.1	7.1	(5.6)
	Breach	--	12.3	10.6	9.2	8.1	6.8	5.2	--	--	--
2000-lb GP AN-M66	Moderate	--	--	29.8	25.9	23.0	21.0	19.3	17.8	16.3	15.2
	Heavy	--	--	20.2	18.1	16.4	14.9	13.7	12.5	11.3	10.4
	Breach	--	--	14.7	13.1	11.8	10.5	9.4	7.9	6.1	--
12000-lb GP T10	Moderate	--	--	--	--	49.0	46.5	41.5	39.0	36.5	34.5
	Heavy	--	--	--	36.0	33.5	32.0	29.0	27.5	26.0	24.5
	Breach	--	--	--	26.0	24.0	23.0	21.5	20.0	18.5	17.5
22000-lb GP T14	Moderate	--	--	--	--	--	50.0	46.0	43.5	40.5	38.5
	Heavy	--	--	--	--	36.0	33.5	32.0	30.5	28.5	27.5
	Breach	--	--	--	--	26.0	24.5	23.0	21.5	20.5	19.5

[a]Numbers in parentheses are based on meager data.

*First published as EWT-5g (OSRD-5405g).

Table II. Weapon selection table for attack on underground reinforced-concrete walls.

Wall Thickness (ft)	Minimum* Optimum Bomb	Moderate Damage	Heavy Damage	Breaching
		Radius of Damage R_D (ft)		
2	250-lb GP	12.4	8.7	6.3
3	500-lb GP	14.6	10.3	7.4
4	1000-lb GP	18.2	12.9	9.2
5	2000-lb GP	23.1	16.4	11.8
8	12000-lb GP	38.8	27.5	19.8
10	22000-lb GP	47.2	33.8	24.1

*πR_D^2/(bomb weight) is maximum.

1. Analysis of data

The effect of earthshock damage on underground reinforced-concrete structures has been the subject of a number of tests conducted in this country as well as in Britain. Among them are full-scale tests at Camp Gruber[1/] and Richmond Park[2/], as well as model-scale tests at Princeton[3/], Richmond Park[4/] and the Road Research Laboratory[5,6,7/].

1/ Effects of underground explosions, Vol. III, "Resulting damage to structures," by N. Dahl and D. Mayer. Committee on Fortification Design, Interim Report No. 26, June 1944.

2/ Report on trials in Richmond Park with buried 50 kg. S.C. 250 lb. A.S., and 250 kg. S.C. bombs exploded in contact with underground concrete walls, Research and Experiments Dept., Ministry of Home Security, R.C. 413, Nov. 1943, Mar. 1944.

3/ Princeton B program, data unpublished, by A. H. Taub, H. L. Beckwith, D. G. Kretsinger, and W. T. Read, Dec. 1943.

4/ Report on model scale tests on underground reinforced concrete walls with charges exploded in contact, Research and Experiments Dept., Ministry of Home Security, R.E.N. 427, Aug. 1944.

5/ Effect of explosion upon single or double shelter walls, Road Research Laboratory, R.C. 117, June 1940.

6/ Effect of explosion upon shelter walls backed by the ground, Road Research Laboratory, R.C. 112, June 1940.

7/ Recent work with buried charges, Road Research Laboratory, R.C. 220, June 1941.

No appreciable scale effect is revealed among the various experiments, despite the fact that the charge weights range from 1/8 lb to 1000 lb. At Richmond Park, however, it was found that the scale relationship between the model and the full-scale tests was not as close as expected. The two main reasons given were:

(i) The quality of the concrete in the model was much superior to that in the full-size structure; the crushing strength of the former was about 6000 lb/in^2 and that of the latter 2000 lb/in^2 at the time of the respective trials.

(ii) The smaller resistance to movement of the model as a whole caused a larger proportion of the energy to be used in moving the target, with the result that less energy remained to damage the concrete.

On the whole, the main discrepancies in the data are attributed to inherent differences between target walls supported on two sides and those supported on four sides. In general, most of the target walls and experimental conditions in the various sets of tests listed in the foregoing have certain similarities:

(i) They are of "lightly reinforced" type with mild-steel bars totalling approximately 1 percent by volume of concrete.

(ii) Target faces generally have height-to-width ratios of 3:5.

(iii) Span-to-thickness ratio ranges from 5:1 to 15:1.

(iv) The position of the charge is nearly always along the normal through the geometric center of the target. It is evident that any variation from this arrangement will in general result in less damage.

The ratio of maximum deflection d to span length L, in inches per foot, was calculated for all available data. Each point with its value of d/L was entered on Fig. 1, a graph of $t/w^{1/3}$ versus $r/w^{1/3}$, where t is the wall thickness (ft), r the distance from the charge (ft), and w the charge weight (lb). Four separate curves were then drawn, each passing through or close to the points having a given d/L value. The four values of d/L adopted were found to correspond to the following categories of damage: slight, moderate, heavy, and breaching. All the data used in establishing the curves shown in Fig. 1 are given in the Appendix.

It is to be noted that the type of damage is different for walls supported on two sides and those supported on four sides. Apparently walls supported on two sides have a tendency to crack rather than scab, whereas walls supported on all four sides scab more readily though less severely, other circumstances being the same. Despite this difference in the type of damage, the points having the same value of d/L for both kinds of support fall reasonably close together on the plot, and hence can be represented by the same curves. For breaching, the value of d/L becomes meaningless in many instances. Some of the data, however, show near breaching and give a measured deflection of the wall. The curve drawn for d/L = 0.5 may be considered as the approximate limiting condition for breaching.

From the curves in Fig. 1, the radii of effectiveness of GP and SAP bombs for various degrees of damage to underground reinforced-concrete walls have been calculated and tabulated in Table I in the abstract of this paper. The criteria assumed for the four categories of damage are given in Table III.

Table III. Criteria assumed for the four categories of damage.

Description of Damage	Type of Damage		d/L (in./ft)
	2-edge Support	4-edge Support	
Slight	Fine cracks	Fine cracks	0.02
Moderate	Medium cracks	Light scabbing	0.10
Heavy	Heavy cracks and scabbing	Severe scabbing	0.20
Breaching	Breaching	Breaching	0.50

A simple theory of damage to an underground target has been outlined by Newmark.8/ While this gives a rational basis for interpreting the data from the Camp Gruber tests, it cannot be applied to the present case because all the points plotted in the work at hand are for charges detonated relatively close to the wall (within about 3R/2, where R is the radius of the maximum

8/ Effects of underground explosions, Vol. I, "Subsurface and target phenomena," by C. W. Lampson. Committee on Fortification Design, Interim Report No. 26, June 1944.

DAMAGE CRITERIA ASSUMED

Description of Damage	Type of Damage		d/L in./ft.
	2-edge Support	4-edge Support	
Slight	Fine Cracks	Fine Cracks	0.02
Moderate	Medium Cracks	Light Scabbing	0.1
Heavy	Heavy Cracks and Scabbing	Severe Scabbing	0.2
Breaching	Breached	Breached	0.5

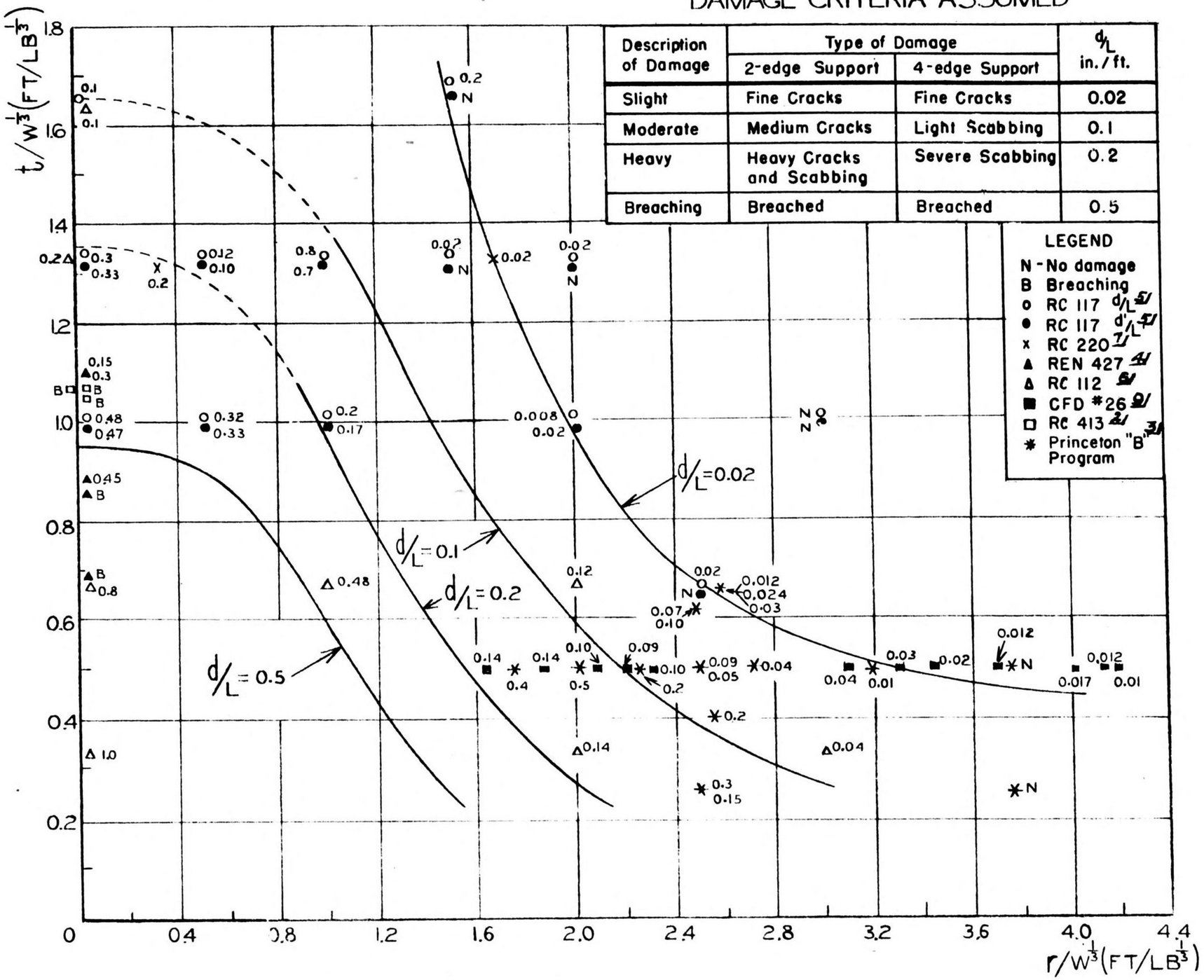

FIG. 1. EFFECT OF EARTH SHOCK ON UNDERGROUND REINFORCED-CONCRETE WALLS.

Princeton University Station
Division 2 NDRC

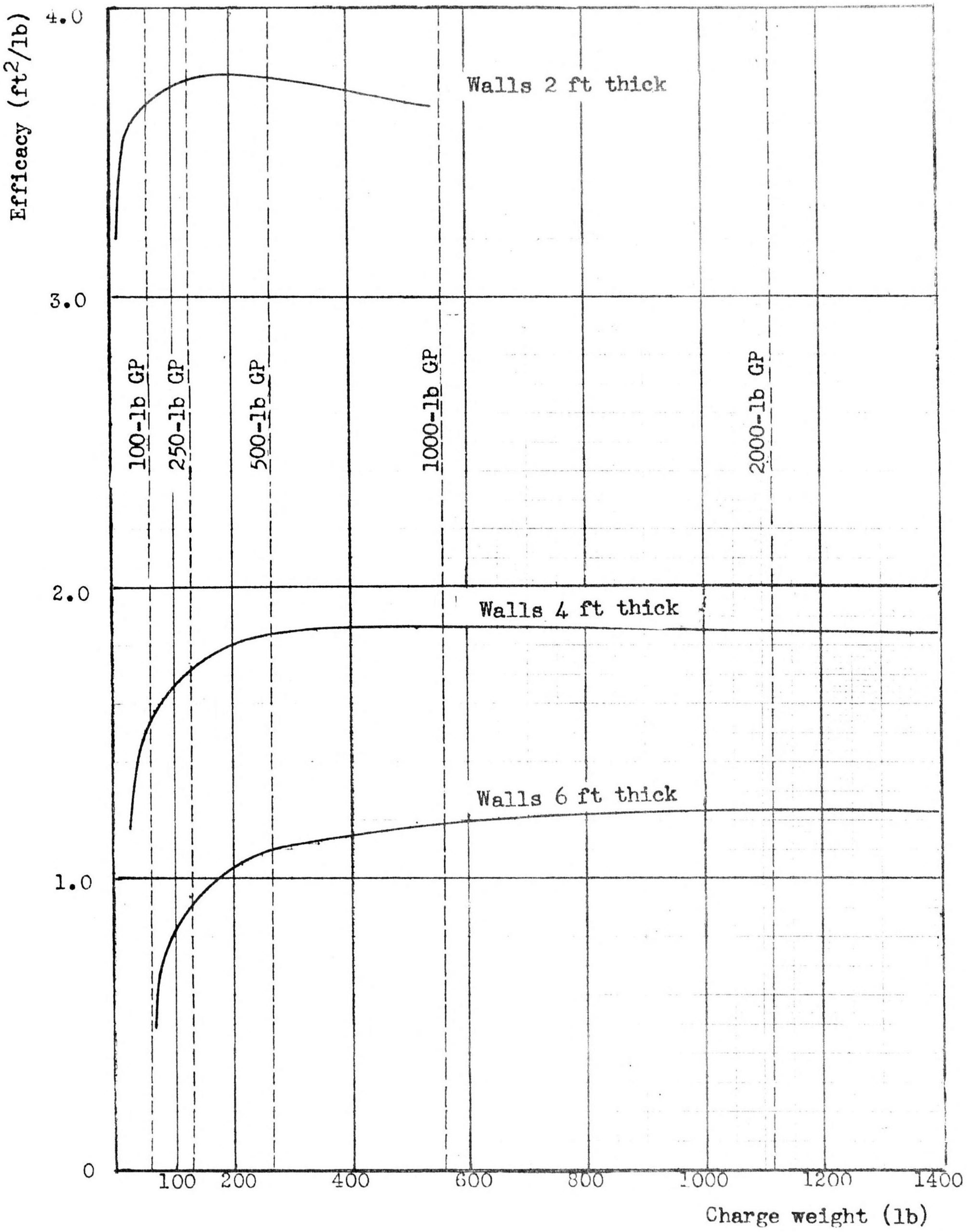

Fig. 2. Efficacy of moderate damage attack on underground reinforced-concrete walls.

Princeton University Station
Division 2 NDRC

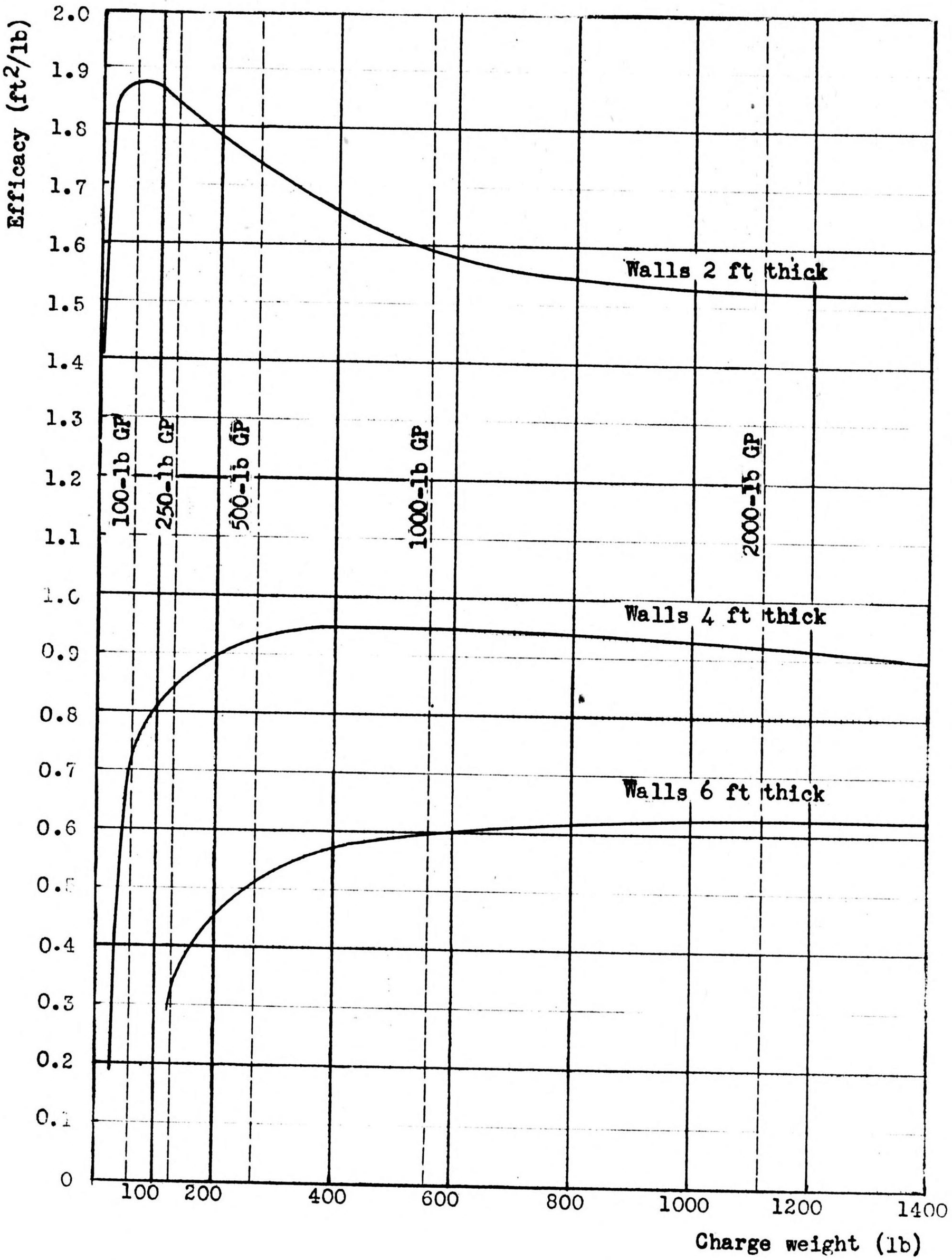

Fig. 3. Efficacy of heavy damage attack on underground reinforced-concrete walls.

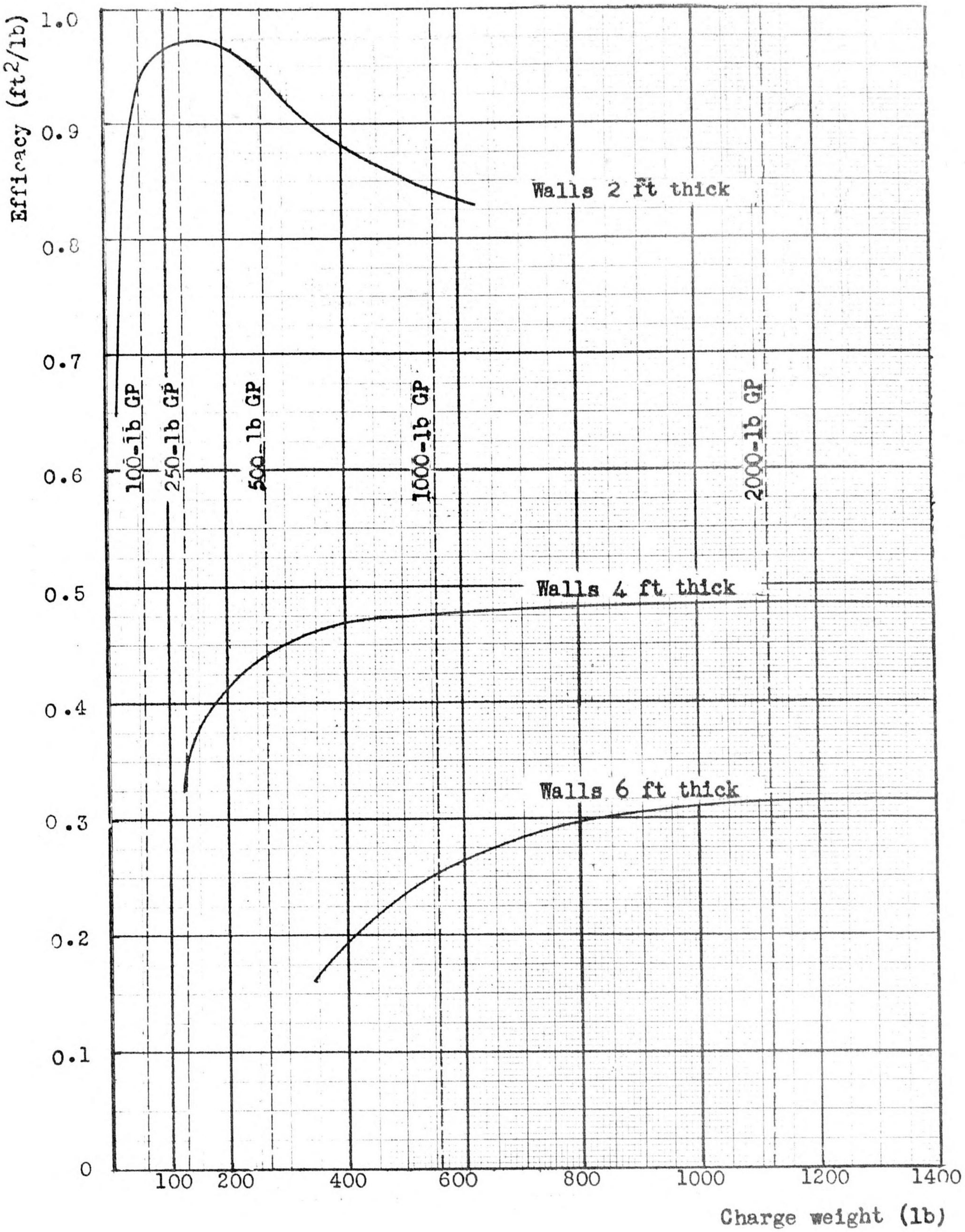

Fig. 4. Efficacy of breaching damage attack on underground reinforced-concrete walls.

crater produced in free soil), while most of the Camp Gruber tests were at greater distances[1,8]. A theoretical interpretation of the present data is, therefore, still lacking.

2. Bomb selection

From Fig. 1 and the test results summarized in Table I, the optimum bombs for area bombing of underground targets with various thicknesses of reinforced-concrete walls can be selected. Figure 1 shows that, for a given thickness of wall, a given bomb has a limiting radius r within which a certain category of damage will result. The vulnerable region for the bomb will be πr^2; its efficacy, $\pi r^2/w$, where w is the weight of explosive charge. Graphically, if a plot is made of efficacy against charge weight, the most nearly optimum bomb can be readily selected. Figures 2, 3, and 4 show the efficacies of various bombs in causing moderate, heavy, and breaching damage to three common thicknesses (2 ft, 4 ft, 6 ft) of reinforced-concrete walls. These curves yield the following conclusions:

(i) The optimum size of bomb for damaging a wall of thickness t is that giving a scaled thickness, $t/w^{1/3}$, of 0.4 to 0.5 $ft/lb^{1/3}$.

(ii) The efficacy of damage rises sharply to the optimum, after which the decrease of efficacy is small for larger charges. This means that it is safer to select a bomb larger than the optimum than one that is smaller. The only exception to this is in the case of doing heavy damage to walls 2 ft thick where the next larger size bomb (500-lb GP) is 6% less effective.

Curves such as these were used to determine the size of bomb giving the greatest efficacy in producing various degrees of damage to different thicknesses of underground reinforced-concrete walls. The results are summarized in Table II in the abstract of this paper.

It must be mentioned, however, that since all bombs larger than the ones recommended in Table II are almost as effective, the real criterion for bomb selection lies in the loading efficiency of the various service bombs in the various service aircraft.

For some purposes, such as the attack on long narrow targets, the optimum bomb is that which maximizes r/w. Reasoning similar to the foregoing shows that for breaching or heavy damage, the optimum bomb is that giving a scaled thickness $t/w^{1/3}$ of 0.8 to 1.0 ft/lb$^{1/3}$. For moderate damage, the optimum is for a value of $t/w^{1/3}$ of about 1.4 ft/lb$^{1/3}$.

APPENDIX

Damage to Underground Reinforced-Concrete Walls

The notation used in the following tabulation of data is

Symbol	Unit	Definition
w	lb	Weight of the charge
t	ft	Thickness of the target wall
r	ft	Perpendicular distance from wall to charge
d'/L'	in./ft	Ratio of doflection at center of target to span of wall for the long span of the wall
d/L	in./ft	Ratio of deflection at center of target to span of wall for the short span of the wall
$t/w^{1/3}$	$ft/lb^{1/3}$	Scaled thickness of the target wall
$r/w^{1/3}$	$ft/lb^{1/3}$	Scaled perpendicular distance from wall to charge

Table III. Damage to underground reinforced-concrete walls.

Target Face Dimensions (ft)	Charge Weight (lb)	Type of Support	$t/w^{1/3}$ ($ft/lb^{1/3}$)	$r/w^{1/3}$ ($ft/lb^{1/3}$)	d'/L' (in./ft)	L'/t	d/L (in./ft)	L/t	Degree of Damage
Reference: RC 117 (see footnote 5)									
2.5 × 1.5	1/8	4 sides	0.67	2.5	0.02	7.5	0	4.5	Fine cracks
			1.0	0	0.48	5	0.47	3	Breaching
			1.0	0.5	0.32	5	0.33	3	Breaching
			1.0	1.0	0.20	5	0.17	3	Heavy cracks
			1.0	2.0	0.028	5	0.02	3	Medium cracks
			1.33	0	0.3	3.7	0.33	2.24	Very heavy cracks
			1.33	0.5	0.12	3.7	0.1	2.24	Heavy cracks
			1.33	1.0	0.08	3.7	0.07	2.24	Medium cracks
			1.33	1.5	0.02	3.7	0	2.24	Fine cracks
			1.66	0	0.1	3	0.03	1.8	Heavy cracks
			1.66	1.5	0.02	3	0	1.8	Fine cracks
Reference: RC 112 (see footnote 6)									
2.5 × 1.5	1/8	4 sides	0.33	0	1.0	15	0.33	9.0	Breaching
			0.33	2.0	0.14	15	0.07	9.0	Medium cracks
			0.33	3.0	0.04	15	0	9.0	Medium cracks
			0.67	0	0.8	7.5	0.33	4.5	Breaching
			0.67	1.0	0.48	7.5	0.17	4.5	Heavy cracks
			0.67	2.0	0.12	7.5	0.03	4.5	Medium cracks
			1.0	0	0.72	5	0.53	3	Heavy cracks
			1.0	1.0	0.28	5	0.07	3	Few heavy cracks
			1.0	2.0	0.04	5	0	3	Medium cracks
			1.0	3.0	0	5	0	3	No damage
			1.33	0	0.2	3.7	0	2.24	Medium cracks
			1.33	2.0	0.02	3.7	0	2.24	Fine cracks
			1.66	0	0.1	3	0	1.8	Medium cracks
Reference: RC 220 (see footnote 7)									
2.5 × 1.5	1/8	4 sides	0.67	2.5	0.02	7.5			Slight
			1.0	2.0	0.02	5			Slight
			1.33	1.67	0.02	3.7			Slight
			1.67	1.5	0.02	3			Slight
			0.67	1.67	0.2	7.5			Scabbing
			1.0	1.0	0.2	5			Scabbing
			1.33	0.33	0.2	3.7			Scabbing
			1.67	--	0.2	3			Scabbing
Reference: R.E.N. 427 (see footnote 4)									
5.33 × 3.35	1 (P.E.)	4 sides	1.1	0	0.15	4.85			Medium cracks
	1 (P.E.		1.1	0	0.30	4.85			Heavy cracks
	4 (P.E.)		0.695	0	Breach	4.85			Breach
	2 (P.E.)		0.873	0	0.45	4.85			Reinforcing cut
	2 (P.E.)		0.873	0	Breach	4.85			Breach
Reference: RC 413 (see footnote 2)									
11.5 × 5.75	53.7	4 sides	1.08	0	1.83 (B)	2.62			Breach
15.67 × 7.87	134.0		1.07	0	1.34 (B)	3.06			Breach
20 × 10	286.0		1.06	0	1.8 (B)	2.57			Breach

Table III. [Concluded.]

Target Face Dimensions (ft)	Charge Weight (lb)	Type of Support	$t/w^{1/3}$ ($ft/lb^{1/3}$)	$r/w^{1/3}$ ($ft/lb^{1/3}$)	d'/L' (in./ft)	L'/t	d/L (in./ft)	L/t	Degree of Damage
Reference: CFD No. 26 (see footnote 1)									
5.0 × 3.5	8	2 sides	0.5	1.62 1.88 2.06 2.10 2.12 3.71 4.12	0.14 0.14 0.10 0.08 0.18 0.012 0.012	5			Not given in report of tests
10.0 × 7.0	64	2 sides	0.5	2.20 2.31 3.64 4.14 4.21	0.09 0.10 0.028 0.014 0.01	5			Not given
15.0 × 10.5	216	2 sides	0.5	2.12 4.19	0.14 0.014	5			Not given
20 × 14.0	512 540	2 sides	0.5	3.29 2.04	0.032 0.12	5			Not given
25.0 × 17.5	1000	2 sides	0.5	2.12 3.15 4.21	0.15 0.044 0.008	5			Not given
	1080			2.06 3.06 3.44 4.05	0.15 0.04 0.02 0.017				
Reference: Princeton "B" Program (see footnote 3)									
2.5 × 1.75	½	2 sides	0.63	2.58 2.58 2.58 2.58 2.55 2.55 2.55 2.55 2.55 2.55 2.52 2.52 2.52 2.52 2.52	0.012 0.024 0.012 0.006 0.072 0.10 0.112 0.148 0.148 0.072 0.06 0.012 0.006 0.05 0	5			Not given in report of tests
2.5 × 1.75	1	2 sides	0.5	2.73 3.19 3.75 1.75 2.24 2.47 2.47 2.02 1.87 2.47 3.12 2.17 2.47 2.52 2.52	0.036 0.012 0 0.40 0.20 0.10 0.148 0.50 1.50 0.148 0.012 0.60 0.124 0.10 0.05	5			Not given
2.5 × 1.75	2	2 sides	0.397	2.7 2.73 2.73 2.55 2.57 2.61 2.7 2.55 2.55	0.136 0.18 0.148 0.20 0.20 0.20 0.06 0.20 0.20	5			Not given
2.5 × 1.75	4	2 sides	0.315	2.8 2.52 2.72 2.83 2.83 2.71 2.71	0.10 0.80 0.28 0.024 0.006 0.148 0.148	5			Not given
2.5 × 1.75	8	2 sides	0.25	2.9 2.5 3.75 3.75 2.5 2.5 2.5 2.5 3.0 2.75	0.05 Breach 0 0 0.30 0.006 0.148 Breach 0.006 0.60	5			Not given
5.0 × 3.5	8	2 sides	0.5	2.5 2.5 2.5	0.086 0.10 0.16	5			Not given

F. EFFECT OF BURIED CHARGES ON CONCRETE SURFACE SLABS*

by D. G. Kretsinger and A. H. Taub

Abstract

Results of tests in which buried charges were detonated under concrete slabs indicate that the thickness t of the slab divided by the cube root of the charge weight w is a measure of the strength of the slab, as is the reinforcing; the strength increases with both of these quantities. At a given depth of the charge the stronger slabs suffer less damage. As the depth increases, the damage decreases. Tamping the charge increases the damage slightly.

Quantitative estimates are given for the limiting values of $t/w^{1/3}$ for which complete destruction of the slab is achieved over the crater area. It is argued that this type of damage will be achieved when the fuze selected is the one that will create the greatest crater area in unsurfaced soil. The presence of concrete slabs of the thicknesses used here does not appreciably affect the diameters of craters produced by the buried charges.

It is felt that these results may be scaled up and applied to the problems involved in selecting bombs and fuzes in the attack of concrete airport runways, road embankments with retaining walls, and concrete floors of heavy structures.

1. Introduction

The purpose of the tests reported herein was to determine the effect of different variables on damage produced by buried charges to concrete slabs in contact with the ground. The charge variables studied were weight, depth of burial, and method of burial. The slab variables were thickness, reinforcing, and restraint. Another purpose was to determine the influence of the presence of a concrete slab on the cratering of a charge in earth.

It is felt that these results may be scaled up and applied to the problems involved in selecting bombs and fuzes in the attack of concrete airport runways, road embankments with retaining walls, and concrete floors of heavy structures.

---

*Formerly published in AES-7 (OSRD-4754), p. 27, and as EWT-1a (OSRD-4918a).

2. Experimental procedure

The slabs used were square in plan area, having 6½-ft sides. Two thicknesses were used, 2 in. and 4 in. Some of the slabs had precast circular holes 5 in. in diameter to simulate the hole made by a bomb in perforating a concrete slab.

Tests were made with and without sand bags to restrain two edges of the slab. In the former case fourteen 75-lb bags were placed on each of two edges of the slab.

Three degrees of reinforcing were used. The 2-in. slabs had either no reinforcing or were reinforced with two mats of 2 × 2-in. No. 12 wire mesh, one in each face. This amounted to about 194 lb of reinforcing per cubic yard of concrete. The 4-in. slabs either had no reinforcing; or had two mats of the type described for the 2-in. slabs, giving a reinforcing of about 97 lb per cubic yard of concrete; or had two mats of 4 × 4 × ¼ in. reinforcing, one in each face, giving a reinforcing of about 194 lb per cubic yard of concrete.

The charges were built up from ½-lb Engineer blocks of TNT, which are rectangular parallelepipeds 1-3/4 × 1-3/4 × 3¼ in. The sizes used weighed ½, 1, 1½, 2, and 4 lb. The 1-lb charge was made by placing two of the blocks end to end to obtain a charge 1-3/4 × 1-3/4 × 6½ in. The 1½-lb charge was made by placing a 1-lb and a ½-lb charge next to each other with their long axes parallel and the center of the ½-lb charge opposite the center of the 1-lb one. The 2-lb charge was obtained by placing two 1-lb charges side by side, giving a charge 1-3/4 × 3½ × 6½ in. The 4-lb charge was obtained by placing two 2-lb ones side by side, giving a charge 3½ × 3½ × 6½ in. The charges were detonated with Engineer caps; the larger charges were boostered with 22-gm Tetryl cylinders.

The charges were buried with their long axis in one of two positions: parallel to or making an angle of 25° with the normal to the slab. In all cases the charge was approximately under the center of the slab. The perpendicular distance between the center of the charge and the bottom of the slab is referred to as the depth of the charge. When the charge axis was tilted with respect to the normal to the slab, the hole in

Fig. 1. A damage: Slab is completely destroyed and only a few isolated pieces of concrete remain.

Fig. 2. B damage: Slab is broken into several large pieces, but they have not been thrown clear of the crater.

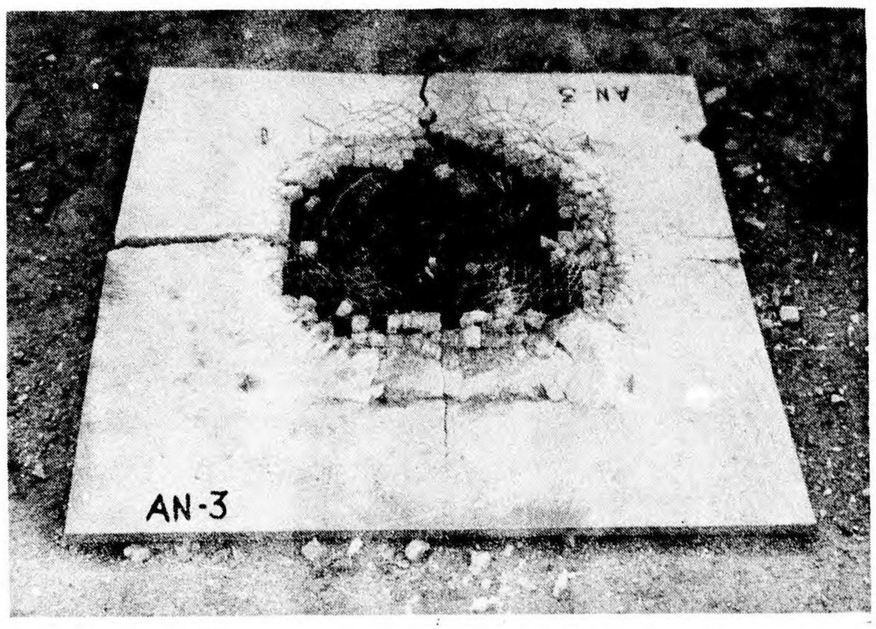

Fig. 3. C damage: Slab has a hole blown in it, with heavy cracks radiating to edges. Concrete pieces remain in place relatively intact.

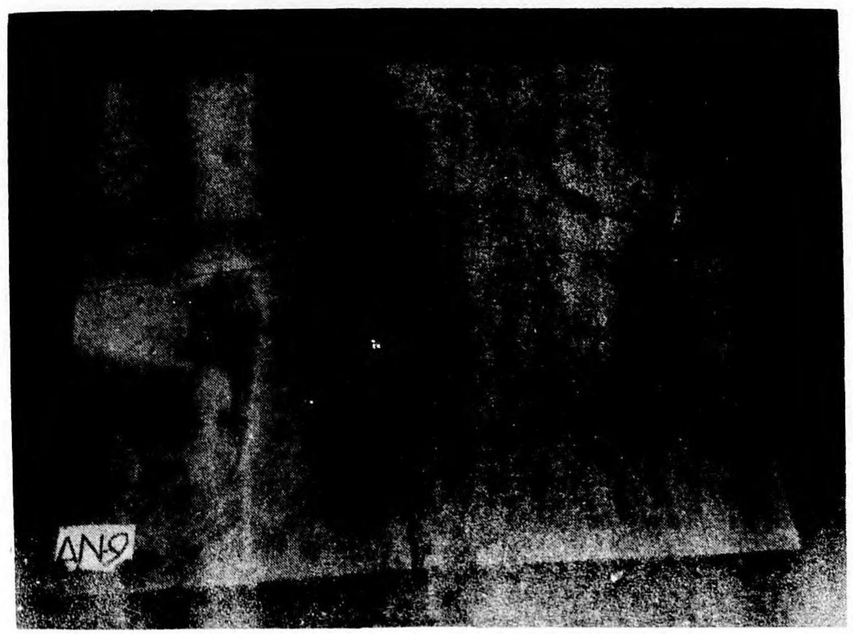

Fig. 4. D damage: Slab experiences heavy radial cracking, some of the cracks extending to edges of slab.

the ground into which the charge was inserted was so tilted. In some cases this hole was filled after the charge was inserted and the fill was compacted. In tests where this was done the charge is said to be a tamped charge.

The charge depths used were determined in terms of fractions of the depths necessary to produce a maximum crater in free earth. Previous experiments in the soil that was used (that in the vicinity of Princeton University Station -- undisturbed, dry, hard, Sassafras clay loam) had shown that this depth is achieved when the depth L (ft) divided by the cube root of the weight of charge w (lb) is 2.5, that is, $L/w^{1/3} = 2.5$. The depths that were used expressed in feet divided by 2.5 times the cube root of the weight of the charge in pounds were chosen to be 0, 1/3, 1/2, 2/3, or 1. The depths of the charges are referred to in the following by the value of this fraction. For example, if w (lb) is the charge weight and the depth is listed as 1/3, then the depth in feet is $(1/3)(2.5w^{1/3})$.

Before the slabs were put in place small amounts of sand were used to level minor inequalities in the ground and to provide a level bearing surface for the slab. The slab and charge were put in place, and the charge was detonated. The slab was then surveyed and the damage was listed as A, B, C, D, or intermediate. Thus B-A damage is intermediate between B and A and closer to B. The definition of these categories is as follows:

A: The slab is completely destroyed and only a few isolated pieces of concrete remain (see Fig. 1).

B: The slab is broken into several large pieces, but these have not been thrown clear of the crater (see Fig. 2).

C: The slab has a hole blown in it, with heavy cracks radiating to the edges. However, the concrete pieces remain in place and are relatively intact (see Fig. 3).

D: The slab experiences heavy radial cracking, some of the cracks extending to the edges of the slab (see Fig. 4).

The slab was then removed and the apparent crater underneath it was profiled. Only the diameters of the apparent craters are reported here.

3. Results

The results of the seventy-two tests performed are listed in Table I. In the first column of the table is listed the number of the test in order

Table I. Damage to concrete surface slabs produced by buried charges.

Slab No.	$\frac{L}{2.5W^{1/3}}$	$\frac{t}{W^{1/3}}$	Category of Damage	Presence or Absence of: Reinforcing	Tamping	Restraint	Bomb Hole	Slant	Slab Thickness (in.)	Charge Weight, W (lb)	$D/W^{1/3}$ (ft/lb$^{1/3}$)	Crater Diameter, D (ft)
64	0	0.167	A	−	−	+	+	+	4	1.0	4.00	4.00
63	0	.210	A	−	−	+	+	+	4	0.5	4.63	3.67
52	0	.333	A	−	−	+	+	+	4	1.0	4.67	4.67
51	0	.420	A	−	−	+	+	+	4	0.5	5.04	4.00
											Avg. 4.59	
24	0	.210	A	+	−	+	−	−	4	4.0	3.57	5.67
32	0	.210	A	+	−	+	+	−	4	4.0	5.13	8.16
21	0	.333	C-B	+	−	+	−	−	4	1.0	3.50	3.50
29	0	.333	A	+	−	+	+	−	4	1.0	4.83	4.83
65	0	.333	C	x*	−	+	+	+	4	1.0	3.83	3.83
											Avg. 4.17	
4	0	.105	A	x	+	−	−	−	2	4.0	3.54	5.63
3	0	.132	C	x	+	−	−	−	2	2.0	3.97	5.00
2	0	.167	C	x	+	−	−	−	2	1.0	4.34	4.34
1	0	.210	C	x	+	−	−	−	2	0.5	3.15	2.50
											Avg. 3.75	
											Grand Avg. 4.17	
8	1/3	0.105	A	x	+	−	−	−	2	4.0	3.98	6.33
7	1/3	.132	A	x	+	−	−	−	2	2.0	4.90	6.17
6	1/3	.167	C	x	+	−	−	−	2	1.0	4.92	4.92
5	1/3	.210	C	x	+	−	−	−	2	0.5	4.04	3.17
											Avg. 4.46	
57	1/2	0.132	A	−	−	+	+	+	2	2.0	5.15	6.50
55	1/2	.167	A	−	−	+	+	+	2	1.0	5.17	5.17
60	1/2	.167	A	−	−	+	−	+	2	1.0	4.66	4.66
53	1/2	.210	A	−	−	+	+	+	2	0.5	3.99	3.17
59	1/2	.210	A	−	−	+	−	+	2	0.5	4.67	3.66
47	1/2	.264	A	−	−	+	+	+	4	2.0	5.13	6.46
43	1/2	.333	B	−	−	+	+	+	4	1.0	5.17	5.17
50	1/2	.333	A	−	−	+	−	+	4	1.0	--	--
41	1/2	.420	D-C	−	−	+	+	+	4	0.5	2.84	2.25
49	1/2	.420	A	−	−	+	−	+	4	0.5	--	--
											Avg. 4.60	
72	1/2	.210	B	+	−	+	+	+	4	4.0	3.98	6.33
27	1/2	.264	A	+	−	+	−	+	4	2.0	5.15	6.50
71	1/2	.264	D	x	−	+	+	+	4	2.0	4.33	5.46
66	1/2	.333	D	x	−	+	+	+	4	1.0	4.25	4.25
70	1/2	.333	C	x	−	+	−	+	4	1.0	5.13	5.13
											Avg. 4.57	
36	1/2	.264	A	+	+	−	+	+	4	2.0	4.90	6.17
35	1/2	.264	A	+	+	+	+	+	4	2.0	5.41	6.83
39	1/2	.264	A	+	+	+	+	−	4	2.0	5.16	6.50
37	1/2	.290	A	+	+	+	+	+	4	1.5	5.23	6.00
68	1/2	.333	C	+	+	+	+	+	4	1.0	4.67	4.67
											Avg. 5.12	
											Grand Avg. 4.81	

*x means heavy reinforcing was present.

Table I. [Concluded.]

Slab No.	$\frac{L}{2.5\ W^{1/3}}$	$\frac{t}{W^{1/3}}$	Category of Damage	Presence or Absence of: Reinforcing	Tamping	Restraint	Bomb Hole	Slant	Slab Thickness (in.)	Charge Weight, W (lb)	$D/W^{1/3}$ (ft/lb$^{1/3}$)	Crater Diameter, D (ft)
58	2/3	0.132	A	-	-	+	+	+	2	2.0	4.23	5.33
56	2/3	.167	A	-	-	+	+	+	2	1.0	--	--
54	2/3	.210	A	-	-	+	+	+	2	0.5	5.45	4.33
48	2/3	.264	A	-	-	+	+	+	4	2.0	5.95	7.50
44	2/3	.333	B	-	-	+	+	+	4	1.0	4.84	4.84
42	2/3	.420	D-C	-	-	+	+	+	4	0.5	1.74	1.38
											Avg. 4.44	
20	2/3	.167	D	x	-	+	+	+	2	1.0	6.00	6.00
18	2/3	.210	D	x	-	+	+	+	2	0.5	6.40	5.08
23	2/3	.264	A	+	-	+	-	-	4	2.0	3.90	4.92
26	2/3	.264	A	+	-	+	-	+	4	2.0	4.23	5.33
31	2/3	.264	A	+	-	+	+	-	4	2.0	5.15	6.50
25	2/3	.333	A	+	-	+	-	+	4	1.0	3.76	3.76
30	2/3	.333	A	+	-	+	+	-	4	1.0	--	--
22	2/3	.333	C-B	+	-	+	-	-	4	1.0	5.66	5.66
67	2/3	.333	D	x	-	+	+	+	4	1.0	--	--
											Avg. 5.01	
12	2/3	.105	A	x	+	-	+	+	2	4.0	4.88	7.75
11	2/3	.132	A	x	+	-	+	+	2	2.0	5.42	6.83
10	2/3	.167	B	x	+	-	+	+	2	1.0	5.25	5.25
9	2/3	.210	D	x	+	-	+	+	2	0.5	6.73	5.34
											Avg. 5.57	
19	2/3	.167	C-B	x	+	+	+	+	2	1.0	6.50	6.50
17	2/3	.210	D	x	+	+	+	+	2	0.5	8.60	6.83
34	2/3	.264	A	+	+	+	+	+	4	2.0	5.30	6.67
38	2/3	.264	A	+	+	+	+	+	4	2.0	6.21	7.83
40	2/3	.290	B	+	+	+	+	-	4	1.5	5.26	6.04
33	2/3	.333	A	+	+	+	+	+	4	1.0	--	--
											Avg. 6.37	
											Grand Avg. 5.31	
16	1.0	0.105	D	x	+	-	+	+	2	4.0	6.20	9.88
15	1.0	.132	D	x	+	-	+	+	2	2.0	5.75	7.25
14	1.0	.167	D	x	+	-	+	+	2	1.0	6.83	6.83
13	1.0	.210	D	x	+	-	+	+	2	0.5	6.72	5.33
											Avg. 6.38	
28	1/2	0.264	A	+	-	-	-	+	4	2.0	5.02	6.50
69	1/2	.333	D	x	-	-	+	+	4	1.0	4.96	4.96
61	1/2	.167	A	-	-	-	+	-	2	1.0	6.13	6.13
45	1/2	.333	A	-	-	-	+	-	4	1.0	6.13	6.13
62	2/3	.167	A	-	+	-	+	+	2	1.0	6.00	6.00
46	2/3	.333	A	-	+	-	+	+	4	1.0	5.25	5.25

of its performance. The second gives the fractional depth of the charge as described in Sec. 2. The third gives the thickness t (ft) of the slab divided by the cube root of the weight w (lb) of the charge. The fourth gives the category of damage in accordance with the classification as just described. In the next five columns plus and minus signs are used to denote the presence or absence of the quantity given at the head of the various columns. In the reinforcing column the x sign is used in addition to denote the presence of very heavy reinforcing. For example, the entries in these columns in the row giving the result of test 65 are to be read as follows: The slab used here had heavy reinforcing; the charge was not tamped; restraining bags were on the slab; there was a precast hole in the slab; and the charge was buried with its long axis making an angle of 25° with the normal to the slab. The tenth column gives the slab thickness in inches; the eleventh the weight of the charge in pounds; the twelfth the apparent crater diameter in feet divided by the cube root of the weight of the charge in pounds; and the thirteenth the crater diameter in feet.

(a) Crater diameters. Table I gives the average value of $D/w^{1/3}$ for each group of tests in which the conditions of reinforcing, tamping, and restraint are the same for a given fractional depth of burial of the charge, as well as the average value of $D/w^{1/3}$ for all the tests in which only the fractional depth is fixed. The latter is called the grand average. The grand averages are within approximately 10 percent of the value of $D/w^{1/3}$ for free earth for the corresponding values of the fractional depth. The latter were obtained from the Weapon Data Sheet 3B1a*[1] by reading the value of $D/w^{1/3}$ corresponding to a value of $L/w^{1/3}$ given by 2.1f, where f is the fractional depth. The grand averages at fractional depths 0 and 1 are slightly above the free-earth $D/w^{1/3}$ increased by 10 percent, and those for fractional depths 1/3 and 1/2 are slightly below the free-earth $D/w^{1/3}$ decreased by 10 percent. The average value of $D/w^{1/3}$ at fractional depth 2/3 is less than 10 percent smaller than the corresponding free-earth $D/w^{1/3}$.

There is no apparent systematic variation of the averages of $D/w^{1/3}$ for fixed fractional charge depth and fixed conditions of reinforcing,

---

1/ Weapon data - fire, impact, explosion, OSRD Report 6053.

tamping, and restraint about the grand average of $D/w^{1/3}$ for fixed fractional charge depth.

Moreover, within the range tested here there seems to be no systematic variation of $D/w^{1/3}$ for fixed charge depth with $t/w^{1/3}$.

The data in Table I are on the whole consistent with the conclusion that the presence of a concrete slab does not alter the crater diameter produced by a charge at a given depth below the surface of the ground by more than 15 percent from that obtained in free earth when the same charge is detonated at the same depth. Of course, the data in Table I apply only for $t/w^{1/3} \leq 0.420$, and it may be expected that for larger values of $t/w^{1/3}$ some influence of the slab will be felt. Such influence will be in the direction of producing camouflets for smaller depths of burial when slabs are present than when they are not. Some evidence for this was found in other tests, which will be reported separately.

(b) Scale laws. The data on crater diameters show that as far as the phenomena in earth are concerned, the usual scale laws hold within the test-to-test variations. This is to be expected if the thickness of the slab plays no important role, for these laws are known to hold in free earth.

The slab thickness has been used in organizing the data in the quantity $t/w^{1/3}$. This variable has been chosen because it is a "nondimensional" measure of the thickness and because data on breaching of underground walls indicate that it, together with the "nondimensional" distance between slab and charge (in this case $L/w^{1/3}$), is an important variable in determining the behavior of the slab.

In tests 72 and 59, 24 and 63, 24 and 1, the same values of $t/w^{1/3}$ and of fractional depth were used, although different thicknesses and charge weights were involved. The difference in damage to the slab is accounted for by the difference in reinforcing, as will be discussed later.

These tests are considered to be a verification of the scaling laws, which are expected to hold in this case because it is felt that at these small distances between charge and slab and for fixed conditions of restraint the forces of gravity are not important. When they are important, scaling in this manner does not take into account all factors.

(c) Damage to slabs. Inspection of Table I shows that the degree of damage can be influenced in a regular manner by the variables $t/w^{1/3}$, fractional depth, reinforcing, tamping, and restraint. The presence or absence of a bomb hole and the slant of the charge seem to produce random changes.

For any fixed fractional depth of charge the damage remains constant or decreases with $t/w^{1/3}$ for fixed conditions of reinforcing, tamping, and restraint. The value of $t/w^{1/3}$ at which this decrease starts, called the limiting $t/w^{1/3}$, is smaller for moderately reinforced slabs than for unreinforced ones and decreases still further for heavily reinforced slabs. Tamping the charge has a tendency to increase this value of $t/w^{1/3}$, as does increasing the restraint. Of these two factors the restraint plays the more important role.

As the fractional depth of charge increases, the value of the limiting $t/w^{1/3}$ remains unchanged or decreases; that is, for a fixed $t/w^{1/3}$ the damage will decrease as the fractional depth increases.

These results are all to be expected if one considers the quantities $t/w^{1/3}$ and the reinforcing as measures of the strength of the slab, and fractional depth and tamping as measures of the strength of the charge.

Table II gives the value of $t/w^{1/3}$ for which damage less than A damage may be expected for various fractional depths under different conditions of reinforcing, tamping, and restraint.

Table II. Limiting values of $t/w^{1/3}$ for A damage.

$L/2.5w^{1/3}$	Limiting Value of $t/w^{1/3}$	Presence or Absence of:		
		Reinforcing	Tamping	Restraint
0	>0.420	−	−	+
1/2	.333	−	−	+
2/3	.264	−	−	+
0	0.333	+	−	+
1/2	.264	+	−	+
2/3	.264-0.333	+	−	+
0	0.105	+	+	−
2/3	≤ .132	+	+	−
1	≤ .105	+	+	−
1/2	0.290	+	+	+
.2/3	0.290	+	+	+
1/3	0.132	x*	+	−

*x means that heavy reinforcing was present.

4. Application to airport runways

Although the tests did not simulate the conditions of restraint obtaining in an airport runway, the results of tests conducted on a model airport runway are in general agreement with those given here and will be reported separately.

When an unsurfaced runway is attacked, bombs and fuzes are chosen to obtain a maximum crater area per pound of bomb consistent with bomb-loading characteristics of the planes used. This usually means small bombs (100-lb GP to 500-lb GP) fuzed for 0.01- to 0.025-sec delay. These bombs are expected to penetrate to a depth that will produce a maximum crater.

Most surfaced runways may be considered as being intermediate between an unsurfaced one and one having a 9-in. layer of unreinforced concrete. A bomb that is fuzed for maximum crater in free earth in attack on such a runway will only achieve a smaller depth in penetrating into the concrete and then the soil. If we assume that the fractional depth is 2/3, then the limiting value of $t/w^{1/3}$ is approximately $\frac{1}{4}$. Hence for charges greater than 27 lb, we will obtain A damage; that is, for the smallest bomb we could use, the 100-lb GP, we will obtain A damage. This is also true when the surface concrete is 12 in. thick.

It is unlikely that fuzing for a longer delay will markedly increase the penetration into the soil below the runway. Hence, we should expect that in almost all cases A damage will be produced in the bombing of surfaced runways.

Whether A damage is a desirable type of damage will, of course, depend upon the repair facilities available. One can conceive of instances where camouflets covered by relatively intact surfacing material would be harder to repair than A damage. However, this is probably an academic question since with present bombs and fuzes A damage will occur except where very deep penetrations are accidentally achieved.

The extent of the damage to the surface of the runway will be confined to a circular area whose radius is slightly larger than the crater radius. This radius in feet is approximately $2.0w^{1/3}$ to $2.5w^{1/3}$ for soil conditions normally found in airfields.

G. RUPTURE OF GLASS BY BLAST*

by J. A. Wise

Abstract

The theory of vibration of rectangular plates is applied to the problem of breakage of glass window panes by air blast from bombs. The results are summarized in Table I.

Table I. Radius of breakage of glass by air blast from bombs.

Glass		Bomb Size (lb) and Type					
Size (in.)	Modulus of Rupture (lb/in^2)	100 GP	250 GP	500 GP	1000 GP	2000 GP	4000 LC
		Radius of Breakage of Glass (ft)					
11 × 14 × 0.12	3000	290	420	540	720	910	1300
	4000	210	300	400	530	670	1000
	5000	140	210	290	390	500	760
11 × 14 × 0.25	3000	70	100	130	170	220	320
	4000	50	80	100	130	160	240
	5000	40	60	70	100	130	180
15 × 15 × 0.12	3000	360	520	680	920	1200	1700
	4000	250	370	490	670	850	1300
	5000	160	240	340	470	610	950
12 × 18 × 0.12	3000	400	580	760	1020	1300	1900
	4000	280	420	550	740	940	1400
	5000	190	290	390	540	690	1060
12 × 18 × 0.25	3000	100	150	190	250	310	450
	4000	80	110	140	180	230	340
	5000	50	80	100	140	180	260
28 × 32 × 0.12	3000	860	1400	2000	2800	3800	6100
	4000	540	910	1300	1900	2600	4300
	5000	250	450	690	1080	1600	2800
28 × 32 × 0.25	3000	290	430	590	810	1050	1600
	4000	190	300	410	560	750	1160
	5000	110	180	260	380	510	820
48 × 48 × 0.12	3000	910	1600	2500	4100	6000	10500
	4000	470	1020	1600	2600	3800	7000
	5000	140	350	670	1100	1700	3500
48 × 48 × 0.25	3000	400	680	990	1500	1900	3200
	4000	250	430	640	980	1300	2200
	5000	100	200	310	510	740	1400
48 × 84 × 0.25	3000	570	1020	1500	2400	3300	5600
	4000	340	610	940	1500	2100	3800
	5000	140	270	430	760	1100	2100

*First published as EWT-5e (OSRD-5405e).

1. Vibrations of and stresses in restrained plates

The basic theory of vibration of rectangular plates is given in numerous publications[1,2,3,4] Tests of the frequency of vibration of panes[5,6] have shown that the frequency of the fundamental mode lies between the theoretical values for simply supported and clamped-edge conditions. A surface of flexure whose form is intermediate to the two cases is assumed, and a theoretical frequency obtained from it agrees quite closely with these tests. From the assumed form of surface, the maximum stresses are obtained; from an assumed modulus of rupture, the maximum static pressure is determined. This is the equivalent static load. From it and the properties of a blast wave, the distance from the detonation of a charge at which rupture would

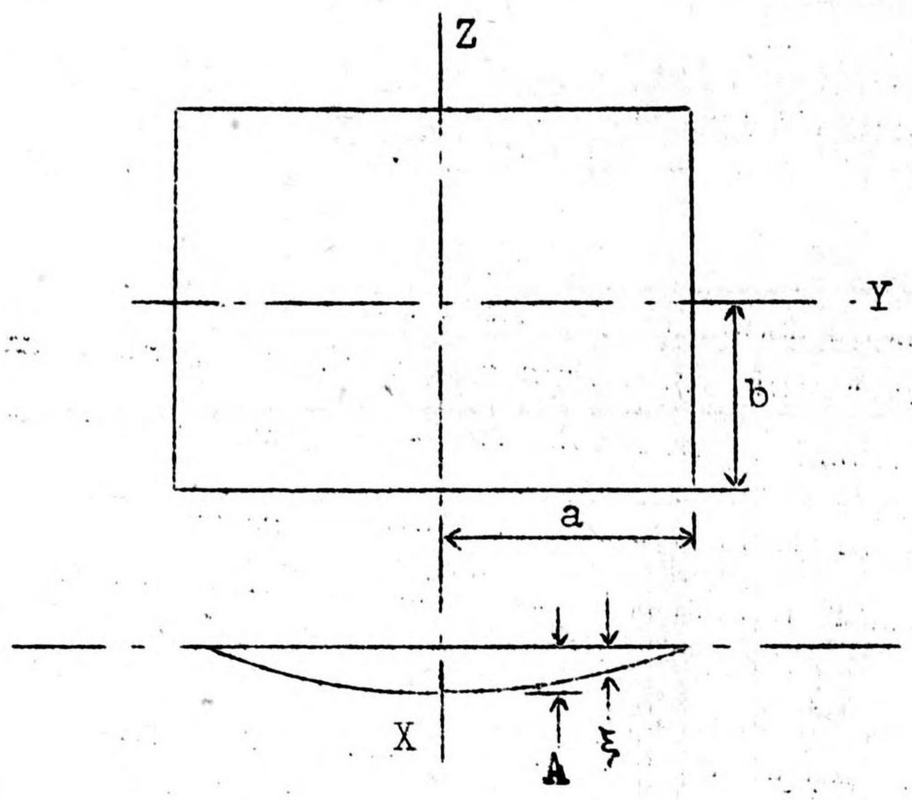

Fig. 1. Surface of flexure, rectangular plate.

1/ Vibration problems in engineering, by S. Timoshenko (Van Nostrand, 1937).

2/ Preliminary note on the measurement of the fundamental frequency of vibration of glass window panes, R.C. 58.

3/ Design of buildings against air attack, R.C. Note No. 6.

4/ Effect of blast on rectangular panels of glass or other elastic materials, by E. B. Phillip, R.C. 163.

5/ The measurement of the fundamental frequency of vibration of glass window panes, R.C. 87.

6/ Results of frequency measurements made on the test windows and rooflights for the Shoeburyness trial of 7th March 1940, R.C. 81.

occur is determined. Panes having a small amount of freedom of motion at supports are also included in the analysis.

Figure 1 shows the rectangular plate to be analyzed.

In addition to quantities indicated in Fig. 1, let h be the thickness of plate, E the modulus of elasticity, and μ Poisson's ratio. The assumed surface is

$$\xi = A\left[1 - \frac{13}{8}\left(\frac{y}{a}\right)^2 + \frac{5}{8}\left(\frac{y}{a}\right)^4\right]\left[1 - \frac{13}{8}\left(\frac{z}{b}\right)^2 + \frac{5}{8}\left(\frac{z}{b}\right)^4\right]. \tag{1}$$

The strain-energy in the plate, W_i, is[7/]

$$W_i = \frac{Eh^3}{12}\cdot\frac{1}{2(1+\mu)}\iint\left\{\frac{1}{1-\mu}\left[\left(\frac{\partial^2\xi}{\partial y^2}\right)^2 + \left(\frac{\partial^2\xi}{\partial z^2}\right)^2\right] + \frac{2\mu}{1-\mu}\cdot\frac{\partial^2\xi}{\partial y^2}\cdot\frac{\partial^2\xi}{\partial z^2} + 2\left(\frac{\partial^2\xi}{\partial y\partial z}\right)^2\right\} dy\,dz. \tag{2}$$

Substituting Eq. (1) in Eq. (2), we obtain

$$W_i = 0.415\,\frac{Eh^3}{1-\mu^2}\,A^2\,\frac{a^4 + 1.09\,a^2b^2 + b^4}{a^3b^3}. \tag{3}$$

The kinetic energy correspondingly is

$$K.E. = \tfrac{1}{2}m\omega^2\iint\xi^2\,dydz, \tag{4}$$

where m is the mass per unit area of plate, and ω is the angular frequency of the fundamental mode. This may be written

$$K.E. = 0.402\,m\omega^2A^2ab. \tag{5}$$

Equating Eqs. (3) and (5) and solving, we get for ω_r, the angular frequency for restrained-edge condition,

$$\omega_r = 1.016\,\frac{h}{a^2b^2}\sqrt{\frac{E}{(1-\mu^2)\rho}\,(a^4 + 1.09a^2b^2 + b^4)}, \tag{6}$$

where ρ is the mass density. The natural frequency in cycles per second is

$$n = \omega_r/2\pi. \tag{7}$$

Table II gives a comparison of measured frequencies[5,6/] with those obtained from Eq. (6). To agree with references, $E/(1-\mu^2) = 10.25 \times 10^6$ was used here.

7/ Drang und Zwang, by A. and L. Föppl (Munich and Berlin: R. Oldenbourg, 1924).

Table II. Comparisons of measured frequencies with those obtained from Eqs. (6) and (7).

Glass Size			Theoretical Frequency, n (cycle/sec)	Measured Frequency, n (cycle/sec)	Reference
Width (in.)	Length (in.)	Thickness (in.)			
9	9	0.12	350	350	5
9	12	.12	278	270	5
9	18	.12	231	230	5
9	36	.12	207	180	5
$11\frac{1}{4}$	$16\frac{1}{2}$	.127	167	200	5
12	18	.12	146	147	6

The work of the pressure forces p,[8] is

$$W_e = \tfrac{1}{2}\int\int p\xi \, dy\,dz = \frac{49}{72} pAab. \tag{8}$$

Equating Eqs. (8) and (3) we get the amplitude

$$A = 1.64 \frac{p a^4 b^4}{\frac{Eh^3}{1-\mu^2}(a^4 + 1.09\, a^2b^2 + b^4)}. \tag{9}$$

The stresses are (tension or compression)

$$\left.\begin{aligned} \sigma_y &= \frac{Eh}{2(1-\mu^2)}\left[\frac{\partial^2\xi}{\partial y^2} + \mu\frac{\partial^2\xi}{\partial z^2}\right], \\ \sigma_z &= \frac{Eh}{2(1-\mu^2)}\left[\frac{\partial^2\xi}{\partial z^2} + \mu\frac{\partial^2\xi}{\partial y^2}\right]. \end{aligned}\right\} \tag{10}$$

The maximum stress if $a > b$ will be σ_z at $(0,b)$

$$(\sigma_z)_{0,b} = 3.49 \frac{p a^4 b^2}{h^2(a^4 + 1.09\, a^2b^2 + b^4)}. \tag{11}$$

2. Vibrations of and stresses in free and simply supported plates

The preceding analysis is applicable to firmly puttied glass panes. In the case of old windows, there may be some shrinkage of the putty and

---

8/ Rayleigh's theorem, by Temple and Bickley (Oxford University Press, 1933).

consequent looseness of pane in the sash. This can be subjected to an approximate analysis by assuming a surface of flexure

$$\xi = A \cos \frac{\pi y}{2\, ra} \cos \frac{\pi z}{2\, rb}, \tag{12}$$

as shown in Fig. 2. In this case the internal strain energy is

$$W_i = \frac{Eh^3}{24(1-\mu^2)} \cdot \frac{\pi^4 A^2}{16\, r^4} \left\{ \frac{(a^2+b^2)^2}{a^3 b^3} \left(1 + \frac{r}{\pi} \sin \frac{\pi}{r}\right)^2 - \frac{8r}{\pi} \cdot \frac{1}{ab} \sin \frac{\pi}{r} \right\}. \tag{13}$$

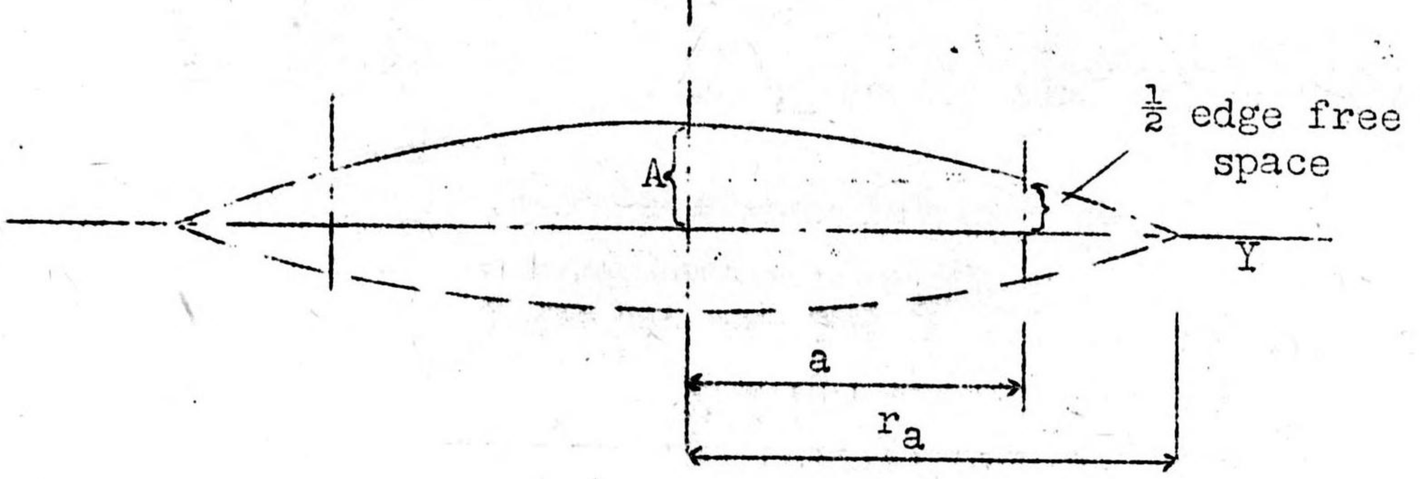

Fig. 2. Surface of flexure.

The kinetic energy is

$$\tfrac{1}{2}\, m\omega^2 \int\int \xi^2\, dy dz = \tfrac{1}{2}\, m\omega^2 A^2 ab \left(1 + \frac{r}{\pi} \sin \frac{\pi}{r}\right)^2. \tag{14}$$

Equating Eqs. (13) and (14), we obtain for the angular frequency for free-edge condition

$$\omega_f = \frac{\pi^2 h\, (a^2 + b^2)}{8\, r^2 a^2 b^2} \sqrt{\frac{E}{3(1-\mu^2)\rho}} \left[1 - \frac{\frac{8r}{\pi}\, a^2 b^2 \sin \frac{\pi}{r}}{(a^2+b^2)^2 \left(1 + \frac{r}{\pi} \sin \frac{\pi}{r}\right)^2} \right], \tag{15}$$

where ρ is the density of material.

For simply supported plates (r = 1)

$$\omega_s = \frac{\pi^2 h (a^2 + b^2)}{8\, a^2 b^2} \sqrt{\frac{E}{3(1-\mu^2)\rho}}. \tag{16}$$

The ratio of ω_f to ω_s is then

$$\frac{\omega_f}{\omega_s} = \frac{1}{r^2} \sqrt{1 - \frac{\frac{8r}{\pi}\, a^2 b^2 \sin \frac{\pi}{r}}{(a^2+b^2)^2 \left(1 + \frac{r}{\pi} \sin \frac{\pi}{r}\right)^2}}, \tag{17}$$

or, if $a/b = \lambda$,

$$\frac{\omega_f}{\omega_s} = \frac{1}{r^2}\sqrt{1 - \frac{\frac{8r}{\pi} \cdot \lambda^2 \sin\frac{\pi}{r}}{(1+\lambda^2)^2\left(1 + \frac{r}{\pi}\sin\frac{\pi}{r}\right)^2}}\,. \tag{18}$$

The maximum stress at the center (0,0) using Eq. (10) is

$$(\sigma_z)_{0,0} = \frac{24p(a^2 + \mu b^2)\sin^2\frac{\pi}{2r}}{h^2 \cdot \frac{\pi^4}{16r^4}\left\{\frac{(a^2+b^2)^2}{a^2b^2}\left(1 + \frac{r}{\pi}\sin\frac{\pi}{r}\right)^2 - \frac{8r}{\pi}\sin\frac{\pi}{r}\right\}}\,. \tag{19}$$

Call this σ_f (for free edge). For simply supported edge ($r = 1$)

$$\sigma_s = \frac{24\,p(a^2 + \mu b^2)}{h^2 \cdot \frac{\pi^4}{16} \cdot \frac{(a^2+b^2)^2}{a^2b^2}}, \tag{20}$$

and the ratio of σ_f to σ_s is

$$\frac{\sigma_f}{\sigma_s} = \frac{r^4 \sin^2\frac{\pi}{2r}}{\left(1 + \frac{r}{\pi}\sin\frac{\pi}{r}\right)^2 - \frac{8r}{\pi} \cdot \frac{\lambda^2}{(1+\lambda^2)^2}\sin\frac{\pi}{r}}\,. \tag{21}$$

The ratios ω_f/ω_s and σ_f/σ_s for various values of $\underline{r}$ are shown in Fig. 3.

3. Comparison with incidents

The reference noted in footnote 2 gives some test values of frequency of vibration for old windows. These vibrated more nearly with the fundamental frequency and mode for simply supported conditions in most cases. In one instance a plate-glass pane, 32.3 × 21 in., unputtied, in a light wooden frame vibrated with a frequency of 8 cycle/sec, as compared with a theoretical simply supported frequency of 15.5 cycle/sec.

This corresponds to a ratio $\underline{r}$ of 1.27 and illustrates the effect of loose-fitting panes. The stress ratio for that case ($\lambda = 1.54$), is $\sigma_f/\sigma_s = 2.02$, showing that the stress for a given pressure would be double that for a simply supported pane, or conversely, only half the pressure would be required for rupture. However, the equivalent static pressure is also much less, and therefore such panes are generally less likely to break.

From the preceding analyses and from comparison with tests, it is concluded that we will have a fair classification of window panes if we consider new, well-puttied panes as restrained; old, but still reasonably well fitting panes as simply supported; and very loose panes as free with an r of, say, 1.25.

From several sources[2,5,9,10] the physical properties of glass have been obtained, and the following values are used herein:

Glass	Modulus of Rupture (lb/in^2)	Young's Modulus (lb/in^2)	Poisson Ratio
Sheet, window	3000 to 4000	10×10^6	0.235
Plate	4000 to 5000	10×10^6	0.235

4. Response to air blast

Air blast will be approximated by

$$p = p_o \left(1 - \frac{t}{\theta}\right) e^{-t/\theta}. \tag{22}$$

This is for "side-on" pressure; for "face-on," the pressure will be doubled.

We will consider a mass m, with a spring constant c representing the elastic restraint, acted upon by the above pressure function, so that

$$m\ddot{x} + cx = p_o \left(1 - \frac{t}{\theta}\right) e^{-t/\theta}. \tag{23}$$

Calling $c/m = \omega^2$, we get

$$\ddot{x} + \omega^2 x = \frac{p_o}{c}\omega^2 \left(1 - \frac{t}{\theta}\right) e^{-t/\theta}. \tag{24}$$

A solution of this equation is

$$x = A \sin \omega t + B \cos \omega t - \frac{p_o}{c} \cdot \frac{\overline{\omega\theta}^2}{(1+\overline{\omega\theta}^2)^2} \left[(1-\overline{\omega\theta}^2) + (1+\overline{\omega\theta}^2)\frac{t}{\theta}\right] e^{-t/\theta}. \tag{25}$$

9/ Comparison of the resistance to blast of glass and various glass substitutes, by E. P. Phillip, REN 120.

10/ Mechanical engineers handbook, by Marks (McGraw Hill, 1941).

The boundary conditions are $x = 0$, $\dot{x} = 0$ when $t = 0$. Thus

$$\dot{x} = \omega \left[A \cos \omega t - B \sin \omega t\right] - \frac{p_o}{\theta c} \cdot \frac{\overline{\omega\theta}^2}{(1+\overline{\omega\theta}^2)^2} \left[2\,\overline{\omega\theta}^2 - (1+\overline{\omega\theta}^2)\,\frac{t}{\theta}\right] e^{-t/\theta}. \quad (26)$$

Thus by Eq. (25)

$$0 = B - \frac{p_o}{c} \frac{\overline{\omega\theta}^2}{(1+\overline{\omega\theta}^2)^2} (1 - \overline{\omega\theta}^2), \quad (27)$$

$$B = + \frac{p_o}{c} \frac{\overline{\omega\theta}^2 (1 - \overline{\omega\theta}^2)}{(1+\overline{\omega\theta}^2)^2}; \quad (28)$$

and by Eq. (26)

$$0 = \omega A - \frac{p_o}{\theta c} \cdot \frac{\overline{\omega\theta}^2}{(1+\overline{\omega\theta}^2)^2} (2\,\overline{\omega\theta}^2), \quad (29)$$

$$A = + \frac{p_o}{c} \cdot \frac{2\,\overline{\omega\theta}^3}{(1+\overline{\omega\theta}^2)^2}. \quad (30)$$

Equation (25) thus becomes

$$x = \frac{p_o}{c} \cdot \frac{\overline{\omega\theta}^2}{(1+\overline{\omega\theta}^2)^2} \left\{2\,\overline{\omega\theta} \sin \omega t + (1 - \overline{\omega\theta}^2) \cos \omega t - \left[(1 - \overline{\omega\theta}^2) + (1 + \overline{\omega\theta}^2)\,\frac{t}{\theta}\right] e^{-t/\theta}\right\}. \quad (31)$$

Equation (31) gives the response to the excitation function, Eq. (22). Differentiating with respect to time, we obtain

$$\dot{x} = \frac{p_o}{\theta c} \cdot \frac{\overline{\omega\theta}^2}{(1+\overline{\omega\theta}^2)^2} \left\{2\,\overline{\omega\theta}^2 \cos \omega t - \overline{\omega\theta}\,(1 - \overline{\omega\theta}^2) \sin \omega t - \left[2\,\overline{\omega\theta}^2 - (1+\overline{\omega\theta}^2)\,\frac{t}{\theta}\right] e^{-t/\theta}\right\}. \quad (32)$$

The maximum response occurs when $\dot{x} = 0$. The equivalent static pressure is $p_e = cx_{max}$. The time of maximum response (t_{max}) and the equivalent static pressure, in terms of $\omega\theta$, are obtainable from Fig. 4. (These are for first-cycle response; damping would reduce subsequent vibrations.)

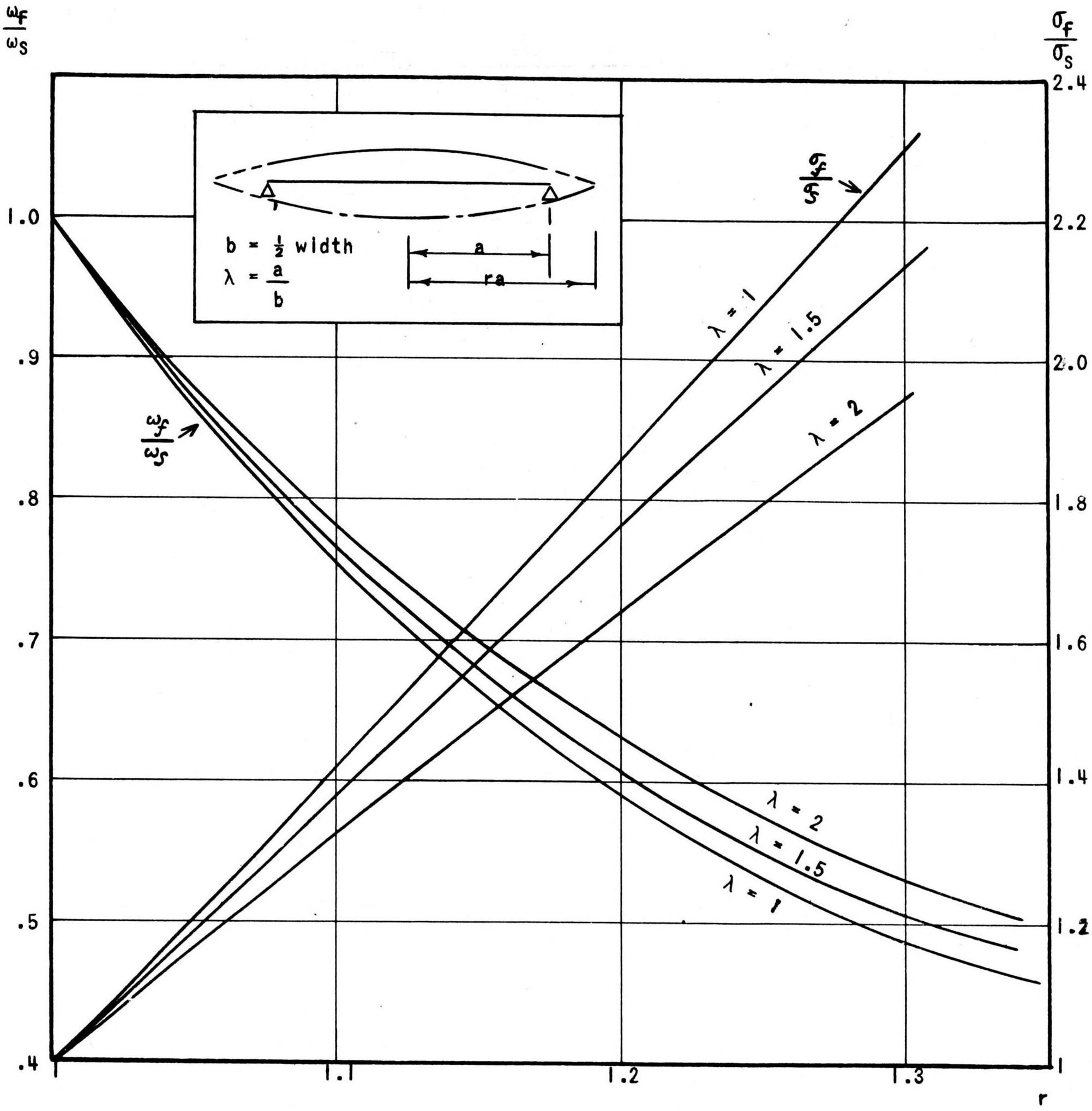

Fig. 3. Relative frequencies and stresses, partially free versus simply supported plates.

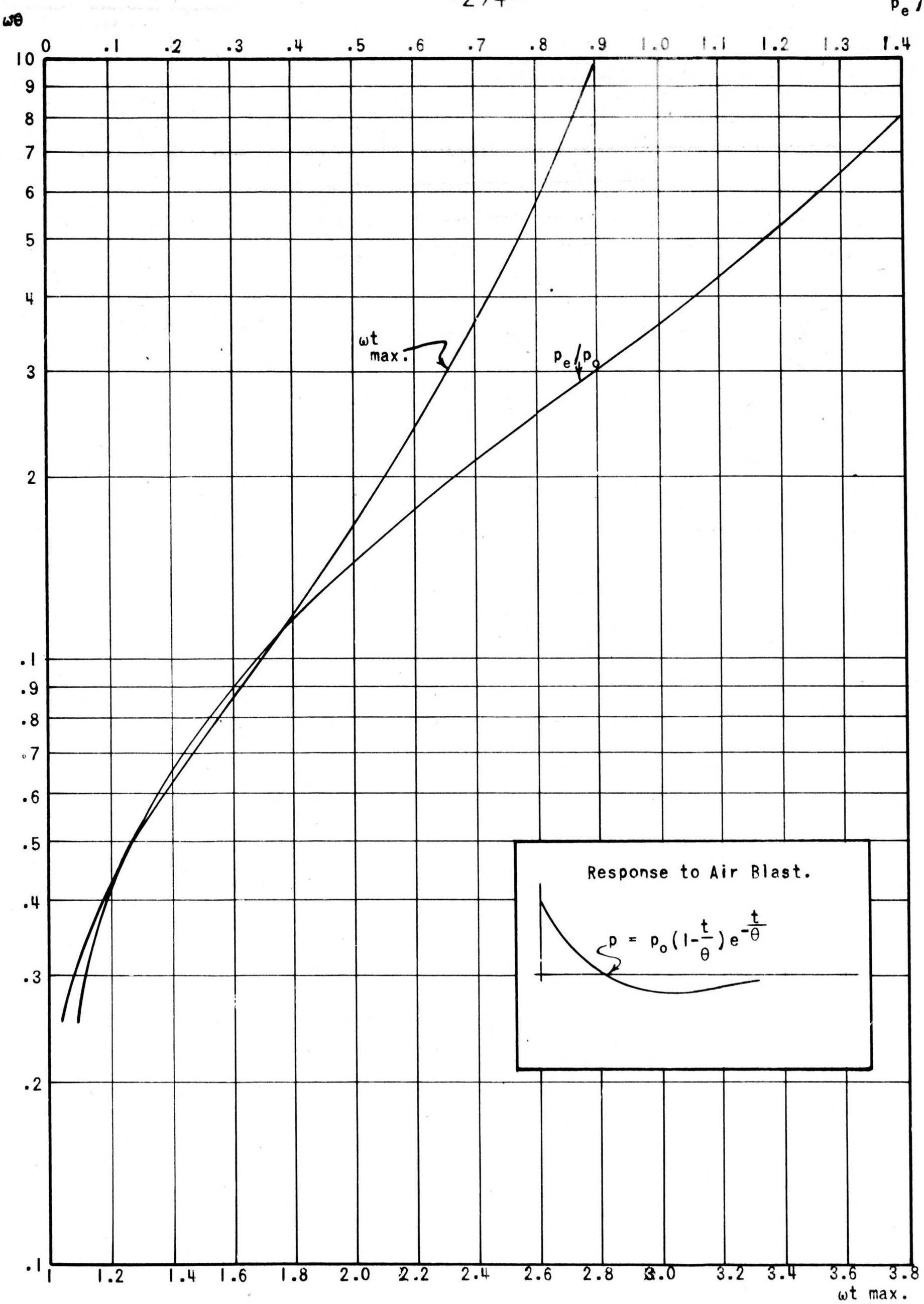

Fig. 4. Response of spring-borne mass to air blast.

5. Application to an incident

As an illustration of the application of the principles herein set forth, we will investigate an incident reported in R.C. 163[4] Fig. 8. In that figure a pane of plate glass 74 × 89 × 0.25 in. at 22 London Road was reported "broken when not expected," by blast from a 50-kg German bomb at a distance of 130 ft. Using Data Sheet 1A5a,[11] we find that the 50-kg SC bomb has a charge of 53.7 lb of TNT or Amatol. Then from Data Sheet 3A2*[11] we find $I = 0.0059$ lb-sec/in^2, and from Data Sheet 3A1,[11] $p_o = 1.17$ lb/in^2 for "side-on" and 2.34 lb/in^2 for "face-on." Therefore $\theta = (0.0059/1.17) \times 2.72 = 0.0137$ sec. The values of ω_r, ω_s, and ω_f ($r = 1.25$) for this pane are, from Eqs. (6), (16), and (17), respectively,

$$\omega_r = 1.016 \frac{0.25}{(44.5)^2} \sqrt{\frac{10.6 \times 10^6}{236 \times 10^{-6}} \left[(1.2)^4 + (1.09)(1.2)^2 + 1\right]} = 58.5 \text{ rad/sec},$$

$$\omega_s = \frac{\pi^2 \times 0.25}{8 \times (44.5)^2} \left[1 + (1.2)^2\right] \sqrt{\frac{10.6 \times 10^6}{3 \times 236 \times 10^{-6}}} = 46.6 \text{ rad/sec},$$

$$\omega_f = 46.6 \cdot \frac{1}{(1.25)^2} \sqrt{1 - \frac{\frac{10}{\pi} (1.2)^2 \, 0.588}{(2.44)^2 \, (1 + 0.234)^2}} = 25 \text{ rad/sec}.$$

The respective values of $\omega\theta$ are

$$(\omega\theta)_r = 0.80, \qquad (\omega\theta)_s = 0.64, \qquad (\omega\theta)_f = 0.34.$$

From Fig. 4, the ratio p_e/p_o for each case is

$$(p_e/p_o)_r = 0.265, \qquad (p_e/p_o)_s = 0.200, \qquad (p_e/p_o)_f = 0.055.$$

The respective equivalent static pressures are (using "side-on" gauge peak pressures)

$$(p_e)_r = 0.310 \text{ lb/in}^2, \quad (p_e)_s = 0.234 \text{ lb/in}^2, \quad (p_e)_f = 0.064 \text{ lb/in}^2$$

11/ Weapon data -- fire, impact, explosion, OSRD Report 6053.

From Eqs. (11), (20), and (21), the maximum stresses are

$$(\sigma)_r = 3.49 \frac{0.310 \times (44.5)^2 \times (1.2)^2}{(0.25)^2 (2.07 + 1.57 + 1)} = 10,600 \text{ lb/in}^2,$$

$$(\sigma)_s = \frac{24 \times 0.234 (44.5)^2 [1 + 0.235/(1.2)^2]}{(0.25)^2 \times \frac{\pi^4}{16} \cdot \frac{(1 + 1.44)^2}{1.44}} = 8250 \text{ lb/in}^2,$$

$$(\sigma)_f = \frac{0.064}{0.234} \times 8250 \times \frac{2.4414 \times 0.346}{(1.234)^2 - \frac{10}{\pi} \cdot \frac{1.44}{(2.44)^2} \times 0.588} = 5140 \text{ lb/in}^2$$

For "face-on" conditions the pressures and stresses would be doubled. Therefore we would conclude from the foregoing that breakage of the window was to have been expected unless it was either (a) exceptionally strong material, or (b) was shielded from the blast in some way. This single incident suffices to explain results of the other incidents in the reference noted[4] for those incidents for which sufficient data were reported.

6. Radii of breakage of glass

Based on the preceding analyses, Table I gives the radii of breakage for glass. Several common sizes of glass are included with various moduli of rupture (3000 lb/in^2 to 5000 lb/in^2). The table gives values for simply supported panes and can be used for restrained panes also, because the radii of breakage for these two types of support are almost exactly the same. For loose-fitting panes the radius of breakage is very nearly half the distance given by the table. The distance at which breakage will occur must necessarily be regarded as a rough approximation; some glass will break at smaller distances and other glass at greater distances. The table gives values for "side-on" position of glass relative to the direction of the blast, since this represents a compromise between "face-on" unobstructed blast (which would give approximately double the distance) and the conditions frequently encountered in incidents in which the glass is partly shielded from the blast. If an estimate of the percentage of glass likely to be broken is

desired, a rough approximation based upon British data[12,13] is given by

$$p = 0.5 - \log_e \frac{d}{d_m}, \tag{33}$$

where

p is proportion of panes broken,
d is distance at which proportion p break,
d_m is mean distance at which 50% are assumed to break,

or

$$d = d_m e^{0.5 - p}. \tag{34}$$

Of course d is limited to the range $0 < p < 1$.

If the glass is "face-on" to the blast and there is no shielding, the distance may be doubled. If the blast is shielded, the distance may be reduced. For interior blast in a building the confined blast may be even more severe than for unobstructed "face-on" conditions. To form an estimate of the percentage of glass broken, a linear relationship between maximum and minimum radii of breakage will usually suffice. For example, assume a 12 × 18 × 0.12-in. window glass, newly installed, subjected to blast from a 1000-lb GP bomb. The minimum radius of breakage is 740 ft and the maximum is 1020 ft (corresponding to 4000 and 3000 lb/in^2 modulus of rupture, respectively). Then

$$p = \frac{d}{280} - 2.64$$

will give, approximately, the proportion of glass broken at distance d.

A report[14] on the Port Chicago explosion states that glass was broken at a distance of 25 mi. The weight of explosive detonated was 2136 tons or 4,272,000 lb. From this, θ is approximately 0.6 sec and p_o is approximately

---

12/ Report of trial to determine the effect of blast on windows at four distances, Shoeburyness, 9 Aug. 1940, EAC. 41.

13/ Summary of report on first trial of window treatments and roof glazing, EAC. 21.

14/ Abstract of explosions, Report I: Port Chicago, California, rewritten 25 May 1945, Army-Navy Explosives Safety Board.

0.05 lb/in.^{2}; $\omega\theta$ will be very large and p_e/p_o will be close to 2. Hence if "face-on" conditions are assumed, p_e will be 2 × 2 × 0.05 = 0.2 lb/in.^{2}, and 12 × 18 × 0.12-in. glass should not be broken, but larger panes such as 24 × 24 × 0.12 in. would be expected to be broken under favorable conditions.

H. BOMBING-DENSITY CALCULATIONS FOR SLOPING TARGETS*

by Joseph A. Wise

Abstract

A formula for the equivalent horizontal area of sloping targets is derived, and a nomogram is given for finding the equivalent horizontal area from the slope and area of the target, direction of approach of aircraft, and angle of impact of bombs.

1. Summary

The bombing density required for a target is usually calculated in terms of number or weight of bombs per unit of horizontal area. If the target or vulnerable portions of it are not horizontal, an equivalent horizontal area A_h can be computed and used in bombing-density computations. The problem can be visualized by imagining that the paths of the bombs as they approach the target are rays of light. The "shadow" thus cast by the target upon a horizontal plane is its equivalent horizontal area. The equivalent horizontal area is derived in terms of the angle of impact of the bombs, the slope of the target, and the relative angle of approach of the aircraft. A nomogram for finding it is given in Fig. 2.

2. Method of calculation

It will be assumed that the target area, or vulnerable area, $\underline{A}$ is a plane oriented as shown in Fig. 1. It is obvious that if we imagine parallel rays of light falling on the target area in the direction of the bomb paths, the "shadow" thus cast upon the horizontal plane will be the equivalent horizontal area because any bombs that would fall within that shadow would hit the target. The true angle of impact of the bombs, $\underline{\alpha}$, is the angle between the bomb path and the normal to the horizontal plane; $\underline{\beta}$ is the bearing of the slope relative to the path of approach of the attacking planes, and $\underline{\gamma}$ is the angle of slope. The angle $\underline{\beta}$ is measured to the axis of the slope, the

---

*First published as EWT-3g (OSRD-5176g).

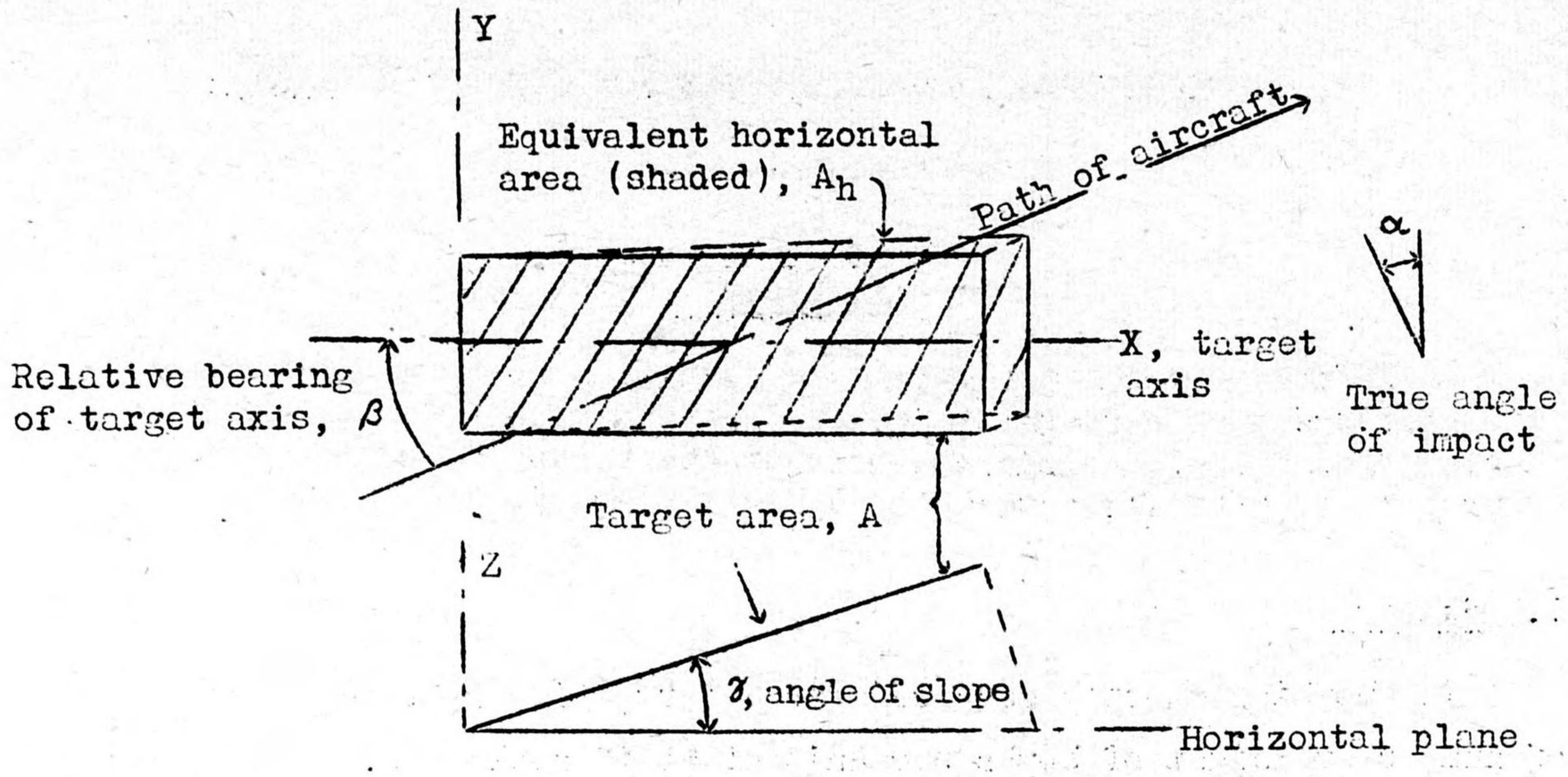

Fig. 1. Target area.

line of steepest slope which is also normal to the intersection of the slope and the horizontal plane. The angle γ is measured in the vertical plane through the axis of the slope.

The projection of the equivalent horizontal area upon a plane perpendicular to the bomb path must be identical with the projection of the actual target area upon the same plane. Using the principle that the projection of a unit area in one plane upon another plane is equal to the sum of the products of the direction cosines of the perpendiculars to the planes, we tabulate the respective direction cosines and then find the desired projections.

Vector	Direction Cosine		
	X	Y	Z
Downward normal to horizontal plane	0	0	-1
Downward normal to target area	$+\sin\gamma$	0	$-\cos\gamma$
Bomb path directed downward	$+\sin\alpha\cos\beta$	$+\sin\alpha\sin\beta$	$-\cos\alpha$

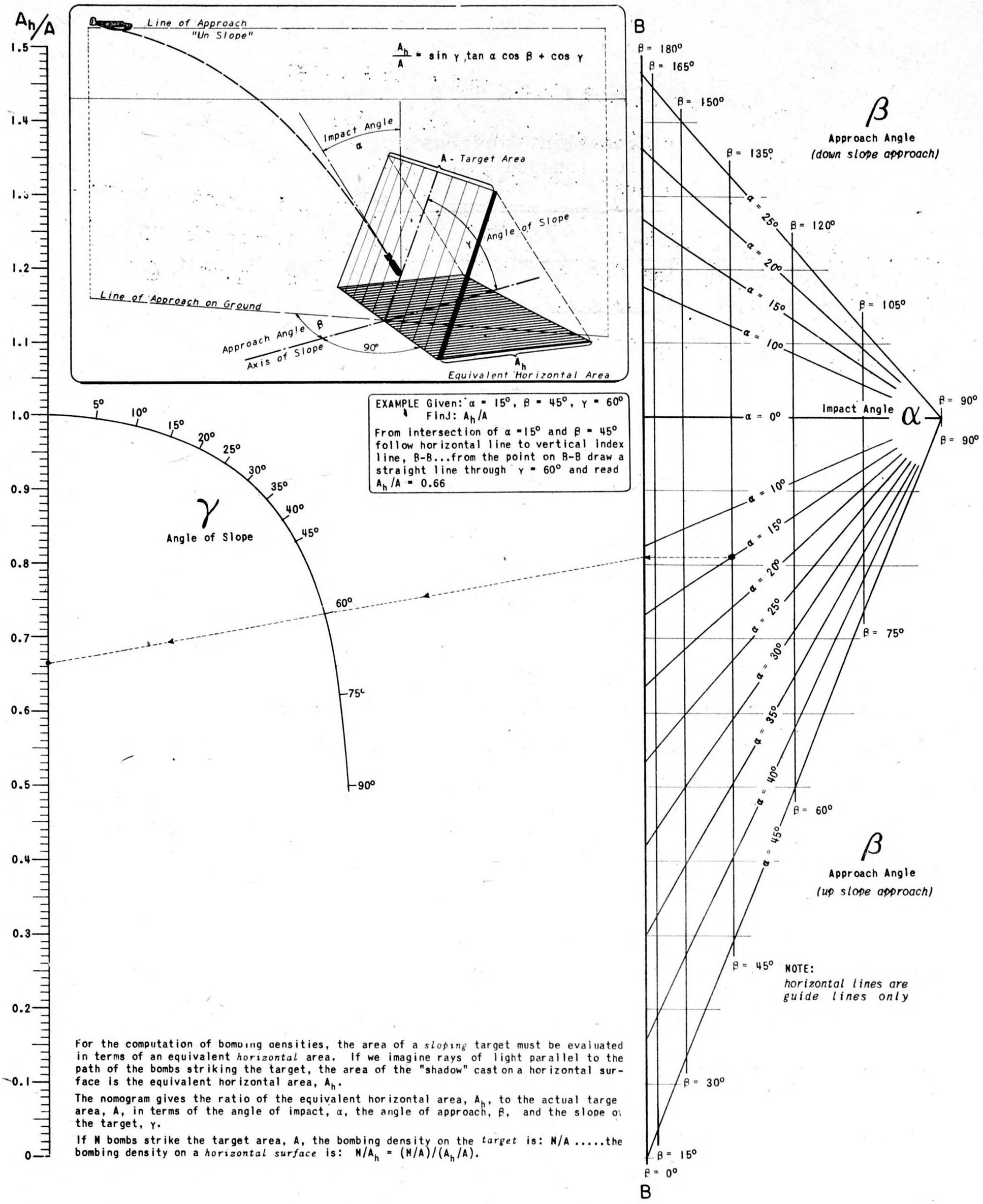

For the computation of bombing densities, the area of a *sloping* target must be evaluated in terms of an equivalent *horizontal* area. If we imagine rays of light parallel to the path of the bombs striking the target, the area of the "shadow" cast on a horizontal surface is the equivalent horizontal area, A_h.

The nomogram gives the ratio of the equivalent horizontal area, A_h, to the actual target area, A, in terms of the angle of impact, α, the angle of approach, β, and the slope of the target, γ.

If N bombs strike the target area, A, the bombing density on the *target* is: N/A .....the bombing density on a *horizontal surface* is: $N/A_h = (N/A)/(A_h/A)$.

FIGURE 2: NOMOGRAM FOR EQUIVALENT HORIZONTAL AREA

Therefore

$$A_h \cos\alpha = A(\sin\gamma \sin\alpha \cos\beta + \cos\gamma \cos\alpha), \quad (1)$$

$$A_h = A(\cos\gamma + \sin\gamma \tan\alpha \cos\beta), \quad (2)$$

$$A_h/A = \cos\gamma + \sin\gamma \tan\alpha \cos\beta. \quad (3)$$

This result is presented in the nomogram, Fig. 2. In using that nomogram, note that β is always less than 90° if the approach is toward the upward slope. It is obvious, of course, that the best angle of approach β is 0° for maximum equivalent horizontal area.

APPENDIX

AN ILLUSTRATION OF THE USE OF DATA SHEETS IN OSRD REPORT 6053: PERFORMANCE OF LARGE BOMBS

by F. G. Roth

Abstract

Data Sheet 7A1 of OSRD Report 6053, Weapon data -- fire, impact, explosion, is a summary of the performance to be expected from the 12000-lb T10 and the 22000-lb GP T14 bombs (see p.305). These performance estimates were made by using other data sheets in this reference report and some additional information. This paper gives details of the methods of making the estimates and illustrates the use of the data sheets for making other estimates of weapon performance.

The data sheets in Weapon data -- fire, impact, explosion [1/] give information on the performance of weapons in terms of scaled variables, and thus may be used to estimate the performance of other weapons. These sheets have been used to estimate the performance of two large bombs, the 12000-lb T10 and the 22000-lb T14. The performance estimates are extrapolations of data for smaller bombs and data for small-scale model experiments with projectiles and explosives. It is believed that the methods of extrapolation are accurate and that the figures given here and summarized in Data Sheet 7A1 of the reference[1/] are of reasonable accuracy. Where actual performance[2/] is known for the British 12000-lb Tallboy and 22000-lb Grandslam the results are in good agreement with the predictions from the data sheets.

In this paper the methods of estimating the performance of the large bombs are explained and will serve as an illustration of the use of the data sheets in Weapon data -- fire, impact, explosion.

The physical dimensions of the two bombs are the same as those of the two large British bombs. The British bombs were filled with Torpex D-1 (desensitized -- nearest U.S. equivalent: HBX) and the U.S. bombs are filled with Tritonal (TNT/Al; 80/20). Since the loading density of Torpex D-1 is 1.66 gm/cm^3 and that of Tritonal is 1.70 gm/cm^3, the explosive weight and the total bomb weight for the U.S. bombs are somewhat greater than for the British equivalents.

In order to estimate the performance of these bombs explosive factors for the charges involved are needed, since most of the information given in

---

1/ OSRD Report 6053.

2/ Study of the requirements, employment, and effectiveness of large bombs, AAF Project No. 4614A471.6, the Army Air Forces Board, Orlando, Fla.

the data sheets is for TNT and the actual performance data for the British bombs is for Torpex D-1. Table I gives the explosive factors, most of which are taken from Data Sheet 1A1½/

Table I. Characteristics and relative effectiveness ratios e for equal volumes of TNT, Torpex D-1 [or HBX], and Tritonal.

Explosive ——→		TNT	Torpex D-1 [HBX]	Tritonal
Composition ——→		TNT(100)	RDX/TNT/Al/wax (42/40/18/1) [RDX/TNT/Al/wax (40/38/17/5)]	TNT/Al (80/20)
Loading density (gm/cm³)		1.57	1.66	1.70*
Impact sensitivity		1.00	0.82	0.94
Air	Peak pressure	1.00	1.17	1.11
	Impulse	1.00	1.20	1.16
Underwater	Peak pressure	1.00	1.13	1.01
	Impulse	1.00	1.25	1.18
	Bubble radius	1.00	1.20**	1.20**
Earth	Crater diameter	1.00	1.16**	1.10**
	Crater depth	1.00	1.20**	1.20**

*This density figure was supplied by E. Bright Wilson, Jr., as that expected from Army loading plants.

**These values are not measured quantities but rather estimates based on Torpex 2 (U.S.) and converted for the purposes of this work.

1. Estimates of performance

(a) Homogeneous armor. -- The thickness of homogeneous armor perforated by these bombs was determined by using the conservative edge of the graph of Data Sheet 2C5*, striking velocities being determined from Data Sheet 1B12. It was realized that these bombs, having cases lighter than SAP and AP bombs, might break up against thick armor. The break-up limit thickness was determined by plotting the known break-up limit thicknesses for GP, SAP, and AP bombs in calibers, against the thickness of the case for each bomb, also in calibers. A smooth curve was drawn, and the caliber thickness which is the limit for perforation without break-up was determined from the calculated case thickness in calibers for each bomb.

The break-up limit for concrete perforation (see next subsection) was determined in a similar manner, and compared with known values of thickness perforated without case failure for these bombs. This showed that the observed values were greater than the estimated values. This can be attributed to the fact that the steel used in the manufacture of the 12000- and 22000-lb bombs is of better grade than that used in the manufacture of our GP and SAP bombs. The break-up limit thickness for concrete has been

WEAPON DATA TENTATIVE

BOMB PERFORMANCE
12,000-lb GP, T10 AND 22,000-lb GP, T14

12,000-lb GP, T10,
United States
"Tallboy-M", *British*

	TPX D-1	Tritonal
Total Wt, W *lb*	11630	11750
Total Chg. Wt, w *lb*	4980	5100
$w^{1/3}$	17.1	17.2
Chg. Wt. Ratio, w/W	43%	43%
Cal. Density, w/d^3	0.21	0.21
Fuze Settings	0.05, 0.25, 0.5, 3.0, 11.0 *sec*, 30, 60 *min*	

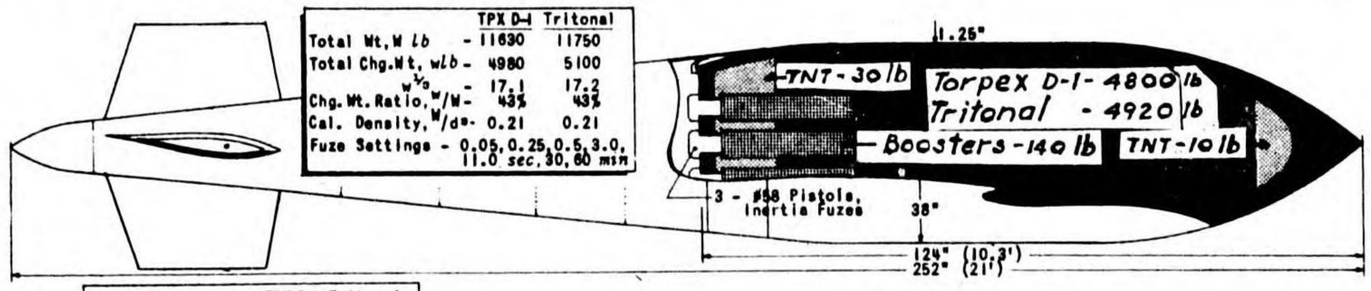

22,000-lb GP, T14,
United States
"Grand Slam", *British*

	TPX D-1	Tritonal
Total Wt, W *lb*	21875	22115
Total Chg. Wt, w *lb*	9200	9440
$w^{1/3}$	20.9	21.3
Chg. Wt. Ratio, w/W	42%	43%
Cal. Density, w/d^3	0.22	0.23
Fuze Settings	0.05, 0.25, 0.5, 3.0, 11.0 *sec*, 30, 60 *min*	

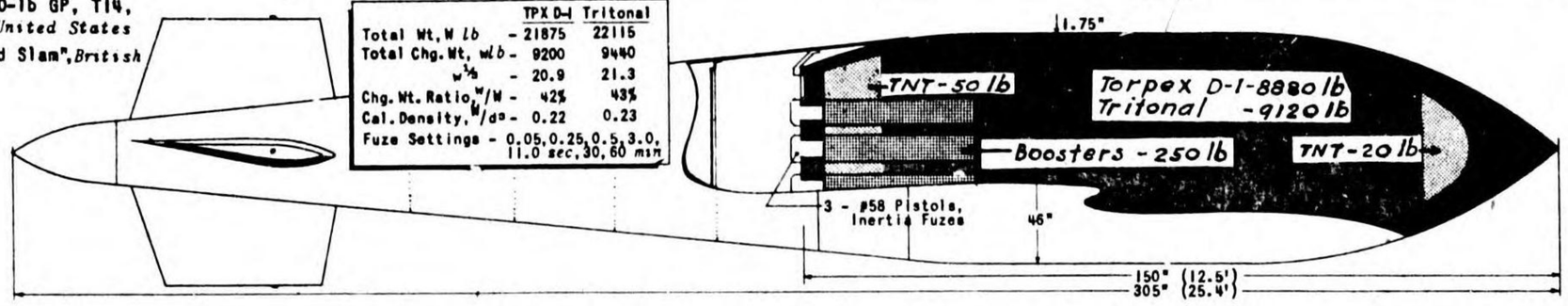

FLIGHT CHARACTERISTICS	Plane Speed, *mph*	12,000-lb GP, T10 (Tallboy-M) Altitude, *ft.* 5000	10000	15000	20000	25000	30000	22,000-lb GP, T14 (Grand Slam) Altitude, *ft.* 5000	10000	15000	20000	25000	30000	REMARKS
Striking Velocity, *ft/sec*	250	670	870	1030	1160	1260	1350	670	875	1035	1170	1275	1375	
Angle of Impact, *degrees*	250	33°	24°	20°	17°	16°	14°	33°	24°	20°	17°	16°	14°	
HOMOGENEOUS ARMOR:	BHN													
Max. Thickness Perforated, *in*	250-300	5.0	5.5-6.6	5.5-6.6	Estimated max. for no case break-up			6.4	7-9.0	7-9.0	Estimated max. for no case break-up			
REINFORCED CONCRETE:	Concrete Strength													
Max. Thickness Perforated, *ft.*	5000 *psi*	6.6*	8.6	10.1	11.5	13.4	13.4	8.2	11.0	13.0	14.8	16.5	16.5	*Ricochet is likely, so these values may not be realized
Inert	3000 *psi*	7.1*	9.6	11.2	13.3	14.9	15.3	8.8	12.3	14.8	17.3	19.5	19.5	
Max. Thickness Scabbed, *ft.*	5000 *psi*	10.1	12.2	13.8	15.8	16.2	17.2	12.4	15.3	17.5	19.3	20.8	22.1	Shaded values indicate zone of probable case break-up or premature detonation..values for 20,000 ft. may be considered as limiting thicknesses for higher altitudes.
Inert	3000 *psi*	10.6	13.2	15.3	17.2	18.3	19.0	13.0	16.7	19.4	21.9	23.5	24.7	
Max. Depth Penetrated, *ft.*	5000 *psi*	2.5	4.4	5.8	7.1	7.8	8.4	3.2	5.8	7.7	9.4	10.4	10.9	
Inert	3000 *psi*	3.0	5.3	7.1	8.8	9.8	11.0	3.9	7.0	9.5	11.7	13.3	13.9	
Max. Thickness Perforated, *ft.*	5000 *psi*	8.0*	10.0	11.5	12.9	13.8	14.7	10.2	13.0	15.0	16.9	17.8	18.6	
Impact + Expl. + Scab	3000 *psi*	8.5*	11.0	12.6	14.7	16.8	17.0	10.8	14.3	16.8	19.2	20.9	21.8	
Max. Thickness Scabbed, *ft.*	5000 *psi*	11.6*	13.7	15.3	16.8	17.7	18.7	14.5	17.4	19.6	21.6	23.2	24.7	
Impact + Expl. + Scab	3000 *psi*	12.1*	14.7	16.8	18.7	19.8	21.1	15.1	18.8	21.5	24.0	25.9	28.1	
Max. Depth Penetrated, *ft.*	5000 *psi*	3.8*	5.7	7.1	8.4	9.2	10.1	5.0	7.6	9.5	11.3	12.4	13.2	
Impact + Explosion	3000 *psi*	4.3*	6.6	8.4	10.1	11.1	12.2	5.7	8.8	11.3	13.5	14.9	15.9	
Ave. Entrance Crater Diam., *ft*	3-5000 *psi*	27	30	33	35	35	35	32	36	40	42	43	43	
Back Crater (Scab) Diameter, *ft*	3-5000 *psi*	Varies from heavy cracks at scab limit to 40 *ft.* when perforated.						Varies from heavy cracks at scab limit to 50 *ft.* when perforated.						
EARTH:	Soil Type													
Penetration Depth, *ft.*	Sand	26	33	39	43	45	47	33	41	49	53	56	59	For penetration *path length* add 20% to 30% to *depth.* Values are given for *uniform* soil.
(With long delay fuze)	Loam	39	48	54	60*	62	65	48	62	67	75	77	80	
	Clay	56	67	76	81	85	87	70	85	95	100	105	111	
Cratering Effect	Explosive	Sand		Sandy Loam		Clay		Sand		Sandy Loam		Clay		Performance values in EARTH dependant upon explosion, are based on *estimated* ratios for relative effectiveness of explosives.
Max. Crater Radius, *ft.*	Torpex D-1	39 - 44		45 - 49		50 - 55		45 - 51		52 - 57		62 - 68		
	Tritonal	37 - 41		41 - 45		48 - 53		44 - 50		50 - 55		59 - 65		
Max. Apparent Crater Depth, *ft*	TPX or Trit	23 - 27		25 - 29		28 - 31		28 - 33		31 - 36		34 - 38		
Displacement in Clay, *inches*		Distance from Explosion, *ft.*						Distance from Explosion, *ft.*						
		70	80	90	100	110	120	80	90	100	110	120	130	
Horizontal:	Torpex D-1	21.2	11.1	7.6	3.4	2.7	2.3	28.6	19.2	13.1	9.3	7.1	5.3	
	Tritonal	20.4	10.5	7.2	3.2	2.5	2.2	27.0	18.0	12.4	8.8	6.7	5.1	
Vertical:	Torpex D-1	13.0	8.3	5.4	3.2	2.1		20.6	14.4	9.7	6.3	5.0	3.3	
	Tritonal	12.4	7.8	5.2	3.0	2.0		19.5	13.4	9.2	6.2	4.7	3.1	
Damage of Underground Piping		Cast Iron			Ceramic			Cast Iron			Ceramic			
Dist. from Explosion, *ft.*	Torpex D-1	63'			104'			77'			128'			
	Tritonal	60'			99'			73'			121'			
Underground R/C Wall Damage *(Average Soil)*		Distance from Explosion, *ft.*						Distance from Explosion, *ft.*						Damage will be *greater* in wet, or clayey soil; *less* in loose or sandy soil.
		0	10	20	30			0	10	20	30	40		
Max. Thickness of Wall Breached, *ft.*:	Torpex D-1	17	16	9				21	20	15	8			
	Tritonal	16	15	9				20	19	14	8			
Max. Thickness of Wall Heavily Damaged, *ft.*:	Torpex D-1	25	23	16	8			30	29	23	14	8		
	Tritonal	23	22	15	8			28	27	22	13	8		
UNDERWATER:		Depth Below Surface of Water, *ft.*						Depth Below Surface of Water, *ft.*						
Maximum Bubble Radius, *ft.*		90	110	130	150			90	110	130	150	170		
	TPX or Trit	50	48	46	45			62	61	57	55	51		
Peak Pressure, *lbs/sq. in.*		Distance from Explosion, *ft.*						Distance from Explosion, *ft.*						
		100	200	300	400	500	1000	100	200	300	400	500	1000	
	Torpex D-1	3050	1360	850	630	500	220	3700	1700	1100	780	600	270	
	Tritonal	2730	1210	760	565	445	198	3340	1530	980	697	536	242	
Impulse, *lb.msec/sq. in.*	Torpex D-1	5290	2660	1750	1350	1060	530	7950	3980	2680	1980	1590	795	
	Tritonal	5000	2560	1650	1250	997	500	7500	3750	2520	1870	1500	750	
AIR:														
Peak Pressure, *lbs/sq. in.*	Torpex D-1	26	5.6	3.2	2.1	1.6	0.8	44	8.2	4.1	2.7	2.0	0.9	
	Tritonal	24	5.3	3.0	2.0	1.5	0.7	42	7.8	3.9	2.6	1.9	0.9	
Impulse, *lb.msec/sq. in.*	Torpex D-1	170	85	57	42	34	17	256	128	86	64	51	26	
	Tritonal	165	82	55	41	33	16	248	124	82	62	99	25	
FRAGMENTATION														
Thickness Perforable by Fragments at Distance 100 ft, *in.*	TPX or Trit	Mild Steel		Concrete		Brick		Mild Steel		Concrete		Brick		
		2 - 3		18 - 26		20 - 30		2½ - 3½		21 - 30		25 - 38		

SOURCE: Physical Characteristics from Ordnance Department, U.S.Army; Performance Data from various British and American model tests

NATIONAL DEFENSE RESEARCH COMMITTEE, DIVISION 2, PRINCETON UNIVERSITY STATION

observed to be at least three times the estimated limit based on data for ordinary GP and SAP bombs. The break-up limit given on Data Sheet 7A1 is 1.4 times that estimated from data on ordinary GP and SAP bombs. This is thought to be somewhat conservative.

(b) Reinforced concrete. -- Depth of penetration into concrete was calculated from the equation given in the "Sources" section of OSRD Report 6053, using values of striking velocity and obliquity from Data Sheet 1B12. The thicknesses perforated or scabbed were determined from the penetration depths by means of the relations given in the abstract of CFD Interim Report No. 28.3/ The limit thicknesses for break-up were determined by using the greatest thickness consistently perforated2/ by the 12000-lb bomb in attacks on German U-boat pens as the limit thickness for the 12000-lb bomb, and using the same thickness in calibers as the limit for the 22000-lb bomb.

The thickness perforated or scabbed by penetration plus explosion was determined by use of the relation for additional penetration by explosion of a projectile, as given in Terminal ballistics and explosive effects.4/

The dimensions of the spall and scab craters were determined by caliber scaling of the craters given in Interim Report No. 20 of the Committee on Passive Protection Against Bombing5/.

(c) Earth. -- (i) Penetration depth. Penetration depth values are given for sand, loam, and clay soil for release altitudes of 5000 to 30,000 ft (5000-ft intervals). The procedure followed was to read directly from the nomogram on Data Sheet 2A2* the value for L where L is the penetration path length. The ratio of radius of ogive to bomb diameter, R/d, for these bombs is about 2.0 or between 1.5 (average) and 3.0 (sharp). Values for the depth of penetration were given instead of the path length because they were considered more usable. They were determined by reducing the path length values, L, by 20% to 30% according to the correction factors as a function of obliquity reported in PTM 103, "Preparation of data sheet 2A2* and 2A2a on penetration into soils."

(ii) Crater radius. From Data Sheet 3B1a* the equation used,

$$D/w^{1/3} = k,$$

gives k, a soil constant for cratering, or the ratio of the maximum crater diameter, D (ft), to the cube root of the charge weight of TNT, w (lb). Values for k were determined from this data sheet as follows:

for clay soil, $k_c = 5.6$,
for sandy loam, $k_\ell = 4.9$,
for sand soil, $k_s = 4.3$.

3/. Interim Report No. 28, Committee on Fortifications Design, National Research Council.

4/ A report by the Committee on Passive Protection Against Bombing, National Research Council, to the Corps of Engineers, U.S. Army, Oct. 1943.

5/ Interim Report No. 20, Committee on Passive Protection Against Bombing (later Committee on Fortifications Design), National Research Council.

Since crater diameter depends on the depth of detonation, the values are given as bracketed between the maximum and 0.9.× maximum to allow for possible variations of about ±50% from the optimum detonation depth. The explosive factors, e, for crater radius for Torpex D-1 and Tritonal from Table I were introduced, and the following formula was developed for determining the maximum crater radius

$$D_{max} = k \cdot w^{1/3} \cdot e \quad \text{or} \quad r_{max} = \frac{k \cdot w^{1/3} \cdot e}{2}.$$

(iii) Crater depth. Data Sheet 3B1a* was also used in a similar manner to determine the crater depth for these bombs. The depth is given by the relation

$$h = k' w^{1/3} e,$$

where h is the crater depth (ft), w is the weight of explosive (lb), e is the explosive factor from Table I, and k' is the soil constant for maximum apparent crater depth as determined from Data Sheet 3B1a*. As in the determination of the crater diameter, allowance for depth of burial at other than optimum values was made by a percentage reduction in the constant k' to allow for about ±50% difference from the optimum in depth of burial. The limits were determined from the curves on the data sheet. The values of the constant used are:

for clay soil, $k'_c = 1.35$ to 1.5,

for sand soil, $k'_s = 1.1$ to 1.3.

Values for sandy loam were interpolated as half way between the values for clay and for sand.

(iv) Earth displacement. Data Sheet 3B2 was used as a basis for determining values for permanent horizontal and vertical earth movement. These values, being based on TNT, were increased intuitively to allow for variation in explosive effectiveness.

(v) Underground piping. Data Sheet 6E1 was used which specifies that the radius of damage, R, to underground piping is equal to a constant times the cube root of the weight of the charge. The following equations were employed:

for ceramic piping, $R = 5.8\ w^{1/3}$,

for cast-iron piping, $R = 3.5\ w^{1/3}$.

Likewise, these values, being for TNT, were increased intuitively to allow for relative explosive effectiveness and for possible depth effects due to the small scaled depth of piping attacked by these bombs.

(vi) Underground reinforced-concrete walls. Data Sheet 6A5* was used in determining damage to underground reinforced-concrete walls. Using the scale variables of the graph, $r/w^{1/3}$ and $t/w^{1/3}$, the thicknesses t which would suffer heavy damage and breaching were obtained for different distances r. To allow for the relative effectiveness of Torpex D-1 and Tritonal, a known factor for Torpex 2 of 1.28 for the equivalent weight of TNT was employed and the resulting damage estimates were then reduced by 3% for Torpex D-1 [and HBX] and by 8% for Tritonal.

(d) Underwater explosion. -- (i) Maximum bubble radius. From Data Sheet 3C2 the following equation was used:

$$R = e\left[k \frac{w}{(h + h_o)}\right]^{1/3},$$

where

R is the maximum bubble radius (ft),
k is the constant for TNT [= 12.2],
w is the charge weight (lb of TNT),
h is the depth of charge (ft),
h_o is the atmospheric head [32 ft of water],
e is the explosive factor [average for Torpex D-1 and Tritonal is 1.20 (Table II)].

(ii) Peak pressure and impulse. From Data Sheet 3C1 the following equations were used to determine values for underwater peak pressure,

$$P = 20{,}400\ e\left(\frac{w^{1/3}}{r}\right)^{1.14},$$

and for underwater impulse,

$$I = 1500\ e\ \frac{w^{2/3}}{r},$$

where

P is the peak pressure (lb/in^2),
I is the impulse (lb-msec/in^2),
w is the charge weight (lb of TNT),
r is the radius or distance from explosion (ft)
e is the explosive factors for pressure and impulse (Table I).

(e) Air blast. -- (i) Peak pressure. Values for peak pressure for an equal volume of TNT were read directly from the nomogram of Data Sheet 3A1 and then multiplied by the explosive factors for Torpex D-1 (e = 1.17) and Tritonal (e = 1.11) from Table I.

(ii) Impulse. Values for the impulse were determined from the equation given in Sheet 3A2a, using the correction given in this sheet for the case thickness. The case-thickness factor S is 0.56 for the 12000-lb bomb and 0.53 for the 22000-lb bomb.

(f) Fragmentation. -- The thickness of mild steel, concrete, or brick perforated by fragments was determined by scaling from smaller bombs on the following basis. At the same distance scaled in terms of $w^{1/3}$ the same thickness of material scaled in terms of $w^{1/3}$ can be perforated. Similar results are obtained if the caliber is used as a scale factor. The thickness of concrete was scaled from the two thicknesses tested and reported in "Passive Protection Bulletin No. 6"7/ by the Office of the Chief of Engineers.

7/ "Passive Protection Bulletin No. 6," Office of the Chief of Engineers, U.S. Army, December 1944.

One wall was seriously damaged and the other was slightly damaged, and the limit thickness was taken as being between the two values. Thicknesses for steel and for brick were determined by using thickness ratios for these materials determined from the data in Tables 21 and 22 of Terminal ballistics and explosive effects. 8/

8/ See reference 4.